Soviet Physics
CRYSTALLOGRAPHY

Vol. 1, No. 3, pp. 205-297

May-June, 1956

IN MEMORY OF A. K. BOLDYREV

March 25, 1956 was the tenth anniversary of the death of the well-known Soviet crystallographer and mineralogist, Anatolii Kapitonovich Boldyrev (1883-1946).

A.K. Boldyrev began his scientific activity while still a student at Petersburg Mining Institute. He specialized in crystallography, mineralogy, and petrography with the famous Russian scientist E.S. Fedorov.

Boldyrev's first great work belonged to this period; this was Fundamentals of the Geometrical Study of Symmetry (1907), which was highly esteemed by E.S. Fedorov, who found in it "extreme strictness of mathematical logic." In this treatise Boldyrev, emphasizing the ambiguous character in the symmetry definitions of E.S. Fedorov, A. Schoenflies, and other authors, developed the idea of J.W. Wulff that the main symmetry transformation was reflection in a plane, and that every symmetry transformation could be reduced to successive reflection in several planes (in particular in one plane). In the same treatment, Boldyrev arrived at a definition of the congruence of figures earlier given by Möbius, but unknown to the majority of crystallographers: "Two systems of points are called mutually symmetric (equivalent) if the distance between any two points in one of them equals the distances between the two corresponding points in the other."

Starting from the concept of mutually symmetric systems and considering all space figures without exception, both finite and infinite, Boldyrev generalized and extended the conclusions of Wulff.

This brilliant start of the scientific activity of the young crystallographer was unfortunately interrupted for a number of years. For participation in the Student Revolutionary Movement he was expelled from the Mining Institute and by the Czar's decree banished first to the Cherdynsk region and later to Nizhnii Tagil.

However, this did not break the will of the student. Even in prison he constructed diagrams important for crystal-optical investigations, connecting the birefringence of the principle sections with the angles between the optic axes of minerals (1912).

The October Revolution enabled Boldyrev to return eight years later to the Mining Institute, where he finished in 1919.

Immediately after finishing at the Institute in 1919, Anatolii Kapitonovich brilliantly defended his scientific works and became Professor and Director of the Faculty of Crystallography at Leningrad Mining Institute. At the same time, he organized the Fedorov Institute of Crystallography, Mineralogy, Petrography, and the Science of Useful Minerals, the main quest of which was to study and develop the scientific ideas of E.S. Fedorov. To

this period belong a number of Boldyrev's publications devoted to the creative genius of his teacher (Scientific Works of E. S. Fedorov, 1921; Commentary on E. S. Fedorov's "Das Krystallreich", 1926, etc.).

To the same period belong Anatolii Kapitonovich's articles on specific problems in the science of symmetry: "Do mirror-rotation symmetry axes (composite-symmetry axes) of odd denomination exist?" (1923); "Oblique mirror-rotation axes of symmetry" (1923). In the first of these, the possibility that mirror-rotation symmetry axes of odd order could exist was demonstrated, contrary to the generally accepted view of the time. In the second article it was proved that a mirror rotation around an oblique mirror-rotation axis could always be replaced by a mirror rotation around some direct mirror-rotation axis. This gave an exhaustive answer to the earlier unsolved problem as to why oblique mirror-rotation axes were not taken into consideration in deriving symmetry groups.

During the same period, Boldyrev developed a number of methodical questions and constructed an angular compass, a stereographic protractor, and a very simple stereographic grid which found wide application. This grid, later named Boldyrev's Grid, comprises a stereographic projection of a spherical grid of meridians and parallels on the equatorial plane.

In 1920, as a participant at the Fourteenth International Geological Congress, Boldyrev visited Germany and Spain. On returning from this journey, he organized the X-Ray Laboratory in Leningrad Mining Institute, one of the first in our Union.

From then until the end of his creative activity, the x-ray measurement of crystals occupied Boldyrev's attention in a special way.

In 1925, Boldyrev's main treatise on crystal-chemical analysis, Principles of a New Method of the Crystallographic Study of Materials, was published. This clearly formulated the Boldyrev method of defining a crystalline substance from measurements made in a certain way of the angles of crystals, and set out a plan for the creation of his Crystal Index, the first two issues of which were published later (1937 and 1939). Boldyrev's index differed advantageously from Fedorov's (Das Kristallreich) in that it renounced Fedorov's subsidiary problem of the determination of the structure of a crystal from its shape.

The way in which the indexing was done consisted mainly of the goniometric measurement of certain defining angles, finding the corresponding angles in the key of the index, and final selection of a completely fitting substance from the description. Mastering this technique took no more than an hour. The same time was spent in one determination.

In 1925, A. K. Boldyrev also published the results of a survey of the crystallographic nomenclature of simple shapes undertaken on his initiative. This work went on in the Fedorov Institute and occupied the greatest specialists in our country. The revised and improved nomenclature received general assent in the Soviet Union. Subsequently, Boldyrev organized the same critical review of the classification, nomenclature, and symbolism of the 32 forms of crystal symmetry.

In 1926, the two leading publications of Boldyrev appeared: the well-known Course of Crystallography, and the no less well-known Course of Descriptive Mineralogy (first issue).

Boldyrev's Crystallography may even now serve as a reference work for various branches of the subject; in clarity and strictness of layout it is still a good example for modern authors of crystallographic handbooks.

In 1930, Boldyrev's monograph, Rare-Earth Apatites of the Lebyazhin Mine and Ural Mountains, appeared. On the basis of extremely accurate measurements, this convincingly confirmed N. I. Koksharov's crystal-chemical law that in apatite "with increased chlorine content the polar distance to the $(10\bar{1}\bar{1})$ face is reduced."

In 1933, the monograph Some Examples of Work with the Abbe Refractometer and the Accuracy of This Instrument, was published, giving a new development of the method of refractometric measurements.

Analogous results were obtained by Boldyrev in work with a large two-circle Goldschmidt goniometer in the last years of his life, articles describing these being published after his death.

In parallel with the development of these subjects, the painstaking work on the Crystal Index continued, and various issues of the Course of Descriptive Mineralogy appeared (second issue in 1928, third in 1935).

In the last years of his creative activity, Boldyrev showed still greater interest in the x-ray measurement of crystals and the crystal chemistry of minerals. He directed two x-ray measurement laboratories, in the Leningrad Mining Institute and the Central Scientific-Research Geological-Prospecting Institute (now the VSEGEI).

Whereas the main problem of x-ray measurement at this time was the determination of crystal structure, Boldyrev and his students created a second independent aspect of x-ray measurements by

applying this new method to studying the composition of mineral formations and chemical products. Even in its primary role in the field of mineralogy and useful minerals, the x-ray approach solved a number of important problems in connection with the nature of poorly crystallizing specimens of powdery composition. This relates, for example, to the ores of iron, manganese, aluminum, and other metals.

Boldyrev was one of the first to realize that data obtained from x-ray photographs of crystalline powders yielded important constants of the material. In this connection, work was started in a number of laboratories on composing an atlas of standard Debye photographs for minerals. Even in the thirties, Boldyrev's students had prepared x-ray standards for manganese and iron ores, silicates, coals, and other materials.

Boldyrev paid great attention to the methods of x-ray studies; these were treated in his papers with E. F. Alekseeva and G. A. Kovalev, and also in papers by his students, prepared under his direction.

In 1936 to 1938, Boldyrev supervised the preparation of new tables considerably simplifying x-ray calculations. These tables were published in 1950, after his death.

Finding himself at the head of the mineralogical application of x-ray measurements, Boldyrev based a number of important generalizations on the new experimental material.

In 1936, at the Jubilee Mendeleev Congress, Boldyrev came out with a paper on "Atomic and ionic radii in crystals," acquainting the members of the Congress with the fundamental laws of the new crystal chemistry.

In the collection Micas of the USSR appeared an extensive article on "The chemical constitution and crystal structure of micas," giving a detailed critical review of the then-existing data on the structure of micas and introducing a number of corrections matching structural data with chemical composition for this complex group of minerals (1937).

Further development of this theme appeared in "Chemical valence and the broader understanding of isomorphism. Application to the formulas of micas" (1938).

In 1935 to 1937, Boldyrev and his students began the great labor of constructing an X-Ray Mineral Index (1938 and 1939), which in essence constituted a new method of defining matter. This work was greatly in advance of similar efforts abroad and served as a model for the composition of a number of foreign handbooks of the same character (American, Portugese).

In this review we have only dealt with the most important work of A. K. Boldyrev. We have not mentioned his many studies on mineralogy, mineral science, petrography, and chemistry. A full list of these may be found in the Records of the Mineralogical Society (Part 75, No. 3, 1946).

Ten years have passed since the death of this scientist, but the value of his Crystal Index and X-Ray Mineral Index remains as high as ever; further volumes are being prepared by his students.

The honored memory of A. K. Boldyrev will live long in the hearts of all who knew him; his name will take its place among the greatest of Russian crystallographers.

V. I. Mikheev,
I. I. Shafranovskii,
A. V. Shubnikov

X-RAY DETERMINATION OF UNIT CELLS AND SPACE GROUPS OF THE PIEZOELECTRIC CRYSTALS $KLiC_4H_4O_6 \cdot H_2O$, $NH_4LiC_4H_4O_6 \cdot H_2O$, $NaHC_4H_4O_6 \cdot H_2O$ AND $(NH_4)_2C_4H_4O_6$

G. S. Zhdanov, M. M. Umanskii, L. A. Varfolomeeva, Z. I. Ezhkova, and Z. K. Zolina

M. V. Lomonosov State University, Moscow

Translated from Kristallografiya, Vol. 1, No. 3, pp. 271-273, May-June, 1956
Original article submitted March 10, 1956

The number of piezoelectric substances in practical use at the present time is small, but the number of substances which possess piezoelectric properties is quite large. Piezoelectricity can arise in crystals which satisfy certain crystallochemical conditions, which at present are not fully explained. To understand the nature of piezoelectricity, and to achieve success in the synthesis of new piezoelectric materials, it is necessary to appreciate their crystallochemical properties [1].

The first stage in a crystallochemical investigation is x-ray determination of the unit cells and symmetry groups of the crystals. Accurate values of the unit cell constants (linear and angular) are particularly necessary in piezoelectric work, to calculate the angles at which plates must be cut. The present article reports the results of an x-ray determination of the unit cells and space groups of four piezoelectric crystals from the tartrate group, which have the chemical formulas and abbreviated symbols shown in Table 1.

The crystals for the investigation were given to us by the Crystal Physics Department of the Physics Faculty, Moscow State University, which is carrying out a systematic study of new piezoelectrics. A summary of the literature data on the crystals we studied is shown in Table 1. These results indicate that the first two compounds are isomorphous, which might be expected, since it is common to talk about the replacement of a potassium ion by an ammonium ion. The only x-ray data in the literature are for (NH_4Li); they are $a = 7.89$, $b = 14.74$, $c = 6.42$ Å; space group D_2^3 [4].

To determine the symmetry of the crystals, the unit cell dimensions, and the space groups, we carried out (a) goniometer measurements; (b) x-ray diffraction determinations of diffraction symmetry classes; (c) approximate determinations of unit cell dimensions and determination of Bravais lattice type; (d) preparation of photographs on a KFOR x-ray goniometer [5], to find the types of reflection observed; and, (e) determination of x-ray groups from systematic-absence rules [6], these groups in most cases being sufficient, in combination with goniometer and piezoelectric results, to give a unique result for the space group. Densities were also determined pycnometrically. Precision measurements were made of the unit cell constants of single crystals, using oscillation photographs [7] taken with a RKU-114 camera [5].

In determination of the cell constants, reflections obtained at angles of 55 to 86° were considered. For each constant, several reflections were obtained, in not less than two different radiations [Cu, Ni, Co, Fe]. The distances between symmetrical spots on equatorial layer lines of the oscillation

TABLE 1.

Chemical formula	Abbreviated symbol	Crystal system	Symmetry class	a : b : c	References
$KLiC_4H_4O_6 \cdot H_2O$	(K, Li)	Orthorhombic	D_2	0.5479 : 1 : 0.4431	[2a], [2a], [4]
$NH_4LiC_4H_4O_6 \cdot H_2O$	(NH_4, Li)	The same	D_2	0.5392 : 1 : 0.4403	[2b], [2b], [4]
$NaHC_4H_4O_6 \cdot H_2O$	(Na, H)	The same	D_2	0.8180 : 1 : 0.6829	[2c], [2c], [4]
$(NH_4)_2C_4H_4O_6$	$(NH_4)_2$	Monoclinic	C_2	0.1506 : 1 : 1.4383 $\beta = 92°23'$	[2d], [2d], [4]

TABLE 2. Summary of Unit Cell Constants, Densities, and Space Groups for the Crystals Investigated

Compound	a (kX)	b (kX)	c (kX)	v (kX)³	ρ	$\rho_{X\ ray}$	Space group
(KLi)	7.839±1	14.318±1	6.326±1	710.0	2.01	1.981	$D_2^3 - P2_12_12$
(NH_4Li)	7.860±1	14.615±2	6.414±2	736.9	1.73	1.721	$D_2^3 - P2_12_12$
(NaH)	8.663±2	10.580±4	7.230±4	662.7	—	1.905	$D_2^4 - P2_12_12_1$
$(NH_4)_2$	7.067±1	6.116±3	8.790±1	379.6	1.608	1.611	$C_2^2 - P2_1$
	$\beta = 92°25' \pm 1'$						

photographs (to determine the angles of reflection) were measured with an error not exceeding 0.2 mm. The x-ray photographs were obtained at room temperature (18-20°C), without thermostatic control. The estimates of accuracy shown in Table 2 were obtained from an analysis of probable errors.

The investigations of the external forms of the crystals and the goniometer measurements confirmed the results published in the literature. Determinations from oscillation photographs of the repeat distances along the principal and diagonal directions showed that all the compounds investigated had primitive Bravais lattices. The x-ray goniometer measurements showed up the appearance of characteristic sets of reflections. For (KLi) and (NH_4Li), reflections of types *hkl*, *hk*0, *h0l*, 0*kl*, and 0*0l* were observed for any indices, and 0*k*0 and *h*00 only for even indices, leading to the space group D_2^3. For (NaH), reflections of type *hkl*, *hk*0, 0*kl*, and *h0l* were observed for any indices, and *h*00, 0*k*0, and 0*0l* only for even indices, which led to the space group D_2^4. With $(NH_4)_2$, the 0*k*0 reflections typically appeared only when k = 2n, and reflections of all other types appeared for any combination of indices, giving two possible space groups C_2^2 and C_{2h}^2. Since this crystal belonged to class C_2 [2], its space group is C_2^2.

The results of our determinations of unit cell constants, densities, and space groups are shown in Table 2. The x-ray results confirm that the (KLi) and (NH_4Li) crystals are isomorphous. The space groups of the crystals were determined without ambiguity. All the crystals belonged to groups in which piezoelectricity could arise. From the results on cell dimensions and densities, it follows that the first three compounds contain four formula units in the unit cell, and the last one has two. The space groups D_2^4 and C_2^2 have only one complex each, with a multiplicity corresponding to the number of particles found in the cells of the substance. Therefore, the (NaH) and $(NH_4)_2$ crystals contain only structurally equivalent tartrate ions. In the space group D_2^3, there are both two-fold and four-fold complexes. The characteristic symmetry of a two-fold complex particle is 2, that of a four-fold complex particle is 1. Thus, in the first two isomorphous crystals, models are also possible with structurally nonequivalent tartrate ions.

We would like to use this opportunity to thank V.A. Koptsik for the gift of crystals, and for discussing some of the results of the investigation.

LITERATURE CITED

1. V.A. Koptsik, Collection: First Conference on Crystal Chemistry [in Russian] (1954), p. 126; "A study of new piezoelectric crystals," Izv. AN SSSR, Ser. fiz., 20 (1956).
2. P. Groth, Chemische Kristallographie (Leipzig, 1910), Vol. 3, pp. 330, 331, 314, 323, 325.
3. Gmelins, Handbuch der anorganischen Chemie 22, 1084 (1938); 23, 467 (1936); 21, 854 (1928); 23, 408 (1936).
4. Sprenkels, Proc. Konin. nedel. Akad. Weten., 57, 524-528 (1954). See Ref. Zh. Khim., 18, 22 (1955).
5. M.M. Umanskii, Collection: Application of X Rays to the Study of Materials [in Russian] (1949), p. 401.
6. G.S. Zhdanov, ZhÉTF, 15, 703 (1945); G.S. Zhdanov and V.A. Pospelov, ZhÉTF, 15, 709 (1945).
7. M.M. Umanskii and S.S. Kvitka, "X-ray analysis of inorganic crystals," Izv. AN SSSR, Ser. fiz., 15, 147 (1951).

SOVIET PHYSICS – CRYSTALLOGRAPHY VOL. 1, NO. 3 MAY-JUNE, 1956

STUDY OF THE FORM OF POTENTIAL RELIEF FOR IONS IN CRYSTALS OF THE PEROVSKITE TYPE

L. N. Syrkin

Institute of Silicate Chemistry

Translated from Kristallografiya, Vol. 1, No. 3,
pp. 274-286, May-June, 1956
Original article submitted August 1, 1955

The coefficients of the potential-energy expansion of an ion in a crystal are calculated in terms of a small displacement on the basis of elementary laws of interaction. The form of the potential relief of the ion is studied for several crystals. The computing formulas obtained are applied to barium titanate.

Introduction

In order to explain the spontaneous polarization of ferroelectric crystals, existing molecular theories use either the model of local minima [1] or that of an anharmonic oscillator [2, 3].

In both cases, the theory clearly contains semiempirical elements in the form of various assumptions regarding the form of the potential relief for a ferroelectrically active ion.

It would seem appropriate, in constructing a molecular theory of ferroelectric and antiferroelectric phenomena, to start exclusively from the elementary laws of interaction, without introducing any additional assumptions on the form of the potential relief.[1] On certain simplifying assumptions, it is possible to establish the way in which the form of the potential relief depends on the atomic constants. Such an examination of the form of the potential relief in ferroelectric crystals is particularly useful in that, first, it can give new information on the structure and properties of the crystals and, second, it can improve the choice of model for each type of ferroelectric crystal.

In this paper we shall consider barium titanate crystals from this point of view. The method of calculation may, however, be applied to other crystals. We shall everywhere consider the crystal to be purely ionic, although a number of authors have expressed the view that the potential-energy minima arising at ions in a ferroelectric crystal are inevitably associated with a covalent character of the bond.

Furthermore, Devonshire [4] noted that there might be asymmetric equilibrium positions for the oxygen ion in barium titanate, even on the purely ionic model. It was shown that the titanium ion could not have such equilibrium positions. The corresponding calculations, however, were carried out in an insufficiently general form, and important aspects of the phenomenon were not considered. Hence, Devonshire's conclusions are also not fully reliable in this respect and require refinement.

We must also make a comment concerning the role of the internal field. Clearly, the internal field by itself cannot lead to the appearance of additional potential wells. On the contrary, if it is large enough, the number of potential minima may be reduced [2].

We shall consider an unpolarized crystal, since the effect of the internal field on the form of potential relief can, in principle, be taken into account. By the coordinates of the ions we shall everywhere understand their time-averaged values.

Expansion of the Potential Energy of an Ion in a Crystal with Respect to a Small Displacement, Without Allowing for the Polarizability of the Ions

We write the expression for the potential energy U' of an ion in a rigid lattice in the form

$$U'(x, y, z) = \sum_{i,k} U'_{ik}(x, y, z) -$$

[1] And also on internal fields.

$$= \sum_{i,k}{}' \left[\frac{q_0 q_{ik}}{r'_{ik}} + \lambda_k (r'_{ik})^{-n} - \mu_k (r'_{ik})^{-6} \right]. \quad (1)$$

All the ions are assumed to be unpolarized, and the indices i and k, respectively, indicate the number of the ion in the sublattice and the number of the sublattice. The summation extends over all surrounding ions. U'_{ik} is the interaction energy of the ion considered (which we shall subsequently call the central ion) with ion number ik; q_0 and q_{ik} are the charges of the central and ik-th ion; r'_{ik} is the corresponding distance between the ions; n, λ_k, μ_k are constants depending on the nature of the two interacting ions.

Expression (1) is approximate. For a more exact calculation, the power law for the forces of repulsion must first of all be replaced by an exponential; this is done, for example, in the paper by Born and Mayer [5].

We shall consider crystals with symmetry m · 2:m, i.e., having three mutually perpendicular symmetry planes, which we shall take as the coordinate planes. We shall choose the system of coordinates so that the origin coincides with the symmetry position of the central ion.

If we assume the possibility of a displacement of the central ion without displacements of the surrounding ions (this assumption is equivalent to neglecting correlation in the motion of neighboring ions), then

$$\vec{r}'_{ik} = \vec{r}_{ik} - \vec{r}, \quad (2)$$

where $\vec{r}_{ik} = \vec{r}_{ik}(x_{ik}, y_{ik}, z_{ik})$ is the radius vector of the ik-th surrounding ion in the undisplaced position, and $\vec{r} = \vec{r}(x, y, z)$ is the radius vector of the displaced central ion.

Let us expand the right-hand side of (1) in a Taylor series in the small quantities x, y, z, retaining terms up to the fourth order of smallness inclusive:

$$U'(x, y, z) = U(0, 0, 0) + \sum_{ik} \sum_{m=1}^{4} \frac{1}{m!} \left[x \frac{\partial}{\partial x} + y \frac{\partial}{\partial y} + z \frac{\partial}{\partial z} \right]^m U'_{ik}(0, 0, 0). \quad (3)$$

In view of the symmetry, (3) only contains derivatives constituting even functions of the operators $x(\partial/\partial x)$, $y(\partial/\partial y)$, $z(\partial/\partial z)$. Hence, the result of calculation from formulas (1) and (3) may be written

$$U'(x, y, z) = U(0, 0, 0) - \alpha'_1 x^2 - \alpha'_2 y^2 - \alpha'_3 z^2 + \beta'_1 x^4 + \beta'_2 y^4 + \beta'_3 z^4 + \ldots \gamma'_1 x^2 y^2 + \gamma'_2 x^2 z^2 + \gamma'_3 y^2 z^2, \quad (4)$$

where

$$\alpha'_1 = -\frac{1}{2} \sum_{ik} \frac{\partial^2}{\partial x^2} U'_{ik}(0, 0, 0),$$

$$\gamma'_1 = \frac{1}{4} \sum_{ik} \frac{\partial^4}{\partial y^2 \partial z^2} U'_{ik}(0, 0, 0),$$

$$\beta'_2 = \frac{1}{24} \sum_{ik} \frac{\partial^4}{\partial y^4} U'_{ik}(0, 0, 0). \quad (5)$$

Analogous expressions are obtained for the other coefficients.

Allowance for the Polarizability of the Ions

Formulas (1) and (3) are written on the assumption that all the ions retain spherical form, independently of the possible displacement of the central ion. In reality, however, the ions have finite polarizability, so that the central ion, on moving from the origin of coordinates (where the electric field is zero), acquires an electric moment $\vec{p}^{(1)}(x, y, z)$ under the influence of the field $\vec{E}_C = (x, y, z)$. Clearly, $\vec{p}^{(1)} = \alpha_0 \vec{E}_C$.

Let us find the additional "polarization" energy $U_p^{(1)}$ of an ion with polarizability α_0 when it suffers a small displacement. At first, the polarizability of the surrounding ions will be considered zero:

$$U_p^{(1)} = -(\vec{p}^{(1)}\vec{E}_C) + \int_0^{E_C} \vec{p} d\vec{E}_C = -\alpha_0 E_C^2 + \frac{1}{2}\alpha_0 E_C^2 = -\frac{1}{2}\alpha_0 E_C^2. \quad (6)$$

Here we have taken account of the energy of the induced dipole in the external field and its internal energy.[2]

The electric field of the surrounding ions acting on the central ion ($\vec{E}_C$), equals

$$\vec{E}_C = -\vec{\nabla}_{\vec{r}} = -\frac{1}{q_0} \vec{\nabla} U_C(x, y, z), \quad (7)$$

where

$$U_C = \sum_{ik} \frac{q_0 q_{ik}}{r'_{ik}} = \sum_{ik} U_{Cik}. \quad (8)$$

[2] Later calculations are effected on the Born point model.

The right-hand side of expression (8) may be expanded in terms of the small quantities x, y, z by means of a formula analogous to (3). This gives an expansion for the Coulomb energy U_C exactly analogous to that for the total energy U[1]:

$$U_C(x, y, z) = U_C(0, 0, 0) - A_1x^2 - A_2y^2 - A_3z^2 + B_1x^4 + B_2y^4 + B_3z^4 + C_1x^2y^2 + C_2x^2z^2 + C_3y^2z^2. \quad (9)$$

The coefficients A, B, C are calculated from formulas (5), where, instead of U^1_{lk} we must put U_{Clk}.

Combining (6), (7), and (9), we obtain

$$U_p^{(1)} = \frac{2\alpha_0}{q_0^3}[-(A_1^2x^2 + A_2^2y^2 + A_3^2z^2) + 4(A_1B_1x^4 + A_2B_2y^4 + A_3B_3z^4) + 2C_1(A_1 + A_2)x^2y^2 + 2C_2(A_1 + A_3)x^2z^2 + 2C_3(A_2 + A_3)y^2z^2]. \quad (10)$$

Summing the right-hand sides of (4) and (10), we obtain an expansion for the potential energy of the ion allowing for its polarizability:

$$U(x, y, z) = U(0, 0, 0) - \alpha_1x^2 - \alpha_2y^2 - \alpha_3z^2 + \beta_1x^4 + \beta_2y^4 + \beta_3z^4 + \gamma_1x^2y^2 + \gamma_2x^2z^2 + \gamma_3y^2z^2, \quad (11)$$

where the coefficients are calculated from the formulas

$$\alpha_1 = \alpha_1' + \frac{2\alpha_0}{q_0^3}A_1^2,$$

$$\beta_2 = \beta_2' + \frac{2\alpha_0}{q_0^3}A_1B_1,$$

$$\gamma_2 = \gamma_2' + \frac{4\alpha_0}{q_0^3}C_2(A_2 + A_3), \text{ etc.} \quad (12)$$

In a number of cases it is also necessary to allow for the polarizability α_k of the surrounding ions, since the corresponding contribution to the potential energy of the central ion may be of the same order as the quantity $U_p^{(1)}$ determined from (10).[3]

In order to find the dependence of the "polarization" energy on the interaction of surrounding ions, we must first of all calculate the electric field $\vec{E}^{(2)}_{lk}$, acting on the ik-th such ion. (Here we shall suppose that when the central ion moves, only the ions closest to it in each sublattice are polarized.)

$$\vec{E}^{(2)}_{lk} = \frac{3\vec{r}'_{lk}(\vec{p}^{(1)}\vec{r}'_{lk})}{(r'_{lk})^5} - \frac{\vec{p}^{(1)}}{(r'_{lk})^3} + \frac{q_0\vec{r}'_{lk}}{(r'_{lk})^3} - \frac{q_0\vec{R}_{lk}}{R^3_{lk}}. \quad (13)$$

In the absence of displacement of the central ion $r'_{lk} = r_{lk}$, $\vec{p}^{(1)} = 0$ and $\vec{E}^{(2)}_{lk} = 0$, and the action of the Coulomb field of the central ion is completely compensated by that of the ion disposed relative to the ik-th ion in a position symmetrical to that of the origin of coordinates [last term in formula (13)].

(The meaning of the vectors is illustrated in Fig. 1 for the particular case of a plane lattice.)

If, however, $r \neq 0$, the electric moments $\vec{p}^{(2)}_{lk}$, induced by the central ion at the surrounding ions will differ both in magnitude and direction. Hence, their reaction on the central ion will not be mutually compensated and there will be a "reactive" electric field acting on the central ion together with the field $\vec{E}_C$ [see (7)].

Clearly,

$$\vec{p}^{(2)}_{lk} = \alpha_k\vec{E}^{(2)}_{lk}. \quad (14)$$

Calculation of the reactive field $\vec{E}_r^{(2)}$, with due allowance for (13) and (14), gives

$$\vec{E}_r^{(2)} = \sum_{lk}\left[\frac{3(\vec{p}^{(2)}_{lk}\vec{r}'_{lk})\vec{r}'_{lk}}{(r'_{lk})^5} - \frac{\vec{p}^{(2)}_{lk}}{(r'_{lk})^3}\right] = \sum_{lk}\left\{\frac{\alpha_k}{(r'_{lk})^6}\left[\frac{3\alpha_0\vec{r}'_{lk}(\vec{r}'_{lk}\vec{E}_C)}{(r'_{lk})^3} + 2q_0\vec{r}'_{lk} + \alpha_0\vec{E}_C\right] - \frac{\alpha_k q_0}{(r'_{lk}R_{lk})^3}\left[\frac{3\vec{r}'_{lk}(\vec{r}'_{lk}\vec{R}_{lk})}{(r'_{lk})^5} - \vec{R}_{lk}\right]\right\}, \quad (15)$$

in which the summation is taken over the nearest surrounding ions.

Since the field acting on the central ion (in the approximation considered) equals $\vec{E}_C + \vec{E}_r^{(2)}$, we obtain the following expression for the polarization energy, allowing for the polarizability of the nearest ions, in analogy with (6):

$$U_p^{(2)} = -\frac{\alpha_0}{2}[\vec{E}_C + \vec{E}_r^{(2)}]^2. \quad (16)$$

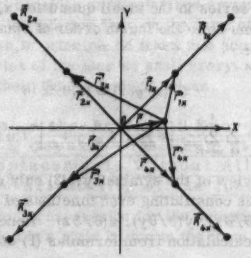

Fig. 1.

[3] This fact was not considered in Devonshire's paper.

Calculation of $U_p^{(2)}$ should be effected by expanding expression (15) into a Taylor series in x, y, z. In view of their complexity, we shall omit the expressions in question. In every case, an expansion analogous to (11) is obtained, the coefficients α, β, γ being known functions of the atomic constants.[4]

Study of the Nature of the Potential Relief of an Ion for a Small Displacement

We showed earlier how to calculate the coefficients α, β, γ in the expansion for the potential energy of an ion in terms of the small displacement $\vec{r}(x, y, z)$.

We must now study under what conditions minima may exist in the potential relief of the ion.

Since expansion (11) is formally similar to the well-known expansion of the thermodynamic potential with respect to the polarization-vector components, we may use the method employed by Ginzburg [2] in thermodynamic theory and generalized by Shirobokov and Kholodenko [6, 7]. Without describing the calculation in detail, we shall present the main results.

The coordinates of the extremal values of potential energy are found from a number of solutions of the system of equations

$$\frac{\partial U}{\partial x} = \frac{\partial U}{\partial y} = \frac{\partial U}{\partial z} = 0, \tag{17}$$

where U(x, y, z) is determined from (11).

System (17) has 27 solutions, which may be divided into four groups:

$$1.)\quad x = \pm\sqrt{\frac{\Delta_x}{\Delta}},\quad y = \pm\sqrt{\frac{\Delta_y}{\Delta}},\quad z = \pm\sqrt{\frac{\Delta_z}{\Delta}}. \tag{18}$$

Here, Δ, Δ_x, Δ_y, Δ_z are the principal and complementary determinants of system (17). The group contains eight solutions:

$$2.)\quad x = 0,\ y = \pm\sqrt{\frac{2\alpha_2\beta_3 - \alpha_3\gamma_3}{4\beta_2\beta_3 - \gamma_3^2}},\quad z = \pm\sqrt{\frac{2\alpha_3\beta_2 - \alpha_2\gamma_3}{4\beta_2\beta_3 - \gamma_3^2}}. \tag{19}$$

Another eight solutions of this group are obtained from (19) by cyclical substitution of the unknowns and the indices on the coefficients. Generally speaking, the twelve solutions of this group are not equivalent.

$$3.)\quad x = y = 0,\quad z = \pm\sqrt{\frac{\alpha_3}{2\beta_3}}. \tag{20}$$

The remaining four solutions of this group are obtained by cyclical substitution from (20):

$$4.)\quad x = y = z = 0. \tag{21}$$

Let us analyze solutions (18)-(21) for two particular cases.

A. Let the coefficients of expansion (11) be connected by the relations

$$\alpha_1 = \alpha_2 = \alpha_3 = \alpha,\ \beta_1 = \beta_2 = \beta_3 = \beta,\ \gamma_1 = \gamma_2 = \gamma_3 = \gamma. \tag{22}$$

This case obtains for the Ti^{++++} and Ba^{++} ions in a $BaTiO_3$ crystal and for analogously situated ions in other crystals of the perovskite type. The solutions of system (17) can be simplified and, instead of (18)-(21), we have, respectively,

$$|x| = |y| = |z| = \sqrt{\frac{\alpha}{2(\beta+\gamma)}}\ \text{(8 solutions)}, \tag{23}$$

$$x = 0,\ |y| = |z| = \sqrt{\frac{\alpha}{2\beta+\gamma}} \tag{24}$$

(12 solutions allowing for cyclical substitution of x, y, z)

$$x = y = 0,\ z = \pm\sqrt{\frac{\alpha}{2\beta}},\ \text{etc., (6 solutions)}, \tag{25}$$

$$x = y = z = 0. \tag{26}$$

If we examine solutions (23)-(26) for stability by the usual methods, we find the following necessary and sufficient conditions for a minimum (the requirement that the solutions be real, also being satisfied).

1. If $\alpha < 0$, there is only one minimal solution of (26), independent of the quantities β and γ.

2. Solutions (23) and (25) can only give a potential-energy minimum on satisfying the conditions $\alpha > 0, \beta > 0$, and also the following additional limitations:

$$-\beta < \gamma < 2\beta \tag{27}$$

[condition for the solution of (23) to be minimal], or

$$\gamma > 2\beta \tag{28}$$

[condition for the solution of (25) to be minimal].

[4] The polarization energy is calculated by successive approximations, up to second-approximation accuracy.

3. Solution (24) gives no potential-energy minimum for any values of α, β, γ [unless the sixth powers are taken into account in the expansion of formula (11)].

For clarity we may present the results in the form of a graph in the plane of coefficients β, γ (Fig. 1).

B. The coefficients of expansion (11) are connected by the relations

$$\begin{aligned} &\alpha_1 = \alpha_2 = \alpha, \quad \alpha_3 \neq \alpha; \\ &\beta_1 = \beta_2 = \beta, \quad \beta_3 \neq \beta; \\ &\gamma_1 = \gamma, \quad \gamma_2 = \gamma_3 \neq \gamma. \end{aligned} \tag{29}$$

Relations (29) hold for the oxygen ions in the perovskite structure. Here, the solutions of system (17) take the form

$$1)\ |x| = |y| = \sqrt{\frac{2\alpha\beta_3 - \alpha_3\gamma_3}{2(2\beta\beta_3 + \beta_3\gamma - \gamma_3^2)}},$$

$$|z| = \sqrt{\frac{\alpha_3(2\beta+\gamma) - 2\alpha\gamma_3}{2\beta_1(2\beta+\gamma) - 2\gamma_1^2}}; \tag{30}$$

$$2)\ x = 0,\ y = \pm\sqrt{\frac{2\alpha\beta_3 - \alpha_3\gamma_3}{4\beta\beta_3 - \gamma_3^2}},$$

$$z = \pm\sqrt{\frac{2\alpha_3\beta - \alpha\gamma_3}{4\beta\beta_3 - \gamma_3^2}}; \tag{31}$$

$$y = 0,\ x = \pm\sqrt{\frac{2\alpha\beta_3 - \alpha_3\gamma_3}{4\beta\beta_3 - \gamma_3^2}},\quad z = \pm\sqrt{\frac{2\alpha_3\beta - \alpha\gamma_3}{4\beta\beta_3 - \gamma_3^2}}; \tag{32}$$

$$z = 0,\ |x| = |y| = \sqrt{\frac{\alpha}{2\beta+\gamma}}; \tag{33}$$

$$3)\ x = y = 0,\ z = \pm\sqrt{\frac{\alpha_3}{2\beta_3}}; \tag{34}$$

$$y = z = 0,\ x = \pm\sqrt{\frac{\alpha}{2\beta}}; \tag{35}$$

$$x = z = 0,\ y = \pm\sqrt{\frac{\alpha}{2\beta}}; \tag{36}$$

$$4)\ x = y = z = 0. \tag{37}$$

In the same way as in case A, we can obtain the conditions for the solutions of (30-(37) to be real and minimal.

1. The null solution (37) only gives a minimum for $\alpha < 0$, $\alpha_3 < 0$.

2. All solutions for which $z \neq 0$ (i.e., 30, 31, 32, 34) give minima if $\alpha_3 > 0, \beta_3 > 0$.

3. The solutions (apart from 37) for which $z = 0$ give minima if $\alpha > 0$, $\beta > 0$.

Apart from this, there are the following additional limitations imposed on the coefficients by the condition that solutions (30)-(36) should be real and minimal: for solution (30) ($z \neq 0$),

$$-2\beta < \gamma < 2\beta,\ \alpha > \frac{\alpha_3\gamma}{2\beta_3},\ \alpha_3 > \frac{2\alpha\gamma}{2\beta+\gamma}; \tag{38}$$

for solutions (31) and (32) ($z \neq 0$),

$$\gamma > 2\beta,\ \alpha > \frac{\alpha_3\gamma_3}{2\beta_3},\ \alpha_3 > \frac{\alpha\gamma_3}{2\beta}; \tag{39}$$

for solutions (33) ($z = 0$),

$$-2\beta < \gamma < 2\beta,\ \alpha_3 < \frac{2\alpha\gamma_3}{2\beta+\gamma}; \tag{40}$$

for solutions (35) and (36) ($z = 0$),

$$\gamma > 2\beta,\ \alpha_3 < \frac{\alpha\gamma_3}{2\beta}; \tag{41}$$

for solutions (34) ($z \neq 0$),

$$\alpha < \frac{\alpha_3\gamma_3}{2\beta_3}. \tag{42}$$

The smallest limitation on the coefficients is imposed by the minimum condition of solution (37), which corresponds to the symmetrical disposition of the ion in the origin of coordinates ($x = y = z = 0$). This case is apparently most frequently realized in crystals. We also find a comparatively small number of limitations for the coefficients in the minimum condition for solution (34), when the potential-energy minima are disposed on the principal axis of symmetry (z axis). The potential energy U_{min} at the bottom of the potential well here equals

$$U_{\min} = U(0,0,0) - \frac{\alpha_3^2}{4\beta_3}. \tag{43}$$

It is plain that, independently of the type of symmetry, for no values of coefficients α, β, γ can we simultaneously have solutions belonging to different groups. This fact is especially obvious for case A, as illustrated in Fig. 2, where region I stands for solution (25), region II for solution (23), and region III for solution (26).

The similarity between some of the results obtained and those of Shirobokov and Kholodenko [6,7] is purely formal, since there is no one-to-one correspondence between the coefficients of the series expansions for the thermodynamic potential and the potential energy. Hence, the fact that one or another of the solutions in question may exist for a given crystal does not provide us with direct conclusions on the nature of phase transformations.

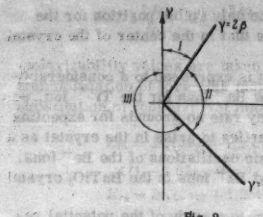

Fig. 2.

It follows from the discussion of this section that the potential relief for the ion has different forms according to the relation between the coefficients, the value of which is ultimately determined by the atomic constants. As a particular case, we have both the model of the anharmonic oscillator (for $\alpha < 0$) and that of local minima (solution 25 with the additional condition $\alpha^2 \ll 4\beta$). A number of intermediate cases may also be established.

In order to draw specific conclusions for each sort of ion we must calculate the corresponding coefficients of the expansion.

Some Numerical Results

Let us turn to a study of the potential relief for the Ti^{++++}, Ba^{++}, and O^{--} ions in the $BaTiO_3$ crystal. We shall use the values of force constants given in [4] for the potential-energy expression (1).

It is easy to see that the values of all the derivatives entering into coefficients α, β, γ in accordance with (5) may be expressed in terms of the coordinates of the surrounding ions x_{1k}, y_{1k}, z_{1k}. The corresponding formulas will not be shown. These can easily be obtained by differentiating the expression for $U_{1k}(x, y, z)$ with respect to x, y, z, afterwards setting $x = y = z = 0$.

In order to calculate the coefficients α', β', γ', and also A, B, C, we must carry out a summation of the (5) type. Then coefficients α, β, γ are determined by means of formulas (12) or (15) and (16).

We shall show first of all that the coefficient $A = 0$ for the Ti^{++++} and Ba^{++} ions; this corresponds to setting the elastic component of the electric forces for small displacements of Ti^{++++} and Ba^{++} equal to zero (similarly for analogously situated ions in other crystals of the perovskite type).

It is clear that the expression $\frac{\partial^2}{\partial x^2}[(r'_{ik})^{-1}]_{x=y=z=0}$, summed over all ions of the k sublattice for a central ion belonging to the l sublattice, constitutes the structure coefficient of the internal field first introduced by Skanavi

$$\sum_i (r_{ik})^{-3}(2x_{ik}^2 - y_{ik}^2 - z_{ik}^2) = Q_k^l,$$

where, in the case of barium titanate, k and l take values from 1 to 5, corresponding to the barium sublattice, three oxygen sublattices, and a titanium sublattice. As shown by Kozlovskii [9], all the quantities Q_k^l may in this case be expressed in terms of two new coefficients Q_1 and Q_2, the following relationships being valid:

$$\begin{aligned} &Q_k^l = Q_k^k, \quad Q_k^k = 0. \\ &Q_1^2 = Q_1, \quad Q_2^3 = Q_1, \quad Q_4^4 = -2Q_1, \quad Q_5^5 = 0, \\ &Q_3^2 = -2Q_1, \quad Q_4^3 = Q_1, \quad Q_4^5 = Q_1, \quad Q_5^4 = Q_2, \\ &Q_5^3 = Q_2, \quad Q_5^4 = -2Q_2. \end{aligned} \tag{44}$$

In Kozlovskii's paper, Q_1 and Q_2 were calculated with insufficient accuracy; more accurate results were given by Slater [3]. By using these we may write

$$Q_1 = \frac{4.334}{(2a)^3}, \quad Q_2 = -\frac{15.040}{(2a)^3}, \tag{45}$$

where $a = 2$Å (half the lattice constant).

It is not hard to see that coefficient A is directly calculated in terms of Q_1 and Q_2.

For the Ti^{++++} ion, we have

$$A_1 = A_2 = A_3 = A = -\frac{1}{2} q_{Ti} \sum_{k=1}^{5} q_k Q_k^5 = 0. \tag{46}$$

For the Ba^{++} ion,

$$A_1 = A_2 = A_3 = A = -\frac{1}{2} q_{Ba} \sum_{k=1}^{5} q_k Q_k^1 = 0. \tag{47}$$

For the O^{--} ion, considering that the Ti^{++++} ions are disposed in the direction of the z axis, we obtain

$$\begin{aligned} A_1 = A_2 = A &= -\frac{1}{2} q_O \sum_{k=1}^{5} q_k Q_k^5 \\ &= 4\varepsilon_0^2 (Q_1 + Q_2) = -5.35 \varepsilon_0^2 a^{-3}, \\ A_3 = -\frac{1}{2} q_O \sum_{k=1}^{5} q_k Q_k^4 &= -8\varepsilon_0^2 (Q_1 + Q_2) = 10.70 \varepsilon_0^2 a^{-3}, \end{aligned} \tag{48}$$

where

$$\varepsilon_0 = 4.8 \cdot 10^{-10} CGSE.$$

Thus, for small displacements of the Ti^{++++} and Ba^{++} ions, elastic forces only appear as a result of the repulsion of the electron shells (and Van der Waals interaction). It follows that the polarization

energy $U_p^{(1)}$ also vanishes [from (10) with A = 0]. Allowing for the polarizability of the surrounding ions produces nothing new. Carrying out the calculation by means of (15), and remembering that A = 0, we obtain

$$E_{rx}^{(2)} = Px^3 - Qx(y^2 + z^2), \tag{49}$$

where P and Q depend on the charges and polarizabilities of the ions.

Analogous formulas are obtained for $E_{ry}^{(2)}$ and $E_{rz}^{(2)}$ also.

Putting (49) into (16), and noting that $E_C = 0$, we obtain $U_p^{(2)} = 0$ up to an accuracy of terms containing sixth powers of x, y, z.

Calculation of the remaining expansion coefficients leads to the following results (all quantities expressed in cgs units):

$$\alpha_{Tl} = -5.1 \cdot 10^8, \quad \beta_{Tl} = 5.8 \cdot 10^{21}, \quad \gamma_{Tl} = -10.4 \cdot 10^{21},$$

$$\alpha_{Ba} = -1.3 \cdot 10^8, \quad \beta_{Ba} = 0.61 \cdot 10^{21}, \quad \gamma_{Ba} = 2.2 \cdot 10^{21}.$$

Hence,

$$U_{Tl} = U_{Tl}(0, 0, 0) + 5.1 \cdot 10^8 r^2 - 5.8 \cdot 10^{21} r^4 + 2.2 \cdot 10^{22}(x^2y^2 + x^2z^2 + y^2z^2), \tag{50}$$

$$U_{Ba} = U_{Ba}(0, 0, 0) + 1.3 \cdot 10^8 r^2 + 0.61 \cdot 10^{21} r^4 - 0.2 \cdot 10^{22}(x^2y^2 + x^2z^2 + y^2z^2), \tag{51}$$

where

$$r^2 = x^2 + y^2 + z^2.$$

In view of the approximate nature of the calculation, the numerical results obtained are on the whole of a qualitative character.

We see from (50) and (51) that the potential relief for the Ti^{++++} and Ba^{++} ions does not possess spherical symmetry (this was not allowed for in Devonshire's paper [4]).

Let us examine the potential relief from the point of view of the possible existence of minima for the displaced ion. According to the conclusions reached above, such minima cannot exist for Ti^{++++} or Ba^{++}, since the corresponding elastic coefficients are greater than zero ($\alpha < 0$).

For the Ti^{++++} ions, there are eight symmetrically disposed potential-energy maxima (on the diagonals of a cube). Calculation by formula (23) gives

$$x_0 = y_0 = z_0 = \sqrt{\frac{\alpha}{2(\beta + \gamma)}} \approx 0.7\text{Å}. \tag{52}$$

It is clear that such a large displacement of the ion from its equilibrium position can only ensue on melting. Hence, the only stable position for the Ti^{++++} or Ba^{++} ion is that in the center of the crystal cell.

Anharmonicity is expressed to a considerably lower extent for the Ba^{++} than for the Ti^{++++} ion, so that there are at any rate no grounds for expecting ferroelectric properties to arise in the crystal as a result of anharmonic oscillations of the Ba^{++} ions. The positions of the Ba^{++} ions in the $BaTiO_3$ crystal are most stable.

Let us now turn to a study of the potential relief for the O^{--} ions. In this case, a substantial part is played by the polarization energy. Calculation of coefficients B and C gives

$$B_1 = B_2 = B = -4.94 z_0^2 a^{-3},$$
$$B_3 = -19.4 z_0^2 a^{-5},$$
$$C_1 = C_2 = C = -28.3 z_0^2 a^{-3},$$
$$C_3 = 59.1 z_0^2 a^{-5} \tag{53}$$

(in the summation the fourteen closest surrounding ions were considered).

If, like Devonshire, we neglect the polarizability of the surrounding ions when calculating the polarization energy, i.e., use formula (10), assuming $\alpha_O = 2.4 \cdot 10^{-24}$ cm^3 for oxygen, we obtain from (12)

$$\alpha_1 = \alpha_2 = \alpha = -1.64 \cdot 10^8 < 0, \quad \alpha_3 \approx 0. \tag{54}$$

From this we may deduce, with Devonshire [4], that the existence of potential minima for the oxygen ion outside the center of the cell is doubtful (it follows from 54 that if such minima exist they must be situated in pairs in the direction of the axis joining the O^{--} ion with the nearest Ti^{++++} ions). If, however, we consider the finite polarizability of the surrounding ions, the result becomes more definite.

Calculating the reactive field by formula (15), allowing for the polarizability of the fourteen closest surrounding ions, we obtain

$$E_{rx}^{(2)} \approx (2\alpha_{Ti} + 1.25\alpha_{Ba} + 1.75\alpha_O)(\alpha_O E_{Cx} + q_O x). \tag{55}$$

$$E_{ry}^{(2)} \approx (2\alpha_{Ti} + 1.25\alpha_{Ba} + 1.75\alpha_O)(\alpha_O E_{Cy} + q_O y). \tag{56}$$

$$E_{rz}^{(2)} \approx (8\alpha_{Ti} + 0.5\alpha_{Ba} + 2.5\alpha_O)(\alpha_O E_{Cz} + q_O z). \tag{57}$$

In order to calculate the correction to the coefficient α, it is clearly sufficient in $E_{rx}^{(2)}$, $E_{ry}^{(2)}$, $E_{rz}^{(2)}$ to consider only terms linear with respect to x, y, and z.

If we consider that $\alpha_O = 2.4 \cdot 10^{-24}$ cm^3; $\alpha_{Ba} = 1.7 \cdot 10^{-24}$ cm^3; $\alpha_{Ti} = 0.27 \cdot 10^{-24}$ cm^3, and

$$F_{Cx} \approx \frac{2Ax}{q_O}, \quad E_{Cy} \approx \frac{2Ay}{q_O}, \quad E_{Cz} = \frac{2Az}{q_O} \qquad (58)$$

(polarizability values are taken for free ions), then transformation of formulas (55), (56), and (57), and substitution of (58) and (48) into these gives

$$E_{rx} = 2z_0(2\alpha_{Ti} + 1.25\alpha_{Ba} + 1.75\alpha_O) \times (1 - 2.67\alpha_O a^{-3}) a^{-6} x + O(x^3), \qquad (59)$$

$$E_{ry} = 2z_0(2\alpha_{Ti} + 1.25\alpha_{Ba} + 1.75\alpha_O) \times (1 - 2.67\alpha_O a^{-3}) a^{-6} y + O(y^3), \qquad (60)$$

$$E_{rz} = 2z_0(8\alpha_{Ti} + 0.5\alpha_{Ba} + 2.5\alpha_O) \times (1 + 5.35\alpha_O a^{-3}) a^{-6} z + O(z^3). \qquad (61)$$

We thus see that the reactive field is only substantial for displacement of the central ion along the z axis ($E_{rx} = E_{ry} \ll E_{rz}$). Hence, allowance for the polarizability of the surrounding ions only gives an essentially new result (as compared with Devonshire's data) for the coefficient α_3 in the potential-energy expansion, i.e., α_3 is certainly greater than zero. As regards the coefficient α, for this we only obtain a negligible correction (this is confirmed by numerical calculation).

Let us give the final formula for the coefficient α_3:

$$\alpha_3 = 2\alpha_O z_0^2 a^{-8} [(8\alpha_{Ti} + 0.5\alpha_{Ba} + 2.5\alpha_O)(1 + 5.35\alpha_O a^{-3}) a^{-3} + 5.35]^2 + 10.7 z_0^2 a^{-3} + 3a^{-8}(7\mu_{OT} + 1.5\mu_{OO} - 0.25\mu_{OB}) - a^{-11}(90\lambda_{OT} - 0.4\lambda_{OB} + 3.6\lambda_{OO}). \qquad (62)$$

Computing formulas have also been obtained for the other coefficients. (In calculating coefficients β and γ, we took no account of the polarizability of the surrounding ions.)

The result of the calculation gives $\alpha_3 = 2 \cdot 10^5$ erg $\cdot$ cm^{-2}.

The potential-energy expansion of the oxygen ion in $BaTiO_3$ with respect to a small displacement has the form

$$U_O = U_O(0,0,0) + 1.64 \cdot 10^5 (x^2 + y^2) - 2 \cdot 10^{12} z^2 + 2.1 \cdot 10^{21} (x^4 + y^4) + 9 \cdot 10^{21} z^4 + 10^{22} x^2 y^2 - 0.52 \cdot 10^{22} z^2 (x^2 + y^2). \qquad (63)$$

Thus, for the oxygen ion, the deviation of the potential relief from spherical symmetry is considerably greater than for the Ti and Ba ions.

Study of the potential relief by the method here set out shows that there are only two potential

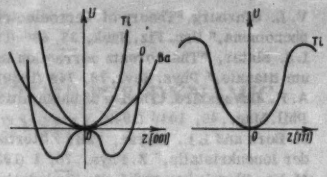

Fig. 3.

minima situated on the z axis symmetrically with respect to the origin of coordinates:

$$z_0 = \pm \sqrt{\frac{\alpha_3}{2\beta_3}} = 0.33\text{Å}.^{5}$$

The depth of the potential wells U_0 is 0.5 eV, i.e.,

$$U_0 \sim kT.$$

Of course, the approximate nature of the calculation means that the values of z_0 and U_0 obtained will not be very reliable, especially in the case of U_0, which depends strongly on α_3 and β_3. The qualitative nature of the result, however, is quite definite.

Figure 3 contains curves giving a schematic picture of the potential energy in the [001] direction for Ti, Ba, and O ions and in the [111] direction for Ti.

From the calculations of this paper we may conclude that, even for a purely ionic bond, the crystal may contain stable positions of equilibrium corresponding to electrical asymmetry in the disposition of the ions. For this, however, special conditions must be satisfied. Covalent bonds superposed on ionic bonds change the character of the spontaneous polarization of a ferroelectric. As regards the Ti and Ba ions, on the purely ionic model their positions in the centers of the unit cells are stable (especially so for the Ba ion). Covalent forces, however, may lead to a displacement of the Ti ion.

The method set out in this paper may be applied to other ferroelectric crystals as well.

I consider it my pleasant duty to thank Doctor of Physicomathematical Science G.A. Smolenskii for valuable comments and interest in this work.

LITERATURE CITED

1. W. P. Mason and B. T. Matthias, "Theoretical model for explaining the ferroelectric effect in barium titanate," Phys. Rev., 74, 1662 (1948).

[5] It is known from experimental data that the displacement of the oxygen ion in $BaTiO_3$ is around 0.12 A.

2. V. L. Ginzburg, "Theory of ferroelectric phenomena," Usp. Fiz. Nauk, 38, 490 (1949).
3. I. S. Slater, "The Lorentz correction in barium titanate," Phys. Rev., 78, 748 (1950).
4. A. F. Devonshire, "Theory of barium titanate," Phil. Mag., 40, 1040 (1949).
5. M. Born and I. E. Mayer, "Zur Zittertheorie der Ionenkristalle," Z. Phys., 75, 1 (1932).
6. M. Ya. Shirobokov and L. P. Kholodenko, "Thermodynamic theory of ferroelectric phenomena in crystals of the barium titanate type," ZhÉTF, 21, 1239 (1951).
7. L. P. Kholodenko and M. Ya. Shirobokov, "Ferroelectric properties of $BaTiO_3$ crystals near the Curie point in the presence of elastic stresses," ZhÉTF, 21, 1250 (1951).
8. G. I. Skanavi, "High dielectric constant of certain crystals," ZhÉTF, 17, 399 (1947).
9. V. Kh. Kozlovskii, "Effective fields in barium titanate," ZhÉTF, 21, 1388 (1951).

SOVIET PHYSICS – CRYSTALLOGRAPHY VOL. 1, NO. 3 MAY-JUNE, 1956

GEOMETRY OF THE DIFFRACTION PICTURE FOR DYNAMIC INTERACTION OF X RAYS WITH A CRYSTAL

I. V. Yavorskii

Lensovet Technological Institute, Leningrad

Translated from Kristallografiya, Vol. 1, No. 3,
pp. 287-290, May-June, 1956
Original article submitted December 31, 1955

The method of solving crystal-diffraction pictures by means of the reciprocal lattice is generally accepted. It is hard to overestimate the value of this extremely convenient method, which makes it possible to represent the field of the chief diffraction maxima clearly and without cumbersome calculations.

It should be noted, however, that in a number of cases the interaction of certain radiations with the crystal leads to the formation of a more complicated picture, the treatment of which causes some trouble. This note relates to the appearance of the so-called superfluous or forbidden maxima.

Without claiming a complete solution of the problem, we may indicate one of the possible reasons underlying such maxima.

It is well known that the use of the reciprocal lattice in solving diffraction problems was brought about by a neat geometrical interpretation of the Wulff–Bragg relation written in vector form [1]:

$$\vec{G}_{h_1h_2h_3} = \frac{\vec{\sigma}_{h_1h_2h_3} - \vec{\sigma}_0}{\lambda}, \qquad (1)$$

where $\vec{G}_{h_1h_2h_3} = h_1\vec{a}_1^* + h_2\vec{a}_2^* + h_3\vec{a}_3^*$ is a reciprocal-lattice vector, σ_0 and $\vec{\sigma}_{h_1h_2h_3}$ are unit vectors of the primary and diffracted waves, λ is the wavelength of the radiation, and $h_1h_2h_3$ are diffraction indices.

The derivation of this relation is based on the kinematical theory of interference; hence, dynamic-interaction effects were not considered in deducing it. One of these effects, the interaction of the diffracted beam with the crystal, was observed by Renninger in studying the diffraction picture of diamond [2].

We shall have to revise the image of the reciprocal lattice by indicating the rules for finding the directions of maxima produced by multiple "reflections," and also consider the question of the unequivocal determination of the x-ray group when such maxima appear on the x-ray diffraction picture.

Let us suppose that condition (1) is satisfied with respect to the 200 maximum (Fig. 1). By construction, the zero of the reciprocal lattice is situated on the direction of the primary beam $\vec{\sigma}_0$ (point 000). The sphere M of radius $2/\lambda$ limits the field of the diffraction maxima.

For a diffracted wave, if we wish to consider possible secondary maxima, the zero of the reciprocal lattice should also be placed on its direction of propagation. Hence, the lattice point 200 transforms into the zero point $(000)_1$. Hence we have to visualize two mutually displaced reciprocal lattices, one (the fundamental) for the primary beam $(\vec{\sigma}_0)$, and the other (auxiliary) for the diffracted beam $\vec{\sigma}_{200} = \vec{\sigma}'_0$. The value of the displacement equals the length of the vector $\vec{G}_{200}$.

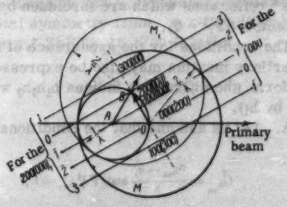

Fig. 1. M and M_1 are the fundamental and auxiliary bounding spheres. The planes $\bar{1}$, 0, $\bar{1}$, $\bar{2}$, $\bar{3}$ of the fundamental lattice coincide with the planes 3, 2, 1, 0, $\bar{1}$ of the auxiliary lattice. The primary maximum 200 is the base for the secondary maxima.

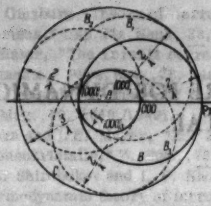

Fig. 2. B is the bounding sphere for the fundamental reciprocal lattice. $B_1B_2B_3$ are some of the positions of shifted bounding spheres for auxiliary reciprocal lattices.

From the auxiliary zero (the 200 point) we describe a sphere of radius $2/\lambda$. We draw an auxiliary reciprocal lattice inside this new bounding sphere M_1 according to the general rules. If any point of the auxiliary lattice touches the interference sphere, a secondary wave will be propagated from the center A to the point. Thus, the interference sphere remains in place; the rotated bounding sphere, however, takes the auxiliary reciprocal lattice with it.

If N is the number of primary diffraction maxima occurring for a given photographic technique, then the number of auxiliary reciprocal lattices will also equal N. A sphere C of radius $3/\lambda$ with center at A limits the space occupied by the displaced auxiliary lattices (Fig. 2). Does this give rise to "superfluous" maxima? Since the auxiliary lattices are obtained from the fundamental by parallel displacement, different planes of the two lattices coincide with each other (Fig. 1).

If this coincidence makes the lattices indistinguishable, no new maxima will arise; otherwise, intermediate points will occur, and if these touch the interference sphere they will produce "superfluous" reflections which are forbidden by the structure factor ($|F|^2 = 0$).

The conditions for the appearance of secondary and tertiary maxima may also be expressed in analytic form (the diffraction indices $h_1h_2h_3$ will be denoted by h_l).

A. Let us assume that the conditions

$$\vec{G}_{h_m} = \frac{\vec{\sigma}_{h_m} - \vec{\sigma}_0}{\lambda} \text{ and } |F|^2_{h_m} \neq 0, \tag{2}$$

$$\vec{G}_{h_n} = \frac{\vec{\sigma}_{h_n} - \vec{\sigma}_0}{\lambda}, \text{ but } |F|^2_{h_n} = 0 \tag{3}$$

are satisfied.

Determining $\vec{\sigma}_0$ from (2) and substituting into (3), we get

$$\vec{G}_{h_n} - \vec{G}_{h_m} = \vec{G}_{h_n - h_m} = \frac{\vec{\sigma}_{h_n} - \vec{\sigma}_{h_m}}{\lambda} = \frac{\vec{\sigma}_{h_n} - \vec{\sigma}_0}{\lambda}. \tag{4}$$

Thus a secondary wave may propagate along the direction of the forbidden maximum $\vec{\sigma}_{h_n}$ on satisfying the following conditions ("indirect excitation").

1. The primary maximum $\vec{\sigma}_{h_m}$ plays the part of the "primary" beam ($\vec{\sigma}_0$).

2. Reciprocal-lattice points h_m and h_n simultaneously ("coincidence!") touch the interference sphere.

3. Vector $\vec{G}_{h_n - h_m}$ of the auxiliary reciprocal lattice equals vector $\vec{G}_{h_k}$ of the fundamental reciprocal lattice and $|F|^2_{h_k} \neq 0$ (Fig. 3).[1]

B. If the auxiliary reciprocal-lattice vector $\vec{G}_{h_n - h_m} = \vec{G}_{h_k}$, but $|F|^2_{h_k} = 0$, then a tertiary wave may propagate in the direction $\vec{\sigma}_{h_e}$ on satisfying the conditions of "secondary indirect excitation" (Fig. 4).

1. There is a secondary maximum $\vec{\sigma}_{h_e}$ ($\vec{G}_{h_e - h_m} = \frac{\vec{\sigma}_{h_e} - \vec{\sigma}_{h_m}}{\lambda}$ and $|F|^2_{h_e - h_m} \neq 0$, which plays the part of a "primary" beam ($\vec{\sigma}_0$);

2. Reciprocal-lattice points h_n, h_m, and h_e simultaneously touch the interference sphere.

3. The relation

$$\vec{G}_{h_n - h_m} - \vec{G}_{h_e - h_m} = \vec{G}_{h_n - h_e} = \frac{\vec{\sigma}_{h_n} - \vec{\sigma}_{h_e}}{\lambda} = \frac{\vec{\sigma}_{h_n} - \vec{\sigma}_0}{\lambda}. \tag{5}$$

is satisfied.

4. The vector $\vec{G}_{h_n - h_e}$ of the auxiliary reciprocal lattice equals the vector $\vec{G}_{h_p}$ of the fundamental reciprocal lattice and $|F|^2_{h_p} \neq 0$.

Clearly, (1), (4), and (5) are the Wulff–Bragg relations for the primary, secondary, and tertiary maxima. The intensity of such maxima is usually low. If, however, a reciprocal-lattice point with zero "weight" ($|F|^2 = 0$) is situated on the interference sphere for the whole time that the x-ray photograph is being taken ("equal–opposite"-slope method), the intensity of the forbidden maximum may become substantial. Then a decision as to whether the crystal belongs to one x-ray group or another,

[1] Only the interference sphere is shown in Figs. 3 and 4.

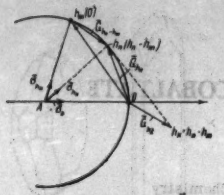

Fig. 3. Forbidden maximum σ_{h_n} realized as a secondary maximum.

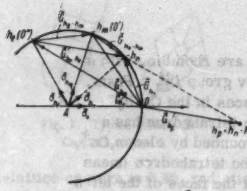

Fig. 4. Forbidden maximum σ_{h_n} realized as a tertiary maximum.

made on the basis of the diffraction picture [3], is subject to doubt.

Out of the 120 x-ray groups, extinctions of the general type (hkl) are absent from 77. In the most unfavorable case, these 77 groups may be reduced to 11 (corresponding to the number of Laue classes). The proof of this is based on the fact that, if primary diffraction maxima with any group of three indices hkl are possible, then "forbidden" primary maxima of the hk0, h0l, 0kl, hh$l$, etc., type may be realized as secondary maxima.

Let us take a specific example.

In the x-ray group mmm Pnnn, primary maxima 0kl, h0l, and hk0 for which the sum of the indices $k + l$, $h + l$, $h + k$ is odd, are absent.

Let us take the indices 021, 201, and 210. If maxima with indices 111, 312, and 121 are taken as "primary" beams, then secondary beams

$$\bar{1}10\,(0-1,\ 2-1,\ 1-1),\ \bar{1}\bar{1}1\,(2-3,\ 0-1,\ 1-2),$$

$$111\,(2-1,\ 1-2,\ 0-1)$$

will propagate in the direction 021, 201, and 210.

Similar differences may be set up for any other group of three indices characterizing forbidden primary maxima. Hence, in the limiting case, in all these 77 x-ray groups the reciprocal lattice is transformed into primitive form. In the remaining 43 x-ray groups there are extinctions of a general type. Corresponding analysis shows that in the limit these groups may be reduced to 12. Thus, under the most unfavorable conditions, the 120 x-ray groups are converted into 23 groups. In practice, of course, not all the secondary maxima will be recorded on the x-ray photograph.

The extinction conditions for many x-ray groups, however, differ very little, so that if even one or two "superfluous" reflections appear on the photograph and are taken for primary maxima, the interpretation of the diffraction picture will be faulty. For example, x-ray groups with the following numbers may not be distinguished [1]: 6-7, 9-10, 11-12, 30-31, 39-40, 42-43, etc.

It must also be noted that the probability of secondary maxima appearing on the x-ray diffraction photograph increases on reducing the wavelength of the radiation used, owing to the rise in the number of reciprocal-lattice points simultaneously touching the interference sphere.

LITERATURE CITED

1. A.I. Kitaigorodskii, X-Ray Structural Analysis [in Russian] (Moscow-Leningrad, 1950).
2. R. James, Optical Principles of X-Ray Diffraction [Russian translation] (IL, 1950).
3. G.S. Zhdanov and V. Pospelov, "Determining crystal symmetry from the x-ray diffraction pattern," ZhÉTF, 15, 709 (1945).

SOVIET PHYSICS - CRYSTALLOGRAPHY VOL. 1, NO. 3 MAY-JUNE, 1956

STRUCTURE OF CESIUM-TETRACHLOROCOBALTATE CRYSTALS Cs_2CoCl_4

M. A. Porai-Koshits

N. S. Kurnakov Institute of General and Inorganic Chemistry

Translated from Kristallografiya, Vol. 1, No. 3,
pp. 291-299, May-June, 1956
Original article submitted December 9, 1955

Crystals of cesium tetrachlorocobaltate Cs_2CoCl_4, are rhombic, with a = 9.737, b = 12.972, and c = 7.392 Å; z = 4, Fedorov group D_{2h}^{16} = Pnam, and the K_2SO_4 type of structure. The Co-Cl distances in the $CoCl_4^{--}$ tetrahedron are the same and equal to 2.26 Å. The tetrahedron has a slight angular distortion. Each tetrahedron is surrounded by eleven Cs^+ ions, of which four lie opposite to the vertices of the tetrahedron (mean distance 3.49 Å), and two opposite to the centers of the faces of the tetrahedron (mean distance 3.94 Å). The configuration as a whole has two planes of symmetry. The coordination numbers of the Cs^+ ion are 11 and 9. The motif of the structure was found from projections of the interatomic function (using the "superimpose and minimize" method) and from electron-density projections. The coordinates were refined by combinations of weighted projections and ultimately by differential synthesis applied to a three-dimensional electron-density distribution. The structure of four-coordination complexes of divalent cobalt and nickel is discussed.

Introduction

The x-ray structural investigation of Cs_2CoCl_4 crystals and other complex compounds of divalent cobalt [1, 2, 3] had as its aim the accumulation of direct structural data regarding a number of questions on the stereochemistry of these compounds. One of the fundamental problems was to elucidate the general nature of the Cs_2CoCl_4 structure in the solid state, and to establish whether it belonged to the class of complex compounds $Cs_2[CoCl_4]$ or to that of double salts $CoCl_2 \cdot 2CsCl$. Study of the structure of the crystals made it possible to establish the presence of complex $CoCl_4^{--}$ ions, to find their configuration, and to determine the nature of the forces binding the complexing atom to its addends.

A brief description of the structure of Cs_2CoCl_4 was given in a review article of the author [2].

Crystallographic Characteristics

Cesium-tetrachlorocobaltate crystals Cs_2CoCl_4 are of blue color with the shape of plates or prisms. Two typical crystal habits are shown in Fig. 1. From goniometric data, the crystals belong to the rhombo-dipyramidal form of symmetry mmm; the ratio of the axes is $a:b:c = 0.755:1:0.568$.

Optically, Cs_2CoCl_4 crystals are biaxial. The refractive indices in white light are $n_g = 1.584$, $n_m = 1.579$, $n_p = 1.575$. The comparatively small birefringence suggests the probable presence of tetrahedral $CoCl_4^{--}$ ions.

The lattice spacings were determined in a precision camera from reflections with $\vartheta > 80°$ belonging to zero layer lines of oscillation x-ray photographs. On the basis of wavelength values of 1.78890 Å for $K\alpha_1$-Fe and 1.93597 Å for $K\alpha_1$-Co, the following spacings were obtained: $a = 9.737_2 \pm 0.0005$ Å, $b = 12.972 \pm 0.001$ Å, and $c = 7.392 \pm 0.003$ Å. The number of formula units of Cs_2CoCl_4 per unit cell was four. From the extinctions, possible space groups were C_{2v}^9 = Pna2 and D_{2h}^{16} = Pnam.

Experimental Technique

The main x-ray structural work was carried out with x-ray diffraction photographs taken in the

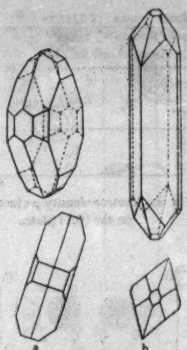

Fig. 1. Typical habits of Cs_2CoCl_4 crystals.

reciprocal-lattice camera in λ Mo radiation. The number of independent reflections on the photographs was 204 hk0, 69 0kl, 73 h0l, 140 hk1, 125 hk2. The total number of independent reflections used in a three-dimensional electron-density synthesis was 950. In order to increase the range of intensities recorded on the photographs, these were taken on several films. The intensities were estimated visually from blackening marks. The crystals had approximately equal dimensions in cross section (about 0.3 mm). The values of $|F(hk\bar{l})|^2$, found after allowing for the kinematic and polarization factors lay in the range 350:1. Conversion to the absolute scale was made after establishing the structural type by comparing the mean values of

$$F_{exp}(hkl)| \text{ and } |F_{theor}(hkl)|.$$

Determination of Structural Type

In the projections of the interatomic function (Patterson synthesis) in the (100) and (010) planes, the main maxima were concentrated along the lines w = 0 and w = ½, indicating that symmetry planes were present, and that the majority of the atoms (and in all cases the Cs and Co) occupied particular positions in the symmetry planes:

$$xy^1/_4;\ \bar{x}\bar{y}^3/_4;\ ^1/_2-x,\ ^1/_2+y,\ ^3/_4;\ ^1/_2+x,\ ^1/_2-y,\ ^1/_4.$$

The main basis for solving the structure was the projection of the interatomic function on the (001) plane (Fig. 2). The symmetry of the structure projection on this plane was C_{2v}^{II} = Pgg; hence, the

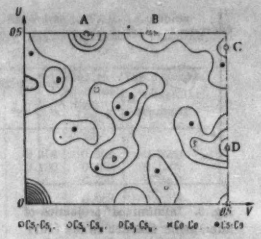

Fig. 2. Projection of interatomic function on the (001) plane.

disposition of the P-function maxima should obey the rules given in Section 7 (group C_{2v}^{II}) of the Patterson table for the characteristics of F and F^2 series.[1]

The selection of the two most intense maxima on the line u = ½ (maxima A and B, Fig. 2), and two such maxima on the line v = ½ (maxima C and D) leads to four possible arrangements of the ends of the Cs–Cs vectors. Figure 2 indicates the disposition of the ends of the Cs–Cs vectors for the only one of the four arrangements which agrees with the general picture of the projection of the P function. The Cs_I–Cs_I maxima are indicated by squares the Cs_{II}–Cs_{II} by circles, and the Cs_I–Cs_{II} by composite symbols.

Thus the projections of the interatomic functions determined the coordinates of the cesium atoms: x_{Cs_I} = 0.355, y_{Cs_I} = 0.098; $x_{Cs_{II}}$ = 0.020, $y_{Cs_{II}}$ = −0.176.

Further analysis of the (001) projection of the interatomic function was carried out by the "superposition and minimization" process [4, 5]. At the first stage of minimization, the key maximum for displacement was that corresponding to the centrosymmetrically connected cesium atoms; at the second stage, the symmetry of the structure projection (lines of glancing reflection) was used. Knowledge of the coordinates of the two symmetrically independent systems of Cs atoms enabled us to carry out a two-fold minimization, and the final distributions were minimized further by simple comparison. The final picture of the "minimized" P-function distribution is shown in Fig. 3. Apart from the two strongest maxima corresponding to the Cs_I and Cs_{II} atoms, the projection shows two more maxima, A and B. One of these must clearly correspond to the Co atom, also occupying a four-fold position in the planes of symmetry.

[1] See A.I. Kitaigorodskii, X-Ray Structural Analysis, p. 497.

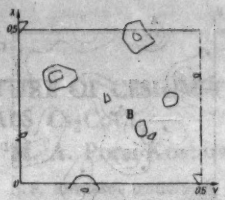

Fig. 3. "Minimized" projection of interatomic function on the (001) plane.

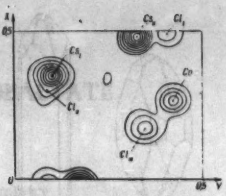

Fig. 4. Electron-density projection on the (001) plane.

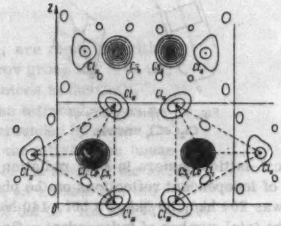

Fig. 5. Electron-density projection on the (100) plane.

The chlorine atoms may occupy either two general eight-fold positions, or four four-fold positions in the planes of symmetry, or two four-fold and one eight-fold position. Since the (001) projection is a projection along a direction perpendicular to the m plane, in the first case the chlorine atoms should give two double-intensity maxima, in the second four weak ones, and in the third one strong and two weaker maxima. The presence of only one maximum on the minimized projection, possibly corresponding to chlorine atoms, is in accordance with the third arrangement.

From the data so obtained, the coordinates of the Cs_I^+ and Cs_{II}^+ ions and the approximate coordinates of the Co and Cl_{III} atoms (eight-fold position), we constructed a first-approximation electron-density projection, which indicated the position of another chlorine atom (Cl_I) and suggested that of a second. The projection obtained after five cycles of successive refinement is shown in Fig. 4. Comparison between the minimized projection and electron-density projection shows that the Cl_I and Cl_{II} maxima were absent from the former, not because of their relative weakness, but because they merged with the maxima corresponding to the cesium atoms. The superposition of the Cs_I and Cl_{II} atoms was especially significant. Thus, after constructing the projection on the (001) plane, only the z coordinate of the Cl_{III} atom remained unknown and the x and y of the Cl_{II} a little indeterminate. Knowledge of all three coordinates of the majority of the atoms in the cell, however, enabled us to calculate the signs of the structure amplitudes for the 0kl reflections and construct the electron-density projection on the (100) plane (Fig. 5). From this projection the following data were determined: the z coordinate of the Cl_{III} atom and the y coordinate of the Cl_{II} atom. Only the x coordinate of the latter remained unknown. The results of determining the coordinates of the atoms from the (001) and (100) projections are given in column 1 of Table 1.

Description of Structural Type

We see From Figs. 4 and 5 that the cobalt atoms are surrounded tetrahedrally by atoms of chlorine. Comparison of the results obtained with published data for K_2SO_4 shows that the two compounds are isostructural.

Thus, the compound Cs_3CoCl_4 is complex in structure. From spectral data [6] the complex ions $CoCl_4^{--}$ are also preserved in solution.

According to the data of Tishchenko and Pinsker [7], tetrahedral structure also occurs in complex ions of $CoBr_4^{--}$. An analogous structure is found in Cs_3CoCl_5 [8]. The reader will find a more detailed discussion of the crystal chemistry of complex Co^{II} and Ni^{II} compounds of the type $Me_2^IMe^{II}X_4$ in the review article [2].

In the crystal, the $CoCl_4^{--}$ tetrahedra retain only one plane of symmetry. Each tetrahedron is surrounded by eleven cesium ions: five of these are Cs_I^+ and six Cs_{II}^+. As we see from Fig. 6, the disposition of Cs^+ ions around the tetrahedron has a very symmetrical character: a plane passing through the Co atom and Cl_{III} atoms divides it into two almost-identical halves. A second symmetry plane of the figure is the true symmetry plane of the whole crystal (this coincides with the plane of the figure). Of the eleven Cs^+ ions, five lie in this

TABLE 1. Atomic Coordinates in the Cs_2CoCl_4 Structure, According to Various Combinations of "Weighted" Projections and Three-Dimensional Differential Synthesis (in Fractions of Cell Dimensions)

Atoms		Projec. $\sigma_z(xy)$; $\sigma_x(yz)$	Combinations of weighted projections $\sigma_z+\frac{1}{x_i}\sigma_x$	$\sigma_x-\frac{1}{x_i}\sigma_z$	$\sigma_z+\frac{1}{z_i}\sigma_z$	$\sigma_x-\frac{1}{z_i}\sigma_x$	Final results from projections	Three-dimen. differential synthesis
Cs_I	x	0.354	0.352	—	—	0.358	0.358	0.3600
	y	0.099_5	0.099	—	—	0.100	0.100	0.1009
	z	—	—	—	—	—	0.250	0.2500
Cs_{II}	x	0.020	0.021	—	0.019	—	0.019	—0.0208
	y	—0.176	—0.176	—	0.176	—	—0.176	0.1762
	z	—	—	—	—	—	0.250	0.2500
Co	x	—0.236	0.232	—	—	—0.232	—0.233	0.2332
	y	0.077	0.078	—	—	0.078	0.078	0.0775
	z	—	—	—	—	—	0.250	0.2500
Cl_I	x	—0.010	—0.009	—	—	—0.006	—0.006	0.0030
	y	0.091	0.090	—	—	0.100	0.100	0.0980
	z	—	—	—	—	—	0.250	0.2500
Cl_{II}	x	—	—	—	—0.307	—	—0.307	—0.3107
	y	0.089	—	—	—0.086	—	—0.086	—0.0867
	z	—	—	—	—	—	0.250	0.2500
Cl_{III}	x	—0.322	—	0.322	—0.325	—0.320	—0.322	—0.3225
	y	0.155	—	0.155	0.152_5	0.156	0.154_2	0.1534
	z	0.493	—	—	—		0.493	0.4984

plane, the remaining six being grouped in threes above and below it. Of the eleven cesium ions, four are situated opposite to the vertices of the tetrahedron, i.e., they are situated roughly in line with the Co–Cl bond. Five Cs^+ ions are situated opposite to the midpoints of the edges of the tetrahedron, on the continuations of straight lines drawn from the Co atom through the middle of the edges. Finally, the last two Cs^+ ions are disposed opposite to the centers of two faces of the tetrahedron.

The Cs^+ ions, in turn, are surrounded by Cl atoms: Cs_I^+ has coordination number 11, and Cs_{II}^+ coordination number 9. The coordination polyhedra are shown in Fig. 7. The environment of Cs_I^+ is similar in character to the close packing of spheres; in the middle layer, however, there are five "spheres" instead of six, one atom taking two of the sites in the spherical packing. The polyhedron of the Cs_{II}^+ ion may be considered as the result of further distortion of the packing, three vertices of the lower layer being replaced by one vertex. The motif of the structure as a whole is shown in Fig. 8 in the form of tetrahedra and coordination polyhedra of the Cs^+.

Refinement of the Atomic Coordinates

The coordinates of the atoms were refined in two stages: first by the method of "weighted" or "generalized" projections [9-12], and second by the method of three-dimensional differential Fourier series [13].

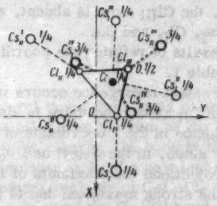

Fig. 6. $CoCl_4^-$ tetrahedron surrounded by Cs^+ ions.

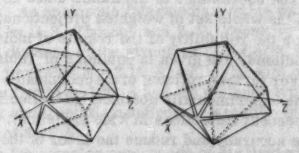

Fig. 7. Coordination polyhedra of Cs_I^+ and Cs_{II}^+ ions.

In our particular case, when all the atoms are disposed in planes situated at approximately equal distances from one another ($z \approx 0$, $z = 1/4$, $z \approx 1/2$, $z = 3/4$), the method of weighted projections is equivalent to that developed earlier by Booth, called "superposition of sections" [14]. This question is considered in more detail in another paper by the author [12].

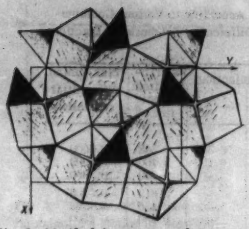

Fig. 8. Motif of the structure of Cs_2CoCl_4 crystals formed out of polyhedra.

The method of superposing cross sections enabled us to refine the x,y coordinates of all atoms in the structure. We calculated four combinations of the weighted projections of the zeroth, first, and second layer lines corresponding to superpositions of the sections z = 0, z = 1/4, z = 1/2, z = 3/4. Two of these, $\sigma_0(xy) + (1/\varkappa_2)\sigma_2(xy)$ and $\sigma_0(xy) - (1/\varkappa_1)\sigma_1(xy)$, are shown in Figs. 9 and 10. In the first projection, the Cl_{III} atom is absent, and in the second the Cs_I, Cl_I, and Co.

The results of refining the coordinates are given in Table 1.

The greatest divergence occurs in the coordinates of the Cl_I atom, and there is also considerable divergence in the x coordinate of Cs_I. This is natural, since, in the $\sigma_0(xy)$ and $\sigma_0(xy) + (1/\varkappa_2) \cdot \sigma_2(xy)$ projections the maximum of the Cl_I atoms lies near the strong maximum due to the Cs_{II}, and the Cs_I maximum considerably overlaps that of the Cl_{II}; in the $\sigma_0(xy) - (1/\varkappa_1)\sigma_1(xy)$ projection, however, these superpositions do not occur.

The coordinates of the atoms taken as final from the whole set of weighted projections, allowing for the reliability of the results of individual projections, are given in column 6 of Table 1.

For further refining of the coordinates we took all the experimentally obtained hkl reflections (950 independent reflections in λ Mo radiation). To improve accuracy and reduce the labor of the calculations, we used the differential-synthesis method of [10].

The computing was carried out on an electronic computer. The machine time for one cycle of refinement (including the time for calculating the signs of the structure amplitudes) was 30 min, i.e., five minutes per atom. After the first cycle of refinement, the sign of only one structure amplitude was changed; after the second cycle, all signs remained constant. The third cycle thus gave a correction associated simply with the assumptions on

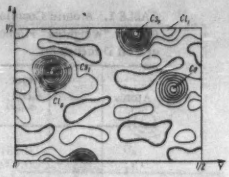

Fig. 9. Superposition of "weighted" electron-density projections $\sigma_0(xy) + \frac{1}{\varkappa_2}\sigma_2(xy)$

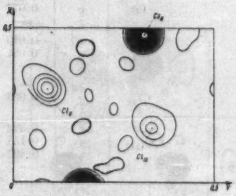

Fig. 10. Superposition of "weighted" electron-density projections $\sigma_0(xy) - \frac{1}{\varkappa_1}\sigma_1(xy)$

which the actual method of differential synthesis was based [neglect of higher terms in the Taylor expansion of the function $(\partial\rho/\partial x)_y$]. This correction was negligible. The coordinates of the atoms obtained from the three-dimensional differential synthesis are given in the last column of Table 1. The mean discrepancy, as compared with the results obtained from the weighted projections, was of the order of 0.0018 (in fractions of the cell edge). The greatest discrepancy was 0.004 in the x coordinate of the Cl_{II} atom [not counting the discrepancy of 0.005 in the z coordinate of the Cl_{III} atom found earlier, less accurately, from a projection on the (100) plane]. The probable errors calculated from Cruickshank's formula [15] were: $\varepsilon(x)_{Cs} = 0.003$ Å, $\varepsilon(x)_{Co} = 0.005$ Å, $\varepsilon(x)_{Cl} = 0.009$ Å, $\varepsilon(Co-Cl) = 0.01$ Å.

Interatomic Distances and Character of the Chemical Bonds

The coordinates of the atoms obtained by the three-dimensional synthesis were taken as final.[2] The interatomic distances and valence angles in the complex $CoCl_4^{--}$ ions are shown in Table 2.

[2] In the article published in the Transactions of the Institute of Crystallography, No. 10 [9], the distances are given on the basis of results obtained in projection. In the present paper all interatomic distances are refined ones.

TABLE 2. Interatomic Distances (in A) and Valence Angles in the Cs_2CoCl_4 Structure

Distances and valence angles in complex $CoCl_4^{--}$	Distances to Cs^+ ions lying oppos. to the vertices of the tetrahedron	Distances to Cs^+ ions lying oppos. to midpoints of edges of the tetrahedron	Distances to Cs^+ ions lying opposite to the faces of the tetrahedron
$Co-Cl_I = 2.26_1$	$Cl_I - Cs_I^I = 3.54_6$	$Cl_{II} - Cs_{II}^{II} = 3.42_0$	$Cl_{III} - Cs_{II}^{III} = 3.06_3$
$Co-Cl_{II} = 2.26_0$	$Cl_{II} - Cs_{II}^{II} = 3.48_4$	$Cl_I - Cs_{II}^{II} = 3.57_6$	$Cl_{III}^I - Cs_{II}^{III} = 3.66_1$
$Co-Cl_{III} = 2.26_0$	$Cl_{III} - Cs_{II}^{III} = 3.47_1$	$Cl_{III} - Cs_{II}^{II} = 3.48_4$	$Cl_{II} - Cs_{II}^{III} = 4.03_9$
$Co-Cl_{III}^I = 2.26_0$	$Cl_{III}^I - Cs_{II}^{III} = 3.47_1$	$Cl_I - Cs_{II}^{II} = 3.84_1$	$Cl_{III} - Cs_I^I = 4.08_2$
$Cl_I - Cl_{II} = 3.84_9$		$Cl_{III} - Cs_{II}^{IV} = 3.48_9$	$Cl_{III}^I - Cs_{II}^{II} = 4.08_2$
$Cl_I - Cl_{III} = 3.68_2$		$Cl_I - Cs_{II}^{IV} = 3.84_1$	$Cl_I - Cs_{II}^{II} = 4.13_4$
$Cl_I - Cl_{III}^I = 3.68_2$		$Cl_{II} - Cs_I^{IV} = 3.73_3$	
$Cl_{II} - Cl_{III} = 3.64_0$		$Cl_{III} - Cs_I^{IV} = 3.81_2$	
$Cl_{II} - Cl_{III}^I = 3.64_0$		$Cl_{II} - Cs_I^{IV} = 3.73_3$	
$Cl_{III} - Cl_{III}^I = 3.67_4$		$Cl_{III} - Cs_I^{IV} = 3.81_2$	
$\angle Cl_I - Co - Cl_{II} = 116°20'$			
$\angle Cl_I - Co - Cl_{III} = 109°20'$			
$\angle Cl_{II} - Co - Cl_{III} = 107°20'$			
$\angle Cl_{III} - Co - Cl_{III}^I = 108°50$			

The $CoCl_4^{--}$ tetrahedra are little distorted; all the Co–Cl distances are the same and equal to 2.26_0 Å; the mean Cl–Cl distances are 3.69_3 Å.

In the second column of Table 2 we have the Cs–Cl distances for the four cesium ions lying on the continuations of the Co–Cl bond lines. The mean distance is here 3.49_3 Å, i.e., close to the sum of the ionic radii. In the third column of Table 2 we have the Cs–Cl distances for the five cesium ions lying opposite to the midpoints of the edges of the $CoCl_4^{--}$ tetrahedron. The mean distance here is rather greater, 3.67_3 Å. Finally, in the fourth column, we have the distances to the two ions situated opposite to the centers of the two tetrahedral faces. The mean distance here is still larger, 3.94_5 Å.

In the coordination polyhedron of the Cs_I^+ ion (an 11-hedron) the mean Cs–Cl distance is 3.84_4 Å, and in that of the Cs_{II}^+ ion (12-hedron), 3.54_3 Å, i.e., considerably smaller.

All the Co–Cl distances in Cs_2CoCl_4 are the same (within the limits of experimental error) and equal to 2.26 Å. This value is close to the sum of the covalent radii normally taken for the Co atom with a tetrahedral environment (1.22 Å [16]) and the Cl atom with a single bond (0.99 Å). A similar value, 2.22 Å, was obtained for the Cu–Cl distance in the structure of Cs_2CuCl_4 [7] belonging to the same structural type. Both these values are considerably smaller than the sum of the ionic radii (2.50 to 2.60 Å); clearly, the bond in these compounds is predominantly of a covalent character. X-ray structural analysis of $CsCoCl_3 \cdot 2H_2O$ showed that in this compound the Co–Cl bond was also of a nonionic nature [8].

In the structure of Cs_3CoCl_5 [8], the Co–Cl distance is rather larger than in Cs_2CoCl_4, being 2.34 Å. An analogous intermediate value was obtained by G. S. Zhdanov and Z. V. Zvonkova for the Co–N distance in the structure of $K_2Co(NCS)_4 \cdot H_2O$ [19]. Here Co–N = 2.15 Å, while the sum of the covalent radii is 1.92 Å and the distance typical for purely electrostatic nondipole interaction is of the order of 2.45 Å.

In the complex compounds of divalent nickel with square coordination, no divergence from the distances characteristic of the covalent bond was found for nickel-addend distances of this kind. It is interesting to note, however, that in one of the complex compounds of divalent platinum, $Pt(NH_3)_2Cl_2$-trans, the Pt–N distance is also considerably larger than the ordinary covalent value: 2.17 ± 0.04 Å instead of 2.00 Å [20].

The author thanks A. S. Antsyshkina for help in the initial stages of the work, and N. P. Trifonov for carrying out the calculations on the computer.

LITERATURE CITED

1. M.A. Porai-Koshits and A.S. Antsyshkina, "Structure of crystals of dichlorotetrapyridinenickel and dichlorotetrapyridinecobalt," Izv. sektora Platiny AN SSSR, 29, 19 (1955).
2. M.A. Porai-Koshits, "X-ray structural study of complex compounds of divalent cobalt and nickel," Tr. Inst. Kristallogr., 10 (1954).
3. M.A. Porai-Koshits, "Refining the structural parameters of triaminodirhodanonickel (II) and cesium tetrachlorocobaltate crystals," Izv. AN SSSR.
4. J.R. McLachlan, "The determination of crystal structures from x-ray data without a knowledge of the phases of the Fourier coefficients," Proc. Nat. Acad. Sci. Am., 37, 115 (1951).
5. M.J. Buerger, "A new approach to crystal structure analysis," Acta Cryst., 6, 531 (1951).
6. M.L. Schultz and E.F. Lilek, "Absorption spectra of some double salts containing cobaltous chlorides," J. Am. Chem. Soc., 64, 2748 (1942).
7. G.N. Tishchenko and Z.G. Pinsker, Electron-Diffraction Study of Complex Compounds of Divalent Cobalt and Nickel, Author's abstract, Master's dissertation [in Russian] (Moscow, 1953).
8. F. Wells and H.M. Powell, "The structure of cesium cobalt chloride (Cs_3CoCl_5)," J. Chem. Soc., London, 359 (1935).
9. G.J.B. Clews and W. Cochran, "The structures of pyrimidines and purines III. An x-ray investigation of hydrogen bonding in aminopyrimidines," Acta Cryst., 2, 46 (1949).
10. R.F. Raeuchle and R.E. Rundle, "The structure of $TiBe_{12}$," Acta Cryst., 5, 85 (1952).
11. W. Cochran and H.B. Dyer, "Some practical applications of generalized crystal-structure projections," Acta Cryst., 5, 634 (1952).
12. M.A. Porai-Koshits, "Relation between the methods of 'weighted projections' and 'superposition of sections' used in the structural analysis of crystals," Tr. Inst. kristallogr., 11 (1956).
13. A.D. Booth, "A differential Fourier method for refining atomic parameters in crystal structure analysis," Trans. Faraday Soc., 42, 444 (1946).
14. A.D. Booth, "Two new modifications of the Fourier method of x-ray structure analysis," Trans. Faraday Soc., 41, 434 (1945).
15. D.W.J. Cruickshank, "The accuracy of electron-density maps in x-ray analysis with special reference of dibenzyl," Acta Cryst., 2, 65 (1949).
16. J. d'Ans and E. Lax, Taschenbuch für Chemiker und Physiker (Berlin, 1943).
17. L. Helmholtz and F.F. Kroo, "The crystal structure of cesium chlorocuprate Cs_2CuCl_4 and the spectrum of the chlorocuprate ion," J. Am. Chem. Soc., 74, 1176 (1952).
18. O. Stelling and T. Olsson, "Röntgen spektroskopische Untersuchungen einiger fester Chlorosalze," Z. Phys. Chem., 7, 210 (1930).
19. G.S. Zhdanov and Z.V. Zvonkova, "Crystal structure of rhodanides. II. Crystal structure of potassium tetrarhodanocobaltate," Zh. Fiz. Khim., 24, 1339 (1950).
20. M.A. Porai-Koshits, "Structure of platinum trans-dichlordiamine crystals," Tr. Inst. Kristallogr., 9, 229 (1954).

STUDY OF THE STRUCTURE OF SOME FOUR-COMPONENT ALLOYS OF Tl—Sb—As—Se

Z. G. Pinsker and V. I. Khitrova

Institute of Crystallography, Academy of Sciences of the USSR

Translated from Kristallografiya, Vol. 1, No. 3,
pp. 300-305, May-June, 1956
Original article submitted March 23, 1956

The structures of films obtained by vacuum sublimation of alloys of composition $Tl_2Se[{}^1/_2Sb_2Se_3 \cdot {}^1/_2As_2Se_3]$ were studied by electron diffraction. After prolonged annealing, two crystalline phases with rhombic unit cells were formed: (I) $a = 4.15$, $b = 4.48$, $c = 11.85$, and (II) $a = 3.99$, $b = 4.43$, $c = 11.55$ Å. The structure was analyzed by Φ^2 and Φ series and the reliability factor minimized; this showed that both phases had the same structure as $Tl_2Sb_2Se_4$ [1], the antimony atoms being statistically replaced by arsenic. The probable composition of phase (I) is $Tl_2[Sb_{0.75}As_{0.25}]_2Se_4$ and that of phase (II) is $Tl_2[Sb_{0.25}As_{0.75}]_2Se_4$. The Fedorov group is

$$D_{2h}^{7} - Pmna;\ Tl\,\text{in}(e)\,(^1/_4 y, 0, ^1/_2),\ (Sb, As)\,\text{in}(e)\,(000,\ ^1/_4 y ^1/_2),$$
$$Se\,\text{in}(h)\,(0\,yz,\ 0\,\bar{y}\bar{z},\ 0\,y^1/_2 - z,\ 0\,\bar{y}^1/_2 + z)\ \text{with}\ y \approx {}^1/_3;\ z = 0.206.$$

This paper, together with [1], forms part of an intensive study of the electrical properties and structure of multicomponent semiconducting alloys [2, 3]. The physical properties were determined and preliminary x-ray studies made with samples of alloys prepared by fusing the components in sealed quartz ampoules, while a more detailed structural analysis was made by electron diffraction on thin films sublimed from such alloys in vacuum. In studying the $Tl_2Se - Sb_2Se_3$ system, complete agreement was reached between the results of work in these two directions. Kolomiets and Goryunova [2] showed that "all the results obtained by studying the electrical and photoelectric properties of this series indicate that it contains compounds corresponding to the formula $Tl_2Se \cdot Sb_2Se_3$." Independently of this, Z.G. Pinsker et al., after studying the structure of sublimed layers of composition $n \cdot Tl_2Se \cdot m \cdot Sb_2Se_3$, found only one phase apart from Tl_2Se and Sb_2Se_3; this had the composition $Tl_2Sb_2Se_4$ (or $TlSbSe_2$), and its structure was established by Pinsker, Semiletov, and Belova [1]. This phase has a rhombic unit cell: $a = 4.18$, $b = 4.50$, and $c = 12.00$ Å, with one molecule of $Tl_2Sb_2Se_4$ in the unit cell. The Fedorov group is $D_{2h}^{7} - Pmna$ (or $D_{2h}^{18} - Cmmm$). The structure is characterized by plane centered lattices of Sb – Tl parallel to ab. Between these lie plane zigzag chains of Se atoms along directions parallel to the a axis.

The structure studied corresponds to a quite definite compound or phase of constant composition, as indicated by the constancy of the lattice spacing measured in different experiments.

In the present investigation, we studied the structure of certain four-component alloys of Tl – Sb – As – Se given to us by N.A. Goryunova and B.T. Kolomiets. In studying similar systems [3], these authors established the existence of a gradual transformation to the amorphous state as arsenic replaced antimony. They represented the alloys in question as a "pseudo-binary section" $Tl_2Se \cdot [xAs_2Se_3(1-x)Sb_2Se_3]$ of the "pseudo-tertiary" system $Tl_2Se - As_2Se_3 - Sb_2Se_3$. The extreme alloys in the "pseudo-binary" section are $Tl_2Se \cdot Sb_2Se_3$ and $Tl_2Se \cdot As_2Se_3$. X-ray and microstructural studies carried out by the authors of [3] showed that, while the first alloy had crystalline structure, the second, containing arsenic, was a typical glass, and the intermediate alloys were a mixture of crystalline and glassy or amorphous phases, of which the crystalline phase was assigned the constant composition $Tl_2Sb_2Se_4$.

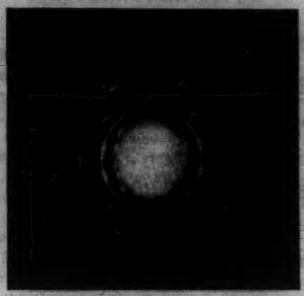

Fig. 1. Electron-diffraction photograph of $Tl_2[Sb,As]_2Se_4$. As content 20% (atomic).

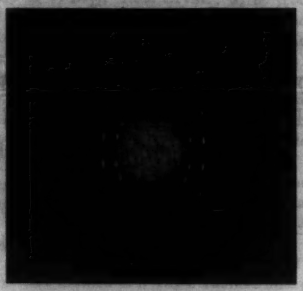

Fig. 2. Electron-diffraction photograph of $Tl_2[Sb,As]_2Se_4$. As content 75% (atomic).

For electron-diffraction examination we took two alloy samples prepared in two different ampoules. Both had the same composition, corresponding to the formula $Tl_2Se\ [1/2As_2Se_3 \cdot 1/2Sb_2Se_3]$, but the external form of the samples indicated that they had different structures. The first sample contained comparatively coarse crystals, while the crystal structure of the second was less obvious to the unaided eye. The two samples were vacuum-evaporated in a series of experiments onto various substrates; the films obtained were annealed for various periods at temperatures of 110 to 120°C, the annealing being interrupted at various stages and the films examined by electron diffraction. It was found that before annealing the sublimed films were amorphous. Annealing for 6 to 7 h with slow cooling led to the formation of a partly crystalline product, the electron-diffraction photographs (Figs. 1 and 2) having considerable background in addition to diffraction maxima from the crystalline phase. On comparing the films obtained by sublimation of the two samples, we found that the first gave the more rapidly crystallizing layers and hence the weaker electron-diffraction background. The process of crystallization induced by annealing was indicated by the appearance of "polycrystalline" rings followed by "oblique-texture" pictures from an oriented film. An important result was that electron-diffraction pictures very similar to those taken from $Tl_2Sb_2Se_4$ [1] were obtained. Study of the diffraction photographs showed that, in all experiments involving sublimation of the first sample, a crystalline phase with a rhombic unit cell was formed (a = 4.15, b = 4.48, and c = 11.55 Å), whereas, on sublimation of the second sample, a crystalline phase with rhombic unit cell a = 3.99, b = 4.43, and c = 11.85 Å developed. We may suppose that these phases correspond to composition with antimony partly replaced by arsenic ($R_{Sb} > R_{As}$) in the $Tl_2Sb_2Se_4$ lattice with the formation of analogous structures. This conclusion diverges somewhat from that of the authors of [3] mentioned above, according to which alloys of composition $Tl_2Se \cdot [xAs_2Se_3\ (1-x)\ Sb_2Se_3]$ consist of crystalline ($Tl_2Sb_2Se_4$) and amorphous ($Tl_2As_2Se_4$) phases. In other words, the authors in question deny the possibility of dissolution or the replacement of antimony by arsenic in $Tl_2Sb_2Se_4$, while our own results directly indicate that such dissolution or substitution takes place. Apparently the difficulties arising during the x-ray study of these alloys prevented the presence of the transitional phases from being established.

In view of the less- intense background on the electron-diffraction photographs of the phase with the larger cell (taken from the first sample), these were studied more fully. Indexing the photographs led unequivocally to the same extinctions, and hence the same Fedorov group as in the case of $Tl_2Sb_2Se_4$.

For further study, the experimental reflection intensities were estimated visually. The oblique-texture diffraction pictures comprised arcs superimposed on polycrystalline rings. In estimating the intensities, parts of the rings free from arcs were chiefly used, and conversion to experimental structure amplitudes was effected by means of the formula

$$|\Phi_{exp}| = |\sqrt{I_{exp}/pd^4}|.$$

The values of Φ^2_{exp} obtained were used to calculate one-dimensional cross sections of the three-

dimensional Patterson series in the directions [100], [010], [001], [110], [101], and [011], and also through the midpoints of the *a* and b axes and through the point [½ ½ 0] parallel to the c axis.

The disposition and number of maxima on these sections (except for one apparently false maximum) correspond to the model established for $Tl_2Sb_2Se_4$, if we suppose that the antimony atoms in the lattice are statistically replaced by arsenic. In the corresponding model, the Sb atoms occupy positions 000, ½ 0 ½, the Tl atoms ½ ½ 0 and 0 ½ ½, and the Se atoms 0yz, $0\bar{y}\bar{z}$, $0y\frac{1}{2}-z$, and $0y\frac{1}{2}+z$ with $y \approx \frac{1}{2}$; the value of parameter z in our structure, according to the Φ^2 series, was ~0.266.

Assuming the structure to have been established to a first approximation, we therefore attempted to refine the composition of this phase by minimizing the reliability factor. Starting from a statistical replacement of half the Sb atoms by As, we obtained the following values from 60 reflections:

$$R = \Sigma||\Phi_{exp}| - |\Phi_{theo}||/\Sigma|\Phi_{exp}| = 37\%.$$

By varying the arsenic content, we reduced the value of R to 21% for ~20% (atomic) As, i.e., considerably less than in the first sample as a whole.

The normalization of the experimental structure amplitudes to the theoretical was effected with respect to the first 30 reflections. The theoretical amplitudes were then multiplied by the temperature factor with B = 0.7; the value of B was established from experiment (see Fig. 4).

By comparison with the results obtained for 50 at.% As, the signs only changed for five structure amplitudes.

The cross section of the three-dimensional potential series were calculated for the x = 0, x = ½, and y = ½ planes (Fig. 3). We see from this figure that the structure of the phase studied fully imitates that of $Tl_2Sb_2Se_4$ with statistical replacement of some of the antimony atoms by arsenic (Fig. 5). The value of parameter z for Se (0.266) given earlier was confirmed.

Study of the electron-diffraction pictures obtained on subliming the second sample showed that here also the crystalline phase had a structure similar to that of $Tl_2Sb_2Se_4$. The fact that the background was stronger than that for the first sample indicated a greater content of the amorphous component. The intensities of the reflections were thus measured less accurately.

As regards the extinction law, this was established quite reliably and led to the same symmetry.

In determining the experimental reflection intensities on electron-diffraction photographs of the oblique-texture type or from polycrystalline films (with multiple exposures), we used microphotometers of the MF-2 (visual) and MF-4 (recording) types. We constructed one-dimensional cross sections of the three-dimensional Patterson series in all the directions previously studied for films of the first sample, and also the projection of the Φ^2 series on the yz plane. These calculations led us to the

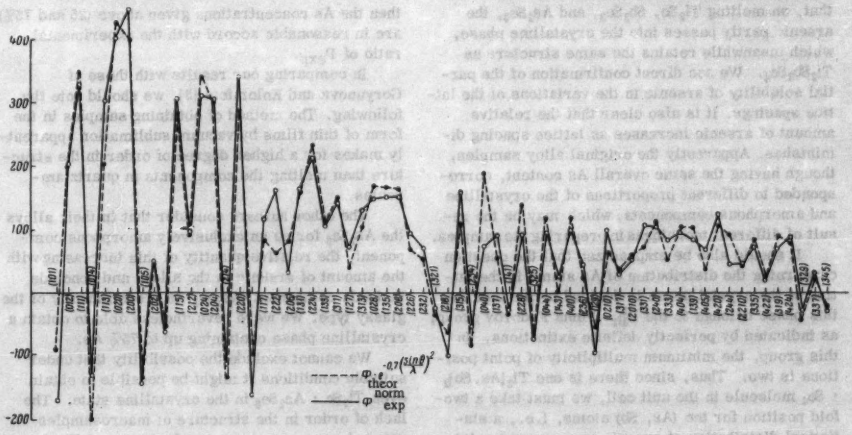

Fig. 3. Comparison between experimental and theoretical structure amplitudes.

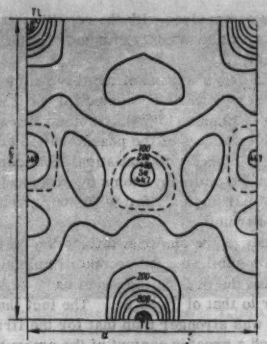

Fig. 4. Cross section of three-dimensional potential series for the plane $y = \frac{1}{2}$ in the $Tl_2[Sb,As]_2Se_4$ lattice.

same structural model, with $y \simeq \frac{1}{2}$ and $z = 0.266$. The factor R was minimized for a 75% As content.

The following comments should be made in connection with the results given. The structural study of a multicomponent system by itself constitutes a difficult problem. The difficulty of the investigation is greater in our case because of the absence of direct data on the composition of the phases, since the compositions of the crystalline and amorphous components are evidently different. In addition to this, it may be considered certain that, on melting Tl_2Se, Sb_2Se_3, and As_2Se_3, the arsenic partly passes into the crystalline phase, which meanwhile retains the same structure as $Tl_2Sb_2Se_4$. We see direct confirmation of the partial solubility of arsenic in the variations of the lattice spacings. It is also clear that the relative amount of arsenic increases as lattice spacing diminishes. Apparently the original alloy samples, though having the same overall As content, corresponded to different proportions of the crystalline and amorphous components, which may be the result of different techniques in preparing the samples.

It should also be emphasized that the question concerning the distribution of As atoms in the lattice of the crystal phase is decided by the fact that this phase belongs to the D_{2h}^{7} – Pmna Fedorov group, as indicated by perfectly definite extinctions. In this group, the minimum multiplicity of point positions is two. Thus, since there is one $Tl_2[As,Sb]_2 \cdot Se_4$ molecule in the unit cell, we must take a two-fold position for the (As, Sb) atoms, i.e., a statistical distribution of arsenic atoms over the lattice points.

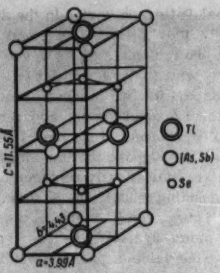

Fig. 5. Model of $Tl_2[Sb,As]_2Se_4$ structure.

As well as the reduction in lattice spacings on passing from the first sample to the second, there is an increase in the P ratio, i.e., the ratio of the height of the Tl maximum to that of (Sb, As), in the potential cross sections; this ratio changes from 1.36 to 1.57. These values are obtained from the heights of the maxima by suitable normalization of Φ_{exp}. If we use the theoretical relationship [4, 5]

$$P = \varphi_{0,Tl}/\varphi_{0,(Sb,\ As)} = (Z_{Tl}/Z_{Sb,As})^{2/3}$$

with

$$Z_{Sb,As} = \frac{n \cdot Z_{Sb} + mZ_{As}}{n+m},$$

then the As concentrations given above (25 and 75%) are in reasonable accord with the experimental ratio of P_{exp}.

In comparing our results with those of Goryunova and Kolomiets [3], we should note the following. The method of obtaining samples in the form of thin films by vacuum sublimation apparently makes for a higher degree of order in the structure than melting the components in quartz ampoules.

The other authors consider that in their alloys the As_2Se_3 forms an exclusively amorphous component, the relative quantity of this increasing with the amount of arsenic in the alloy, and conclude that this component (As_2Se_3) is predominantly of the glassy type. We were nevertheless able to obtain a crystalline phase containing up to 75% As.

We cannot exclude the possibility that under suitable conditions it might be possible to obtain even $Tl_2Se \cdot As_2Se_3$ in the crystalline state. The lack of order in the structure of macrosamples noted above makes x-ray analysis very difficult, since the amorphous component of alloys containing

heavy Tl and other atoms leads to severe background; the small dimensions of the crystals, and the absence of orientation, prevents the experimental material necessary for structural analysis from being obtained.

The degree of order obtained in our alloy films is still not high enough. This is chiefly expressed in the limited number of reflections found on the electron-diffraction pictures (up to $\sin\vartheta/\lambda \approx 0.62$), of which there are fewer than might be expected. Thus, there is a statistical derangement in the lattice of the crystalline component, analogous to that found in metals after working.

The structures studied in the present investigation may evidently be considered as "transitional" phases between $Tl_2Sb_2Se_4$ on the one hand, and $Tl_2As_2Se_4$ on the other, with a continuously increasing As content. This view is in agreement with our statistical distribution of As atoms in the lattices of the phases examined. Usually, however, transitional or intermediate phases have lattice spacings varying continuously with varying composition, whereas we are dealing with two completely definite structures, the unit cells of which have fixed sizes.

One possible explanation of this discrepancy would be that our phases were not obtained in the equilibrium state corresponding to an ordered disposition of Sb and As atoms in the lattice. A final solution to these problems awaits further study of the system.

LITERATURE CITED

1. Z. G. Pinsker, S. A. Semiletov, and E. N. Belova, "Electron-diffraction study of the $Tl_2Sb_2Se_4$ structure," DAN SSSR, 106, 1003-1007 (1956).
2. B. T. Kolomiets and N. A. Goryunova, "Properties and structure of ternary semiconducting systems. I.," ZhTF, 25, 984-994 (1955).
3. N. A. Goryunova and B. T. Kolomiets, "Properties and structure of ternary semiconducting systems. II," ZhTF, 25, 2069-2078 (1955).
4. B. K. Vainshtein, "Study of crystal-lattice potential by electron diffraction," Trudy Inst. Kristallogr., 9, 259-276 (1954).
5. B. K. Vainshtein, "Height of the maxima in electron-density and potential synthesis," Trudy Inst. Kristallogr., 11, 78-84 (1955).

SOVIET PHYSICS – CRYSTALLOGRAPHY VOL. 1, NO. 3 MAY-JUNE, 1956

ELECTRON-DIFFRACTION STUDY OF THE STRUCTURES OF THIN LAYERS OF CADMIUM SULFIDE, SELENIDE, AND TELLURIDE

S. A. Semiletov

Institute of Crystallography, Academy of Sciences of the USSR

Translated from Kristallografiya, Vol. 1, No. 3,
pp. 306-310, May-June, 1956
Original article submitted March 23, 1956

Point electron-diffraction photographs obtained from CdS, CdSe, and CdTe were solved and various cases of the orientation of these crystals relative to mica and NaCl analyzed, as well as that of the cubic and hexagonal forms of the crystal relative to each other.

Cadmium sulfide, selenide, and telluride crystals became the subject of many investigations after a simple method of producing them had been developed (reaction of Cd vapor with H_2S, H_2Se, and H_2Te); they were shown to have valuable properties, in particular, photoconductivity [1]. Photoresistances made of these substances are sensitive over a wide range of radiation, from infrared to ultraviolet, to x rays and γ rays, and also to corpuscular α and β radiation.

In order to explain the various properties of these compounds, certain authors have expressed views on the phase composition of the samples, without making any direct verification of these. Thus, in studying the influence of cadmium impurity on the operation of selenium photoelements [2], it was found that the introduction of cadmium impurity into selenium by simultaneous vacuum evaporation led to a change in the spectral distribution of sensitivity, and even to the formation of a photoelement of a new type, a peculiarity of which was the fact that the sign of the photo emf depended on the wavelength of the incident light. In connection with this, the authors expressed the view that crystals of the cubic and hexagonal forms of CdSe were produced on introducing the cadmium into the selenium.

Until recently, available data [3] indicated that cadmium telluride, in contrast to the sulfide and selenide, had no hexagonal form. Electron-diffraction study by the author [4] of sublimed layers of CdTe, however, established the existence of this form and showed that it had a wurtzite structure with spacings $a = 4.56$ kX, $c = 7.46$ kX.

We should note that before the publication of these data, the authors of [5], studying the properties of cadmium telluride, drew attention to the large scatter in activation-energy values for various samples and a fall in the activation energy for some samples at high temperatures. According to V. P. Zhuze, these phenomena were due to the existence of hexagonal CdTe along with the cubic form in the samples studied. Our results completely support this view.

In the present communication we shall be concerned with the interpretation of point electron-diffraction pictures obtained from films of CdS, CdSe, and CdTe.

Among these electron-diffraction pictures we studied various orientations of the crystals relative to the substrates and of the hexagonal and cubic forms relative to each other. While analyzing the diffraction pictures, we considered the possibility of unequivocally indexing point photographs in cases where the sample contained a mixture of crystals with the structural types of wurtzite and sphalerite, with an exact ratio of the lattice spacings. The samples for study were prepared by vacuum sublimation on to substrates of mica or rocksalt heated to 200 or 300°C.

Figures 1 and 2 show electron-diffraction photographs taken in reflection from a CdTe sample pre-

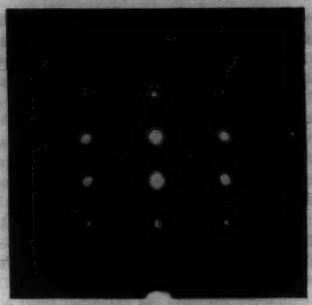

Fig. 1. Electron-diffraction reflection photograph of CdTe (I).

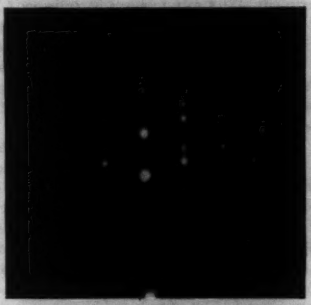

Fig. 2. Electron-diffraction reflection photograph of CdTe (II).

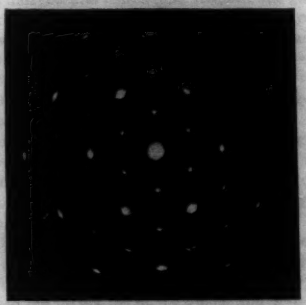

Fig. 3. Electron-diffraction photograph of a single-crystal film of CdTe.

pared by sublimation onto mica heated to 300°C. The diffraction photograph of Fig. 3 was obtained from the same sample after removing it from the mica (the film was removed from the substrate after leaving the sample for a short period on a water surface and then carefully pressing). This diffraction picture was indexed on the basis of a hexagonal lattice, although this did not mean that there were no cubic crystals in the specimen.

The question of the phase composition of this sample was solved after analyzing the reflection photographs. The first of these (see Fig. 1) could be indexed on the basis of either a cubic or a hexagonal lattice. On indexing with hexagonal axes, the disposition of the reflections on the diffraction photograph corresponded to the plane $hh\bar{2}hl$ of the reciprocal lattice (Fig. 4), i.e., the $[\bar{1}100]$ direction in the crystal was parallel to the electron beam (Fig. 5).

On indexing with cubic axes, hhh reflections were situated on the central line and reflections of the $h+2l$, $h-2l$, h type (h and l of the same parity) on the other lines (Fig. 6). This corresponds to a section of the cubic reciprocal lattice by the $(11\bar{2})$ plane, i.e., the $[11\bar{2}]$ direction of a cubic crystal with its (111) face on the substrate was parallel to the electron beam (Fig. 7).

Thus, the choice between one modification and another cannot be made from this electron-diffrac-

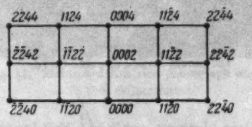

Fig. 4. Plane $hh\bar{2}hl$ of the reciprocal lattice of hexagonal CdTe.

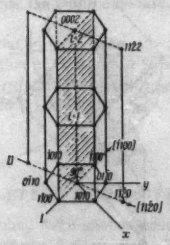

Fig. 5. Two sections of the reciprocal lattice of hexagonal CdTe.

tion photograph. In order to resolve this question, the sample must be turned so that the diffraction pattern gives $h0\bar{h}0$ reflections not coinciding with reflections from the cubic phase, i.e., it must be turned through 30 or 90° in azimuth (see Figs. 5 and 7). Then, in the case of hexagonal crystals, the reflections should appear as in Fig. 8, and in the case of cubic as in Fig. 9. However, the actual disposition of the reflections on the electron-diffraction photograph of Fig. 2, obtained from the same sample after 90° rotation, corresponded to neither the first nor the second case.

Nevertheless, all the reflections of this photograph could be indexed on the basis of a cubic lattice. In fact, if we reflect the lattice shown in Fig. 9 in the [hhh] line, we obtain exactly the same disposition of reflections as in the electron-diffraction picture of Fig. 2 (Fig. 10). Reflection of the lattice of points in the [hhh] line indicates the existence of two orientations (twins) of cubic CdTe crystals. The arrangement for indexing this kind of diffraction pattern is given in detail in [7]. Hence, the main reflections of the photographs analyzed correspond to crystals of the cubic form disposed with the (111) face parallel to the (0001) of the mica and the [110] direction parallel to the $[11\bar{2}0]$ of the mica. The same orientation is found on evaporating silver on the (0001) face of silicon carbide [6], mica, and molybdenite [7].

As well as the main reflections, the electron-diffraction pictures of Figs. 1 and 2 contain weak reflections from the hexagonal phase. The mutual disposition of the cubic and hexagonal forms may be described as $(111)_c \| (0001)_h$ and $[1\bar{1}0]_c \| [11\bar{2}0]_h$.

Thus, analysis of electron-diffraction patterns in reflection and transmission enables us to deter-

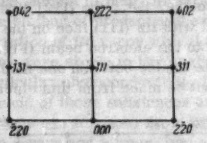

Fig. 6. Plane $h + 2l, h - 2l, h$ of the reciprocal lattice of cubic CdTe.

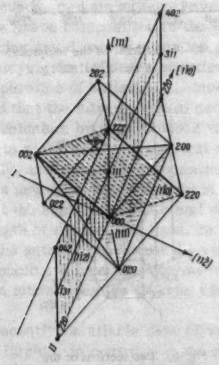

Fig. 7. Two sections of the reciprocal lattice of cubic CdTe.

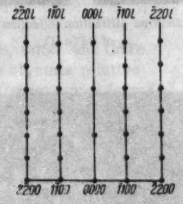

Fig. 8. Plane $h\bar{h}00$ of the reciprocal lattice of hexagonal CdTe.

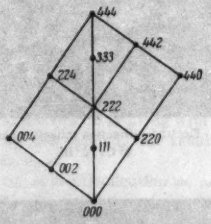

Fig. 9. Plane lhl of the reciprocal lattice of cubic CdTe.

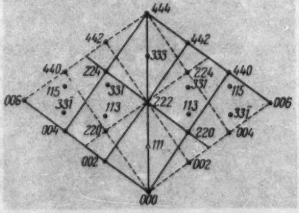

Fig. 10. Arrangement of reflections on the electron-diffraction picture of Fig. 2.

mine the phase composition of the samples, even when many of the reflections from the two phases coincide, as in the case of CdTe.

Apart from the reflections indexed on either a cubic or a hexagonal lattice, the electron-diffraction photographs also showed many superfluous reflections and continuous lines in the form of crosses and hyperbolas. Typical of this case is the diffraction picture of Fig. 11, obtained from the same sample as the previous ones, but turned slightly away from position I (by 2 to 3°). Diffraction pictures with superfluous reflections and continuous lines were also obtained in transmission.

The presence of irrational reflections and continuous lines indicates the complex structure of the CdTe layers. Some of these reflections are situated on lines joining the main reflections, dividing the distance between the latter in ratios of 1 : 3 and 2 : 3. According to present views [7], the presence of these reflections results from twinning of the crystals along the (111) plane in the region of contact between film and substrate.

In the case of CdTe, a possible source of the superfluous reflections and lines lies in stacking faults of the atomic layers, some of which stack on the cubic law and some on the hexagonal; the faults may be either periodic or aperiodic.

Apart from the diffraction photographs of CdTe described, others of a rather different type were obtained (Fig. 12). A characteristic of these was the great diffuseness of the reflections from the hexagonal phase and their partial arrangement on ellipses, this being associated with a large c spacing. An attempt to determine this quantity met with no success, since the individual reflections, in view of the small resolving power of the crystallites, merged into continuous ellipses and gave a picture reminiscent of two-dimensional diffraction. It may be that in this case the hexagonal phase was based on some other kind of packing analogous to one of those of SiC.

On studying samples of CdS and CdSe, both forms of crystals were observed, just as in the case of CdTe; for CdS, subsequent annealing increased the amount of the hexagonal phase, while for CdSe it increased the amount of the cubic phase. These results entirely confirm the views expressed in the paper mentioned earlier [2].

On condensing cadmium and sulfur or selenium onto crystal faces of NaCl or mica, polycrystalline samples are obtained. Annealing these samples leads to the formation of individual and quite large crystallites, oriented in a definite fashion relative to the substrate. If mica sheet is used as substrate,

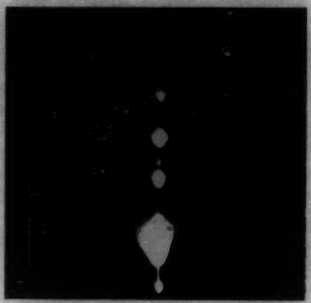

Fig. 11. Electron-diffraction photograph of CdTe with superfluous reflections and lines.

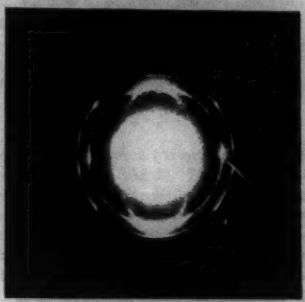

Fig. 12. Electron-diffraction photograph with diffuse reflections.

the hexagonal CdS and CdSe crystals are disposed with their basal faces parallel to the substrate and the $[11\bar{2}0]$ direction parallel to the $[11\bar{2}0]$ of the mica; as regards the cubic crystals, these remain unoriented.

On using NaCl crystals as substrate, the following orientation of CdS and CdSe was observed: $(100)_c \parallel (100)_{NaCl}$ and $[100]_c \parallel [100]_{NaCl}$; $(0001)_h \parallel (100)_{NaCl}$, and $[11\bar{2}0]_h \parallel [100]_{NaCl}$.

LITERATURE CITED

1. R. Frerichs, "The photoconductivity of 'incomplete phosphors'," Phys. Rev., 72, 594 (1947).
2. B. T. Kolomiets and E. K. Putseiko, "Differential spectral photoelements," ZhTF, 17, 818 (1947).

3. Strukturbericht, Bd. I (Leipzig, 1931).
4. S.A. Semiletov, "Electron-diffraction study of the alloy system Cd–Te," Tr. Inst. Kristallogr. 11, 121-124 (1955).
5. B.I. Boltaks, P.P. Konorov, and O.A. Matveev, "Electrical properties of cadmium telluride," ZhTF, 25, 13, 2327-2336 (1955).
6. B.K. Vainshtein and G.G. Lemmlein, "Orientation of silver on silicon carbide," Tr. Inst. Kristallogr., 6, 203-206 (1951).
7. Z.G. Pinsker, Electron Diffraction [in Russian] (Izd. AN SSSR, 1949).

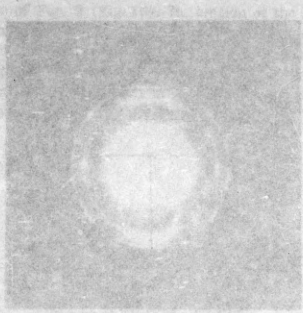

SOVIET PHYSICS – CRYSTALLOGRAPHY VOL. 1, NO. 3 MAY-JUNE, 1956

ELECTRON-DIFFRACTION STUDY OF CRYPTOHALITE

B. K. Vainshtein and M. M. Stasova

Institute of Crystallography, Academy of Sciences of the USSR

Translated from Kristallografiya, Vol. 1, No. 3,
pp. 311-320, May-June, 1956
Original article submitted March 21, 1956

The position of the hydrogen atoms in the structure of cryptohalite $(NH_4)_2SiF_6$ was investigated by constructing Fourier potential series from electron-diffraction data. The lattice spacing was $a = 8.35$ kX. The positions found for the Si, F, and N atoms confirmed earlier x-ray data. The tetrahedral NH_4 groups were distributed statistically in six positions, in each of which the vertices of the tetrahedron (hydrogen atoms) were directed toward four of the 12 fluorine atoms surrounding the NH_4 group. The space group was O_h^5–Fm3m. Analysis of the shape and height of the Si and F potential peaks indicated positive ionization of Si and negative of F.

Introduction

The structure of $(NH_4)_2SiF_6$ was studied by x-ray diffraction by Bozorth in 1922 [1]. At temperatures below 5°C, the substance has a hexagonal form, above 5°C a cubic form with a lattice spacing of $a = 8.337 \pm 0.007$ kX and four molecules per cell. This structural type is illustrated in Fig. 1 and may be described on the basis of the CaF_2 structure if the Ca atoms are replaced by SiF_6 groups and the F by NH_4. The disposition of the Si, F, and N atoms is described by the O_h^5–Fm3m space group. However, bearing in mind the tetrahedral structure of the ammonium ion NH_4, Bozorth [1] indicated that T_d^2–F43m was also a possible space group. The parameter of fluorine in the $(NH_4)_2SiF_6$ structure lay within the limits $0.200 \leq x_F \leq 0.208$.

The main problem of the present investigation was to establish the positions of the hydrogen atoms in the cubic form of cryptohalite by using Fourier potential series obtained from electron-diffraction data [2, 3, 4].

Experimental Part

The samples for electron-diffraction study at room temperature were prepared in two ways. Drying a drop of an aqueous solution of $(NH_4)_2SiF_6$ on a celluloid substrate led to the formation of lamellar texture on this. Photographs of these specimens gave electron-diffraction patterns of the so-called oblique-texture type (Fig. 2). The intensification of the Debye rings on different layer lines directly indicated the cubic symmetry of the crystals studied.

The crystallites in the texture were disposed with the octahedral faces parallel to the substrate, i.e., the texture axis was the [111] direction.

If, as is most frequently the case, the texture axis were the c axis, the number of the layer line n would be equal to the index l of any reflection lying on it. In general, if the texture axis has indices H, K, L and there are layer lines which correspond to perpendicular [HKL] planes in the reciprocal lattice, the indices of the points hkl lying in these planes, i.e., the indices of the reflections of the layer lines, are determined by the condition

$$hH + kK + lL = n, \tag{1}$$

where n is the number of the layer line. In our case [HKL] = [111], so that

$$h + k + l = n. \tag{2}$$

The reflections of the electron-diffraction picture of cryptohalite satisfy the condition characteristic of face-centered lattices: the hkl indices are unmixed. Hence, on even-layer lines we only have reflections with even hkl, and on odd-layer lines only odd ones. For example, the zero-layer line (in

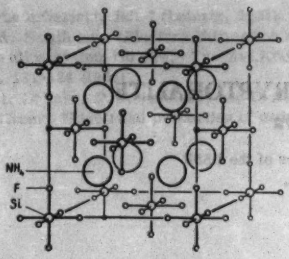

Fig. 1. Structure of $(NH_4)_2SiF_6$ according to x-ray data.

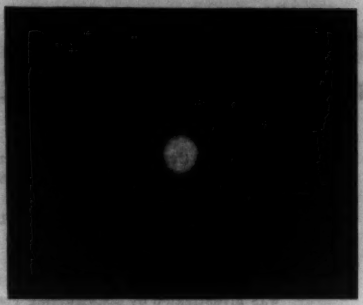

Fig. 2. Electron-diffraction photograph from a texture sample of $(NH_4)_2SiF_6$ crystallites taken at an angle of 55°.

order of increasing hkl) contained the reflections $2\bar{2}0$, $4\bar{2}\bar{2}$, $6\bar{4}\bar{2}$, etc., the first $11\bar{1}$, $3\bar{1}\bar{1}$, $13\bar{3}$, etc., the second 200, $2\bar{2}2$, $4\bar{2}0$, etc.

The disposition of the reflections along the ellipses is determined by successively adding the indices of the texture axis to those of the given reflection. For example, if the $\bar{2}20$ reflection is disposed at n = 0 on an ellipse, the next will be the $2\bar{2}0 + 111 = 3\bar{1}1$ (n = 3) reflection, then 402 (n = 6), etc. Hence, in ellipses of this type, reflections appear on every third-layer line, beginning from the zeroth. The first ellipse is an example of a second type. The sequence of reflections on this is $00\bar{2}$ (n = $\bar{2}$), $11\bar{1}$ (n = 1), 220 (n = 4). Since electron-diffraction pictures of a textured sample must necessarily have a horizontal plane of symmetry, a difference in the sign of n is of no significance, so that reflections on ellipses of the second type appear twice as often, for the very values of n for which reflections are absent in ellipses of the first type, namely, n = 1, 2, 4, 5, 7, 8, ... An analogous disposition of reflections characterizes electron-diffraction pictures of oblique textures of rhombohedral crystals.

On sublimation in air, polycrystalline samples giving photographs of the type of Fig. 3 were obtained.

Both polycrystalline and textured samples were photographed with multiple exposures in order to determine the intensity of the reflections. In the first stages of the work, visual estimates were used. Later, oblique-texture photographs were measured on a microphotometer with an objective reading (MF-2) and photographs of polycrystalline samples on an MF-4 recording microphotometer.

From each group of measurements, photographic-plate blackening curves were constructed and the intensities of the reflections determined. The transformation from intensities I to relative amplitudes was made by the formulas derived in [5]. For texture photographs

$$|\Phi_{hkl}| = \sqrt{I/d_{hkl} \cdot d' \cdot p}, \tag{3}$$

where d_{hkl} is the interplanar spacing of the given reflection, d' is that of the zero-layer line reflection on the same ellipse, and p is the recurrence factor.

For photographs of polycrystalline samples

$$|\Phi_{h\ l}| = \sqrt{I/d^4_{hkl} \cdot p}. \tag{4}$$

In the final calculations, for the majority of reflections we used the values of $|\Phi|$ obtained from the photographs of the polycrystalline specimen. In order to find the $|\Phi|$ of reflections with small recurrence factors (for example, the h00 type), giving very weak rings on the polycrystal photographs, and also for cases in which reflections with different indices merged into a common ring (for example the 511 and 333 types), reflection intensities from texture patterns were used.

From photographs with a standard we found $a = 8.35 \pm 0.03$ kX in agreement with [1]. The smallest interplanar distance (reflection $10 \cdot 6 \cdot 4$) for which the intensity could be measured was 0.677 kX corresponding to $\sin\theta/\lambda = 0.738 \cdot 10^8$. Altogether, 67 independent reflections were used; allowing for the recurrence factors, this gave 1770 terms for constructing the Fourier series.

Fourier Potential Series of the $(NH_4)_2SiF_6$ Structure

The construction of Φ^2 series confirmed the validity of Bozorth's model [1] and his value of the parameter x_F. In order to construct Fourier po-

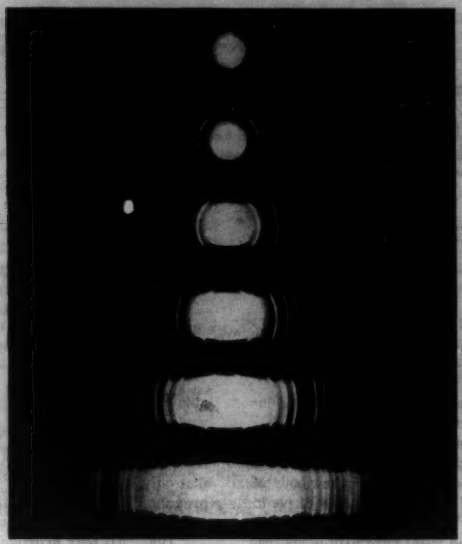

Fig. 3. Electron-diffraction photographs with multiple exposures for a polycrystalline sample of $(NH_4)_2SiF_6$.

tential series, the signs of the structure amplitudes were calculated from the formula

$$\Phi_{hkl} = \Phi_{hkl}(\mathrm{Si,F,N}) + \Phi_{hkl}(\mathrm{H}),$$

$$\Phi_{hkl}(\mathrm{Si,F,N}) = 4f_{Si} + 8f_N \cos 2\pi\frac{h}{4}\cdot\cos 2\pi\frac{k}{4}\cdot\cos 2\pi\frac{l}{4}$$

$$+ 8f_F(\cos 2\pi hx + \cos 2\pi ky + \cos 2\pi lz), \qquad (5)$$

with atomic amplitudes f from the data of [6]. The main part in the calculation of Φ_{hkl} was played by the $\Phi_{hkl}(\mathrm{Si,F,N})$ term, but it was still necessary to consider the $\Phi_{hkl}(\mathrm{H})$, i.e., the scattering by hydrogen atoms. As regards the positioning of these, the following possibilities seemed admissible.

I. The tetrahedral NH_4 groups are rigid. The symmetry of cubic space groups then allows only such a disposition of tetrahedra in the eight octants that the H atoms lie on the space diagonals of the octants. If all the tetrahedra are oriented similarly (model Ia), the symmetry of the structure is T_d^2. The NH_4 group is surrounded tetrahedrally by SiF_6 groups, so that its nearest neighbors are 12 F atoms, three from each SiF_6 group (see Fig. 1). In this model, in half of the octants the H atoms are turned toward the SiF_6 groups and in the other half they are directed into empty vertices of octants $\frac{1}{2}00$). This makes the model improbable from the point of view of crystal chemistry. If the vertices of the rigid tetrahedra are directed toward the SiF_6 groups in all the octants (model Ib), the space group of the structure is O_h^5, with a center of symmetry.

II. The NH_4 groups are distributed statistically over the two orientations considered, as occurs, for example, in the structure of NH_4Cl. The symmetry of this model is O_h^5. In projection on the cube face, models Ia, Ib, and II are indistinguishable. The hydrogen atom in the NH_4 group is easily seen on the Fourier-potential projection under conditions such as exist, for example, in the NH_4Cl structure, as shown in Fig. 4 [7].

III. The NH_4 groups exist in a state of spherical rotation. The symmetry of this model is O_h^5.

IV. The NH_4 groups are distributed statistically over orientations other than those in model II. The need to consider model IV arose in the course of the investigation.

On allowing for scattering by hydrogen atoms, it was found that, among the Φ_{hk0} amplitudes re-

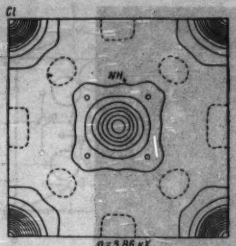

Fig. 4. Potential projection of NH_4Cl structure [7].

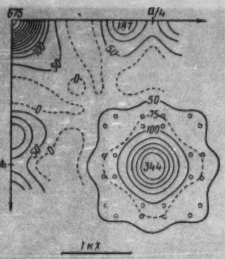

Fig. 5. Potential projection of $(NH_4)_2SiF_6$ structure on the cube face. The isolines are drawn every 50 V · kX. The figures indicate the potential values (V · kX). The circles indicate the positions of the statistically distributed H atoms.

quired for constructing the projection, the signs remained unchanged for all models, and of the Φ_{hkl} amplitudes only one changed sign (weak reflection) in model Ib.

Figure 5 shows the Fourier-potential projection on the cube face constructed from the Φ_{hk0}. The result presented in this figure was verified by constructing similar syntheses from several different values of Φ obtained with different methods of intensity measurement on several series of photographs. The synthesis of Fig. 5 is constructed on the basis of the best and most carefully measured diffraction photographs. According to this projection, models Ia, Ib, and II must certainly be rejected, since these should give a clear H peak, as in Fig. 4. At the same time the presence of H atoms near the peak into which the 2 N are projected is quite apparent, since the 2 N peaks, in contrast to the Si + 2 F and F, have a clear zone of increased potential around them. The protuberances of potential due to the hydrogen atoms are directed in the projection toward the Si + 2 F peak at the origin of coordinates and toward the F peaks.

The existence of these protuberances, confirmed later by constructing a three-dimensional synthesis, compels us to reject model III with the spherical rotation also, as this would (within the limits of error) give a spherically symmetrical distribution of potential around the nitrogen atom.

The directional aspect of the hydrogen protuberances toward the fluorine atom directly indicates that in the $(NH_4)_2SiF_6$ structure the NH_4 tetrahedra are disposed in such a way that the H atoms approach the F. Since a distortion of the valence angles in the tetrahedra is most improbable, we must admit a statistical orientation of the tetrahedra, in each of which the H atoms only approach some of the 12 F atoms symmetrically surrounding the NH_4 group (model IV). This model is conceivable in several variants, reminding one of possible variants of the orientation of the ND_4 group in the high-temperature form of ND_4Br [8], for which a trial-and-error neutron-diffraction method showed that only those models for which the D atoms approached the Br were admissible.

Let us consider various forms of model IV.

IVa. All four hydrogen atoms approach four F atoms in such a way that the $\bar{4}$ axis of the NH_4 tetrahedron coincides with the $\bar{4}$ axis of the cell (Fig. 6a). Six such equivalent orientations of the tetrahedron exist; the H atoms occupy a 192-fold position (j) xyz with weight $1/6$.

IVb. Three H atoms approach the F atoms, so that the three-fold axes remain common to the tetrahedron and the cell (Fig. 6b); there are eight such equivalent orientations. These three H atoms are distributed with weight $1/6$ over the same positions 192 (j) with different parameters; the fourth H atom (weight $1/4$) occupies position 32 (f) xxx on the three-fold axis.

IVc. As a result of the loss of coincidence between the 3-axis of the cell and tetrahedron, two H atoms still come fairly close to F atoms, but the third moves away (Fig. 6c). There are 24 such orientations of the tetrahedron.

IVd. Only one H atom approaches an F, occupying a 96 (k) xxx position with weight $1/12$; the three other hydrogens rotate around the NH... F line (Fig. 6d).

The potential values in the protuberances found in the syntheses can (within the limits of error) only be matched with models IVa and IVb for the positions of the H atoms. In the other two models, the statistical aspect of the H positions is so great that the

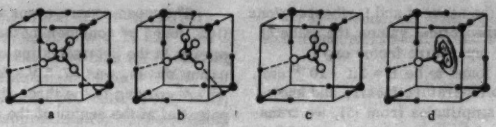

Fig. 6. One octant of the $(NH_4)_2SiF_6$ structure. Variants of model IV with H atoms approaching (a) four, (b) three, (c) two, and (d) one F atom. For each variant only one of the symmetrically possible orientations of the tetrahedron is shown. In the cryptohalite structure, model IV (a) is realized.

potential picture from these would be scarcely distinguishable from that of spherical rotation, which is not supported by the syntheses.

However, like IVc and IVd, model IVb is improbable for another reason. It fails to indicate what makes the nitrogen atom remain exactly in the position ¼ ¼ ¼, without being displaced toward the three, two, or one fluorine atom associated with the H atoms of the NH_4 group. At the same time, in the most-symmetrical model IVa, the N atom is correctly disposed among the four H, occupying the position ¼ ¼ ¼. Thus, model IVa, which agrees best with the synthesis picture (Figs. 5 and 7) is also most natural from the crystal-chemistry point of view.

Owing to the proximity of the xyz and yxz positions (the x and y values being close together, see below), in calculating $\Phi(H)$ we may replace the 192-fold position (j) xyz by the 96-fold (k) $x\,x'z$ [$x' = (x+y)/2$], i.e., suppose that H atoms are disposed in (k) with weight ⅓. This calculation, according to the formula

$$\Phi(H) = 32\frac{f_H}{3}(\cos 2\pi hx \cdot \cos 2\pi kx \cdot \cos 2\pi lz + \cos 2\pi hx \cdot \cos 2\pi lx \cdot \cos 2\pi kz + \cos 2\pi kx \cdot \cos 2\pi lx \cdot \cos 2\pi hz), \quad (6)$$

showed that $\Phi_{hkl}(H)$ did not change the signs of Φ_{hkl}(Si, F, N). The construction of a differential projection of the cube face with subtraction of the Si, F, and N atoms showed maxima corresponding to the model in question.

We then constructed the section of a three-dimensional Fourier potential series along the diagonal plane [110] in which the Si, F, and N atoms were situated, so that near the N–F line one might expect a peak with a weight of around ⅓ H (from two neighboring positions with weight ⅙). In fact, a protuberance of the N potential was found in the corresponding site (Fig. 7). Two other protuberances were comparable in magnitude with this; the appearance of these, however, may be explained (apart from possible errors) by the fact that they coincided with the closest approach of the remaining H atoms to the [110] plane. The three-dimensional differential synthesis gave peaks instead of protuberances; the greatest of these lay almost exactly on the N–H...F line at a distance of 1.03 kX from the "subtracted" N atom. The potential of this peak was 12 V at the maximum, which agrees with the expected value since, according to theoretical calculations [9] and experimental data for the H atom, $\varphi(0) = 30$–40 V, i.e., for ⅓H, $\varphi(0) = 10$–13 V.

Fig. 7. Section of three-dimensional potential series of $(NH_4)_2SiF_6$ in the (110) plane. Isolines drawn every 30 V. Crosses indicate the position of the ⅓ H peak found from differential synthesis.

Normalization of the Series. Measuring Errors. Positions of the Atoms

With increasing $(\sin\theta)/\lambda$, the $|\Phi_{exp}|$ obtained from the formulas of kinematic theory [5] fell off more rapidly than the $|\Phi_{theor}|$ from [6]. On the one hand, this indicated the kinematic character of the scattering (since, in the case of dynamic scattering, for which $|\Phi| \sim I$, use of a formula of the type $|\Phi| \sim \sqrt{I}$ would give a $|\Phi_{exp}|$ too high by comparison with $|\Phi_{theor}|$ on increasing $(\sin\theta)/\lambda$, and on the other hand it indicated the necessity of introducing the temperature factor. By comparing the averaged

values of $|\Phi_{exp}|$ for the nearest and farthest regions of $(\sin\theta)/\lambda$ with the theoretical values, the value of parameter B in the temperature factor $\exp\cdot\{-B[(\sin\theta)/\lambda]^2\}$ was found to be $B = 1.0 \cdot 10^{-16}$ cm^2.

Introducing the temperature factor, and knowing the values of the amplitudes from (5), we transformed to the values of Φ'_{hkl} in volts by way of the formula

$$\Phi'_{hkl}(\text{volt}) = 114.5 \cdot \frac{\Phi_{hkl}}{\Omega}, \qquad (7)$$

where Ω is the volume of the cell in kX^3, in the present case 580 kX^3. Then, from the first 12 strong reflections with small $(\sin\theta)/\lambda$, the experimental amplitudes were normalized to values in volts by the relation

$$\Sigma|\Phi'_{exp}| = \Sigma|\Phi_{theo}|. \qquad (8)$$

The values of the theoretical and experimental structure amplitudes are given in Table 1.

The construction of a three-dimensional Fourier series from the Φ'_{exp} gives the potential distribution in volts; the construction of a projection after multiplying by the length of the projecting edge ($c = 8.35$ kX) gives a projection in units of V · kX [3].

The theoretical term $\Phi_{000} = 7.8$ V was also introduced into the series (average internal potential).

The values of $\varphi'(0)$ in the potential projection at the centers of the peaks were 675 V · kX for Si +2 F, 187 V · kX for F, and 344 V · kX for 2 N, whence $\varphi'(0)_{Si} = 301$ V · kX and $\varphi'(0)_N = 172$ V · kX.

The mean-square error in the potential projection, found by considering the combined effects of errors in the determination of amplitudes and truncation waves, was 17.5 V · kX.

According to the three-dimensional series, the potential at the center of the atoms $\varphi(0)$ was 422 V for Si, 276 V for F, 220 V for N, and 12 V for $\frac{1}{8}$H, i.e., 36 V for H.

The mean-square error in determining the potential was about 6 V.

The reliability factor R was taken for the value of the mean-square error in determining the amplitudes, where

$$R = \Sigma\big||\Phi_{theo}| - |\Phi_{exp}|\big| / \Sigma|\Phi_{exp}|, \qquad (9)$$

is calculated with allowance for the zero amplitudes, i.e., those for which $|\Phi_{exp}| = 0$ but $|\Phi_{theor}| \neq 0$. This value was R = 18.3%; if the zero amplitudes were not counted, then R = 14.8%.

The atoms in the structure of cryptohalite are disposed as follows. In the space group O_h^5, Si occupies the position 4(a)000, N the 8(c) $\frac{1}{4}$ $\frac{1}{4}$ $\frac{1}{4}$, F the 24(e)x00. From the three-dimensional series we find $x_F = 0.200_5$.

The hydrogen atoms are statistically distributed with weight $\frac{1}{8}$ in the position 192(j)xyz. Putting the N–H distance equal to 1.00 kX, we may calculate from model IVa that x = 0.156, y = 0.178, and z = 0.231. From the three-dimensional differential synthesis we found $x' = (x+y)/2 = 0.168$, z = 0.235, which confirms the x and y values in question and directly determines the z. The Si–F dis-

TABLE 1. Experimental and Theoretical Structure Amplitudes (in V · 100)

hkl	Φ_{exp}	Φ_{theor}	hkl	Φ_{exp}	Φ_{theor}	hkl	Φ_{exp}	Φ_{theor}
111	191	+261	800	51	+ 88	10.2.2	—	—21
200	81	+ 86	733	56	— 60	666	—	+ 2
220	224	+182	820	31	— 26	953	32	+28
311	86	+ 60	644	27	+ 23	10.4.0	39	+39
222	236	—217	822	27	— 32	864	4	— 4
400	298	+316	660	72	+ 85	10.4.2	34	+32
331	48	— 12	751	26	+ 31	11.1.1	28	+16
420	44	+ 37	555	87	+107	775	6	— 3
422	49	+ 28	662	—	— 24	880	—	+22
333	110	—118	840	54	+ 50	11.3.1	9	+ 6
511	133	+143	911	45	+ 44	971	22	+10
440	183	+187	753	1	— 6	955	34	+46
531	94	+ 54	842	31	— 35	10.4.4	28	+26
600	126	+117	664	49	+ 56	882	34	—32
442	9	+ 8	931	24	+ 28	10.6.0	39	+51
620	96	+ 75	844	38	+ 36	886	12	+15
533	8	+ 12	933	7	— 7	11.3.3	—	—12
622	56	— 72	771	22	— 20	973	—	— 8
444	104	+125	755	37	+ 34	10.6.2	—	+ 3
711	11	+ 10				12.0.0	—	+34
551	125	+122	10.0.0	38	+ 56	884	—	+ 8
640	71	+ 55	860	19	+ 6	11.5.1	25	+24
642	49	+ 46	10.2.0	54	+ 49	777	28	—43
731	25	— 26	862	2	+ 2	12.2.0	16	—12
553	56	+ 58	951	37	+ 48	12.2.2	10	—10
			773	28	— 35	10.6.4	33	+34

tance equals 1.674 ± 0.006 kX, the N–H is 1.03 ± 0.11 kX, and the H...F, 1.95 ± 0.11 kX.

It should be noted that conditions for observing H atoms with effective atomic number $Z = \frac{1}{2}$ in the cryptohalite structure in the presence of N (Z = 7), F (Z = 9), Si (Z = 14) (approximately corresponding to the determination of an "ordinary" H atom in a structure with mean atomic number 30 for the heavy atoms) are extremely unfavorable. In fact, the height of the peaks corresponding to the statistically distributed H atoms is only twice as large as the error in measuring the potential. Hence, although in electron diffraction the ratio of peak heights differs from the ratio of atomic numbers in the sense favorable toward light atoms (allowing hydrogen to be localized in organic compounds to the high accuracy of about 0.03 kX) in the present case such accuracy could not be attained.

Thus, the data of the present investigation indicate that cryptohalite is represented by model IVa, with a statistical distribution of NH_4 tetrahedra in six orientations, corresponding to the disposition of H near the N–F straight lines. Thermal motion causes constant interchange between these orientations.

The value of the N–H distance in the tetrahedron, 1.03 kX, agrees very well, within experimental error, with data from electron-diffraction, neutron-diffraction, and other determinations, giving the value ~1.00 kX, and again confirms the covalent character of this bond.

The orientation of the NH_4 tetrahedra must be explained by the existence of a weak H–F attraction; this is less clearly expressed, for example, than the hydrogen bond in the NH_4F structure, since the N–H...F distance here is 2.96 kX, while in NH_4F and NH_4HF_2 it is 2.63 kX.

Ionization of the Si and F Atoms

By analyzing the shapes and sizes of the potential peaks we may draw certain conclusions regarding the state of the electron shell of the atoms. It is most convenient to do this for Si and F, since, in the case of N consideration is complicated by the effects of the hydrogen-atom potentials.

Let us first consider a simple model of an atom in the form of a spherical condenser, qualitatively examining the effect of a contraction of the electron shell and the effect of ionization on the resultant potential of the atom, this being given by the difference between the potential of the nucleus and that of the electron shell

$$\varphi_{at} = \varphi_+ - \varphi_-. \qquad (10)$$

For a condenser with a point charge $+Z_1e$ inside a spherical shell of radius R with charge $-Z_2e$,

$$\varphi_+ = \frac{Z_1 e}{r}, \qquad (11a)$$

$$\varphi_- = \begin{cases} \frac{Z_2 e}{R} \text{ for } r \leqslant R \\ \frac{Z_2 e}{r} \text{ for } r > R \end{cases} \qquad (11b)$$

The behavior of the potential in the model of a neutral atom ($Z_1 = Z_2$) is shown in Fig. 8a. We see from the figure that the φ_{at} curve may be obtained by omitting the φ_+ curve, since, for r = R, $\varphi_{at} = 0$. Curves for an anion ($Z_1 < Z_2$) and cation ($Z_1 > Z_2$) are obtained analogously and are shown in Fig. 8b; in contrast to the neutral atom, the cation has a region of positive potential extending to infinity, and the anion has a region of negative potential, which outside the R "boundary" has the value $[(Z_1 - Z_2)/r] \cdot e$. At the center of an atom at rest, the potential tends to infinity $\left(\varphi(0) = \frac{Z_1 e}{r}\Big|_{r=0} - \frac{Z_2 e}{R}\right)$. If, however, we remember the thermal motion, the singular point r = 0 becomes diffused, and φ_+, and hence φ_{at}, take on finite positive values. Taking all this into account, we arrive at the conclusion that positive ionization of the atom "broadens" the potential peak and increases the value of the potential at the maximum $\varphi(0)$, while negative ionization "compresses" the peak and reduces $\varphi(0)$ (Fig. 8b).

Figure 9 shows the form of the Si and F potential peaks in the structure of cryptohalite according to the three-dimensional synthesis from experimental data. For convenience of comparison, the peaks are arbitrarily referred to the same height. The more compressed form of the F and the lower potential at the periphery indicates, in accordance with the foregoing argument, that the ionization is

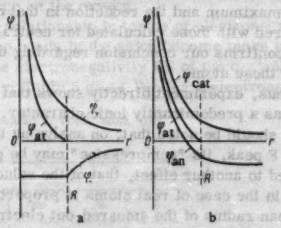

Fig. 8. (a) Superposition of φ_+ and φ_- in the spherical-condenser model of the atom; (b) different behavior of potential for a cation, neutral atom, and anion.

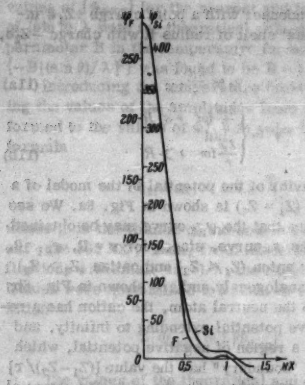

Fig. 9. Potential distribution at Si and F peaks (along directions [110] and [100], respectively), in volts.

negative, while for Si it has the opposite sign. Let us now consider the values of $\varphi(0)_{Si} = 442$ V and $\varphi(0)_F = 276$ V. From theoretical considerations [9] and experimental data confirming these (see, for example [4]), it follows that the ratios of potential-peak heights for neutral atoms in electron diffraction obey a law of the form $(Z_1/Z_2)^{\alpha}$, $\alpha < 1$ (Z = atomic number). Theoretical calculation of $\varphi(0)$ for neutral Si and F, with B = 1 and truncation of the series at $(\sin\theta/\lambda) = 0.74 \cdot 10^8$, shows that we may expect values $\varphi(0)_{Si} \simeq 420$ V and $\varphi(0)_F \simeq 290$ V, i.e., $\varphi(0)_{Si}/\varphi(0)_F = 1.44$ ($\alpha = 0.87$), whereas experiment gives $\varphi(0)_{Si}/\varphi(0)_F = 1.6$, which even slightly exceeds the ratio of the atomic numbers $Z_1/Z_2 = 1.56$.

The increase in the experimental potential at the Si maximum and the reduction in that of F, as compared with those calculated for neutral atoms, again confirms our conclusion regarding the ionization of these atoms.

Thus, experiment directly shows that the Si–F bond has a predominantly ionic character.

It should be noted that, on analyzing the shape of the F peak, its "compression" may be partly attributed to another effect, that of the value of R, which in the case of real atoms is proportional to the mean radius of the smeared-out electron shell. Reducing this also compresses the potential peak, but without reducing $\varphi(0)$ (see Fig. 8a). This reduction, or contraction of the electron shells toward the nucleus, occurs as the shells fill up inside a given period of Mendeleev's system with increasing Z; it may play a considerable part in the case of the F atom, which is next to last in the second period.

Conclusions

Electron-diffraction study of cryptohalite has enabled us to determine the positions of the hydrogen atoms of the NH_4 group; this group is distributed statistically over six positions. The construction of Fourier series reveals weak potential protuberances near the N atom; these come from statistically distributed hydrogen atoms, and lead to the model described in the text. Detection of these atoms roughly corresponds to the detection of an ordinary hydrogen atom in a crystal with heavy atoms of atomic number 30; this shows that H atoms can be determined in such structures by electron diffraction. Analysis of the shape and height of the F and Si potential peaks reveals the state of ionization of these atoms.

LITERATURE CITED

1. Z. Bozorth, "The crystal structure of ammonium fluorosilicate," J. Am. Chem. Soc., 44, 1066-1070 (1922).
2. B. K. Vainshtein and Z. G. Pinsker, "Use of harmonic analysis in electron diffraction," DAN SSSR, 64, 49-53 (1949).
3. B. K. Vainshtein, "Study of crystal-lattice potential by electron diffraction," Tr. Inst. Kristallogr., 9, 259-276 (1954).
4. B. K. Vainshtein, "Electron-diffraction study of crystals with hydrogen bonds," Tr. Inst. Kristallogr., 10, 115-127 (1954).
5. B. K. Vainshtein, "Kinematic theory of the intensities of electron-diffraction reflections," Kristallografiya, 1, 2, 150-158 (1956).
6. B. K. Vainshtein, "Atomic scattering factors of electrons," ZhÉTF, 25, 2, 157-168 (1953).
7. M. M. Stasova and B. K. Vainshtein, "Refining the structure of the NH_4 group in ammonium chloride," Tr. Inst. Kristallogr., 12, 18-24 (1956).
8. H. A. Levy and S. W. Peterson, "Neutron diffraction determination of the crystal structure of ammonium bromide in four phases," J. Am. Chem. Soc., 75, 1536-1542 (1953).
9. B. K. Vainshtein, "Heights of maxima in electron-density and potential syntheses," Tr. Inst. Kristallogr., 11, 78-84 (1955).

REFRACTIONS FOR HYDROGEN BONDS IN INORGANIC COMPOUNDS—PART 2*

S. S. Batsanov and A. S. Sonin

M. V. Lomonosov State University, Moscow
Translated from Kristallografiya, Vol. 1, No. 3, pp. 321-327, May-June, 1956
Original article submitted October 1, 1955

Bonds of type xH...O have been examined by refractometry; the bond refraction is found to vary in the same sense as the effective charge on the oxygen atom.

Part 1 [1] presented refractions for various types of hydrogen bonds, which were found to be dependent on the effective negative charges on the atoms in the bond. For instance, the refraction of $_N$H...O in ammonium salts increases with the charge on the anion containing the oxygen. The method of calculation used here differs from that of [1] in that the refractive index is extrapolated to $\lambda = \infty$ strictly in accordance with Wulff's method [2] (reciprocal of the Lorentz-Lorenz function plotted against square of frequency), which gives results of fixed accuracy for different classes of compound. The altered method of extrapolation may affect the absolute values slightly, but it is without effect on the sequence for different bonds.

Table 1 gives results for potassium and ammonium bromides and iodides, with the values extrapolated to $\lambda = \infty$.

From n_∞ and the measured densities we get the molar refractions listed in Table 2.

These results show that the mean difference of the ionic refractions is $\Delta\bar{R} = R_{NH_4^+} - R_K = 1.60$ cm^3; this may be used with the differences between the molar refractions for potassium and ammonium oxysalts to determine the $_N$H...O refraction.

Table 3 gives the refractive indices of various such salts as measured at fixed wavelengths and extrapolated to $\lambda = \infty$; the molar refractions were calculated by averaging the refractive indices from $\bar{n} = (n_g \cdot n_m \cdot n_p)^{1/2}$. Table 4 gives the $\bar{n}_\infty$, which with the densities (own measurements, or taken from the literature if both salts were measured by the same worker) give the molar refractions (also listed in Table 4). We subtract 1.60 cm^3 from the difference of the molar refractions to give ER (the exaltation of the refraction) due to the hydrogen bonds (Table 4).

The compounds in Table 4 are listed in order of increasing field strength for the central atom in $[EO_n]^{m-}$; $_N$H...O bonds have refractions ranging from 0.17 to 0.50 cm^3 per ammonium ion and varying inversely as the polarizing action of the central atom in the anion, i.e., increasing with the polarity of the E–O bond and hence with the effective negative charge on the oxygen.

The relationship in terms of electronegativity is that the bonds in the anion become more covalent as the electronegativity EN of the central atom increases; Table 5 gives Pauling's electronegativi-

*Part 1 appeared in Vestn. Mosk. Univ.

TABLE 1

Compound	λ (mμ)						
	486	520	555	589	620	656	∞
NH_4Br	1.731	1.724	1.717	1.712	1.707	1.704	1.672
KBr	1.572	1.567	1.563	1.559	1.557	1.555	1.536
NH_4I	1.736	1.722	1.709	1.700	1.693	1.686	1.633
KI	1.687	1.679	1.672	1.667	1.663	1.659	1.628

TABLE 2

Compound	M	d_4^{25}	n_∞	R_∞	ΔR_∞
NH_4Br	97.96	2.432	1.672	15.08	1.53
KBr	119.01	2.738	1.536	13.55	
NH_4I	144.96	2.514	1.633	20.58	1.68
KI	166.02	3.118	1.628	18.90	

TABLE 3

Compound	n	λ (mμ)						
		486	520	555	580	620	656	∞
NH_4HCO_3	n_g	1.568	1.563	1.559	1.555	1.552	1.549	1.527
	n_m	1.548	1.544	1.540	1.536	1.533	1.530	1.509
	n_p	1.430	1.427	1.425	1.423	1.422	1.421	1.410_4
NH_4NO_3	n_g	1.660	1.650	1.643	1.636	1.632	1.628	1.592_5
	n_m	1.630	1.622	1.614	1.610	1.606	1.603	1.574_5
	n_p	1.419	1.417	1.415	1.413	1.412	1.411	1.400_4
NH_4NO_3	n_g	1.655	1.646	1.639	1.632*	1.628	1.624	1.588_5
	n_m	1.518	1.514	1.511	1.508*	1.505	1.503	1.483
	n_p	1.483	1.479_5	1.476_5	1.474*	1.472	1.470_5	1.455_5
KNO_3	n_g	1.484	1.479_5	1.476_5	1.474*	1.472	1.470	1.454_5
	n_m	1.460	1.456_5	1.454	1.452*	1.450_5	1.449_5	1.437_5
	n_p	1.340	—	—	1.345*	—	1.343	1.336
NH_4VO_3	n_m	1.967	1.950	1.938	1.927	1.918	1.911	1.851
	n_p	1.802	1.788	1.777	1.768	1.762	1.756	1.708
KVO_3	n_g	1.941	1.924	1.912	1.901	1.894	1.887	1.831
	n_m	1.877	1.862	1.852	1.842	1.835	1.829	1.777
	n_p	1.749	1.737	1.720	1.720	1.715	1.710	1.668
$(NH_4)_2Cr_2O_7$	n_g	1.897	1.884	1.875	1.864	1.857	1.851	1.798
	n_m	1.815	1.802	1.793	1.783	1.777	1.771	1.723
	n_p	1.741	1.731	1.723	1.716	1.710	1.705	1.664
$K_2Cr_2O_7$	n_g	1.851	1.839	1.828	1.819	1.813	1.807	1.754
	n_m	1.766	1.754	1.746	1.738	1.733	1.728	1.687
	n_p	1.748	1.736	1.728	1.720	1.715	1.710	1.668
$(NH_4)_2HPO_4$	n_g	1.539	1.534	1.530	1.527	1.524	1.522	1.502
	n_m	1.530	1.525	1.521	1.518	1.515	1.513	1.493
	n_p	1.509	1.505	1.502	1.499	1.499	1.497	1.474
K_2HPO_4	n_g	1.519	1.514	1.510	1.507*	1.504	1.502	1.482
	n_m	1.510	1.506	1.503	1.500*	1.498	1.496	1.475
	n_p	1.501	1.497	1.494	1.491*	1.489	1.487	1.466
$(NH_4)_3Co(NO_2)_6$	n_m	1.781	1.762	1.751	1.742	1.734	1.728	1.677
$K_3Co(NO_2)_6$	n_m	1.760	1.742	1.731	1.721	1.713	1.708	1.656

*Not previously reported.

ties together with the ER appropriate to that atom. There is clearly an inverse relation between EN and ER.

The strength of the hydrogen bond also has a regular relation to the bond polarity; the refraction and bond energy increase together.

The refraction of the hydrogen bonds in NH_4NO_3 is only about half of that of those in $(NH_4)_3Co(NO_2)_6$, on account of the difference in the number of hydrogen atoms per oxygen atom (two as against one). The refraction is to be expected to be higher when there is only one hydrogen per oxygen atom, because the electron shells are more extensively distorted by polarization in one direction only.

The $_N$H...O refractions may be compared with the $_O$H...O ones known from ice and certain hydrated compounds; the refraction of the water in the

TABLE 4

Compound	M	σ_4^{25}	$\bar{n}_\infty$	R_∞	ΔR_{NH_3}	ER
$NH_4H_2AsO_4$	158.97	2.317 [3]	1.5385 [4]	21.47	2.10	0.50
KH_2AsO_4	180.02	2.879 [3]	1.5320 [4]	19.37		
$(NH_4)_3Co(NO_2)_6$	389.11	1.965	1.677	74.57	2.07	0.47
$K_3Co(NO_2)_6$	452.28	2.431	1.656	68.35		
$(NH_4)_2HPO_4$	132.07	1.622	1.490	23.54	2.06	0.46
K_2HPO_4	174.18	2.519*	1.474	19.43		
$NH_4H_2PO_4$	115.04	1.799	1.4954 [4]	18.66	2.04	0.44
KH_2PO_4	136.09	2.338	1.4830 [4]	16.62		
$(NH_4)_2Cr_2O_7$	252.10	2.155	1.728	46.59	2.03	0.43
$K_2Cr_2O_7$	294.21	2.683	1.703	42.53		
$(NH_4)_2SeO_4$	179.04	2.1940 [5]	1.5517 [6]	26.06	1.99	0.39
K_2SeO_4	221.15	3.0667 [5]	1.5245 [7]	22.08		
NH_4HCO_3	79.06	1.543	1.482	14.62	1.85	0.25
$KHCO_3$	100.11	2.163	1.464 [8]	12.77		
$(NH_4)_2SO_4$	132.15	1.772 [2]	1.513 [3]	22.42	1.85	0.25
K_2SO_4	174.26	2.666 [3]	1.485 [9]	18.73		
NH_4NO_3	64.05	1.506	1.508	12.68	1.81	0.21
KNO_3	85.10	1.931	1.408	10.87		
NH_4VO_3	116.99	2.304	1.802	21.75	1.79	0.19
KVO_3	138.05	2.840	1.758	19.96		
NH_4NO_3	80.05	1.718	1.520	14.16	1.78	0.18
KNO_3	101.10	2.096	1.427 [9]	12.38		
NH_4ClO_4	117.50	1.9518 [10]	1.4741 [11]	16.92	1.77	0.17
$KClO_4$	138.56	2.5298 [10]	1.4653 [11]	15.15		

*Not previously reported.

TABLE 5

Element	EN	ER	Element	EN	ER
As	2.0	0.50	C	2.5	0.25
P	2.1	0.45	N	3.0	0.18
Se	2.4	0.39	Cl	3.0	0.17
S	2.5	0.25			

latter must be compared with that for ice and for the anhydrous salts, or hydrated ones free from hydrogen bonds.

Table 6 gives results for certain hydrated and anhydrous salts, with extrapolation to $\lambda = \infty$; here, $A = NH_3$ in the coordination compounds.

Table 7 gives the refractions for water of crystallization in hydrates free from hydrogen bonds. The inherent refraction of the water of crystallization is found to be 3.42 cm^3.

Pulfrich [16] gives $\bar{n}_\infty$ for ice as 1.3009; the density is 0.9174 g/cm^3 [17], so the refraction at $\lambda = \infty$ is 3.68 cm^3. The production of two $_OH\ldots O$ bonds thus increases the refraction by 0.26 cm^3, or 0.13 cm^3 per bond.

These $_OH\ldots O$ bonds occur in certain hydrated crystals, especially polyhydrates, in which the water molecules form an array much as in ice, with hydrogen bonds between adjacent water molecules. In addition, these bonds link the water to the anions in gypsum and $K_2HPO_4 \cdot 3H_2O$. These bonds are detectable by refractometry.

Table 8 gives refractions for this class of compound.

In every case, the refraction of the water of crystallization exceeds the inherent values of 3.42 cm^3, which indicates that hydrogen bonds are present; these have refractions equal to or less than those of the $_OH\ldots O$ bonds in ice.

The refractions of $_NH\ldots O$ bonds in ammonium salts range from 0.04 to 0.12 cm^3, while those of the $_OH\ldots O$ ones in ice and hydrated compounds have a smaller range. In each case, the effective negative charge on the oxygen atom is the decisive factor.

TABLE 6

Compound	n	λ (mμ)						
		486	520	555	589	620	656	∞
$NaBr \cdot H_2O$	n_g	1.547	1.539	1.531	1.525	1.520	1.515	1.479
	n_m	1.540	1.532	1.525	1.519	1.514	1.510	1.477
	n_p	1.536	1.528	1.521	1.515	1.510	1.506	1.474
NaBr [12]	n_m	1.652A*	—	1.6459	1.6412	—	1.6347	1.6133
$CaSO_4 \cdot 2H_2O$ [13]	n_g	1.5355	1.5325	—	1.5300	—	1.5276	1.5186
	n_m	1.5285	1.5255	—	1.5230	—	1.5207	1.5116
	n_p	1.5262	1.5231	—	1.5207	—	1.5184	1.5094
$CaSO_4$ [14]	n_g	1.6187	—	—	1.6130	—	1.6106	1.6009
	n_m	1.5808	—	—	1.5752	—	1.5730	1.5637
	n_p	1.5747	—	—	1.5693	—	1.5672	1.5586
$BaCl_2 \cdot 2H_2O$	n_g	1.690	1.686	1.673	1.665	1.661	1.657	1.620
	n_m	1.664	1.654	1.647	1.640	1.636	1.632	1.596
	n_p	1.650	1.640	1.633	1.626	1.622	1.618	1.583
$BaCl_2$	n_g	1.770	1.758	1.750	1.742	1.736	1.731	1.688
	n_m	1.765	1.753	1.742	1.736	1.730	1.725	1.682
	n_p	1.757	1.746	1.737	1.730	1.725	1.720	1.676
$K_2HPO_4 \cdot 3H_2O$	n_g	1.490	1.486	1.483	1.480	1.477	1.475	1.458
	n_m	1.487	1.483	1.480	1.477	1.474	1.472	1.456
	n_p	1.478	1.474	1.471	1.468	1.465	1.463	1.448
$SrCl_2 \cdot 6H_2O$	n_m	1.550	1.545	1.540	1.536	1.533	1.530	1.509
	n_p	1.496	1.492	1.489	1.486	1.484	1.482	1.465
$SrCl_2$	n_m	1.676	1.666	1.658	1.650	1.646	1.642	1.606
$[Co(A_4CO_3)_2]_2SO_4 \cdot 3H_2O$	n_m	1.649	1.639	1.632	1.625	1.621	1.617	1.582
	n_p	1.601	1.593	1.587	1.582	1.578	1.575	1.545
$[Co(A_4CO_3)_2]_2SO_4$	n_g	1.695	1.685	1.678	1.671	1.666	1.662	1.626
	n_m	1.660	1.650	1.643	1.636	1.632	1.628	1.592
	n_p	1.621	1.613	1.607	1.602	1.598	1.595	1.567
$[Pt(A_2(NO_2)_2Cl_2]\,H_2O$	n_g	1.835	1.824	1.813	1.804	1.797	1.791	1.740
	n_m	1.796	1.787	1.776	1.767	1.761	1.756	1.707
	n_p	1.767	1.756	1.747	1.739	1.733	1.728	1.685
$[Pt(A_2(NO_2)_2Cl_2]$	n_m	1.815	1.803	1.793	1.784	1.777	1.770	1.720

* At 501.6 mμ.
** At 545 mμ.
*** At 667.8 mμ.
**** At 535 mμ.

TABLE 7

Compound	M	d_4^{25}	$\bar{n}_\infty$	R_∞	R_{H_2O}
$NaBr \cdot 2H_2O$	138.94	2.165 [15]	1.477	18.14	3.47
NaBr	102.91	3.198 [16]	1.6133	11.20	
$BaCl_2 \cdot 2H_2O$	244.30	3.096 [11]	1.600	26.99	3.43
$BaCl_2$	208.27	3.917 [11]	1.682	20.14	
$[Co(A_4CO_3)_2]_2SO_4 \cdot 3H_2O$	524.27	1.874	1.570	91.79	3.40
$[Co(A_4CO_3)_2]_2SO_4$	470.22	1.958	1.595	81.60	
$[Pt(A_2(NO_2)_2Cl_2]\,H_2O$	410.20	3.040	1.710	52.72	3.36
$[Pt(A_2(NO_2)_2Cl_2]$	392.18	3.138	1.720	49.36	

TABLE 8

Compound	M	d_4^{25}	$\bar{n}_{\infty}$	R_{∞}	R_{H_2O}
$K_2HPO_4 \cdot 3H_2O$	228.23	2.030	1.454	30.45	3.67
K_2HPO_4	174.18	2.519	1.474	19.43	
$CaSO_4 \cdot 2H_2O$	172.18	2.310 [10]	1.513	22.41	3.57
$CaSO_4$	136.15	2.942 [10]	1.574	15.27	
$SrCl_2 \cdot 6H_2O$	266.64	1.9663 [11]	1.494	39.48	3.63
$SrCl_2$	158.54	3.085 [11]	1.606	17.72	

LITERATURE CITED

1. S. S. Batsanov, "Refractions of hydrogen bonds in inorganic compounds. Part 1," Vestn. Mosk. Univ., 9, 95-108 (1954).
2. P. Wulff, "Ein neues Verfahren zur Darstellung des Dispersionsverlaufes im Sichtbaren und Ultravioletten," Z. Phys. Chem., B21, 368-382 (1933).
3. B. Gossner, "Beiträge zur Kenntnis der Isomorphie," Z. Krist., 44, 417-518 (1908).
4. H. Topsöe and C. Christiansen, "Recherches optiques sur quelques series de substances isomorphes," Ann. Chim. Phys., 1, 5-99 (1874).
5. A. Tutton, "Crystallized ammonium sulphate," J. Chem. Soc., 83, 1049-1074 (1903).
6. A. Tutton, "Ammonium selenate," J. Chem. Soc., 89, 1059-1083 (1906).
7. A. Tutton, "The alkali sulphates and selenates," J. Chem. Soc., 87, 1183-1189 (1905).
8. H. Merwin, International Critical Tables, 7, 27.
9. K. Krishnan and A. Dasgupta, "The pleochroism and the birefringence of the NO_3^- ion in crystals," Indian J. Phys., 8, 49-66 (1933).
10. P. Wulff and A. Heigl, "Methodisches zur Dichtebestimmung fester Stoffe," Z. Phys. Chem., A153, 187-209 (1931).
11. A. Tutton, "The alkali perchlorates," Proc. Roy. Soc., A111, 462-491 (1926).
12. K. Spangenberg, "Dichte und Lichtbrechung der Alkalihalogenide," Z. Krist., 57, 494-534 (1922).
13. A. Tutton and A. Hutchinson, "On the temperature of optical uniaxiality in gypsum," Min. Mag., 16, 257-263 (1912).
14. A. Mühlheims, "Über eine neue Art der Axenwinkelmessung," Z. Krist., 14, 202-236 (1888).
15. P. Favre and C. Valson, "Recherches sur la dissociation cristalline," Compt. Rend., Acad. Sci., 77, 577-584 (1873).
16. C. Pulfrich, "Untersuchung über die Lichtbrechungsverhältnisse des Eises und des unterkühlten Wassers," Wied. Ann., 34, 326-340 (1888).
17. S. Artsimovich and I. Parfianovich, "Das Wärmeleitvermögen des Eises," Z. Phys., 56, 441-445 (1929).
18. E. Madelung and R. Fuchs, "Kompressibilitätsmessungen an festen Körpern," Ann. Phys. 65, 289-309 (1921).

REFRACTIONS OF HYDROGEN BONDS IN INORGANIC COMPOUNDS—PART 3

S. S. Batsanoy

M.V. Lomonosov State University, Moscow

Translated from Kristallografiya, Vol. 1, No. 3,
pp. 328-333, May-June, 1956
Original article submitted December 23, 1955

Refractometry has been applied to $_{O}H\ldots N$ and $_{N}H\ldots N$ hydrogen bonds in inorganic compounds; the refraction is found to vary in the same sense as the effective negative charge on the nitrogen.

The first paper in this series [1] was concerned with all types of hydrogen bonds in inorganic compounds; the second [2] dealt with bonds to oxygen. This part deals with bonds to nitrogen.

1. The following trihydrates occur: $K_4Os(CN)_6 \cdot 3H_2O$, $K_4Ru(CN)_6 \cdot 3H_2O$, $K_4V(CN)_6 \cdot 3H_2O$, $K_4Fe(CN)_6 \cdot 3H_2O$, in which the numbers of hydrogen and nitrogen atoms indicate that the water is linked to the $[E(CN)_6]^{4-}$ group by hydrogen bonds. We have previously shown that the tendency to produce hydrogen bonds to the addends increases with the negative charge on the group, so the bonds should weaken as the valence of the metal increases. This is evidently so, for $K_3Fe(CN)_6$ is anhydrous only.

Refractometry provides a means of detecting and measuring these bond strengths.

Table 1 gives the dispersion of the ferrocyanide in its two forms; the n_g for the anhydrous form have not previously been reported.

Table 2 gives molar refractions calculated from the $\tilde{n}_\infty$, as averaged in $\tilde{n} = (n_g \cdot n_m \cdot n_p)^{1/3}$, and the densities (by pycnometer).

The result for the water in the hydrated form is 0.47 cm^3 greater than that for water itself (3.42 cm^3), on account of the two hydrogen bonds; the refraction of one $_{O}H\ldots N$ hydrogen bond is thus 0.24 cm^3.

2. The refraction of an $_{N}H\ldots N$ bond may be deduced from the molar refractions of corresponding ammonium and potassium salts. The best compounds for initial use are the hexacyanides of iron, for these most readily allow one to verify that the negative charge of the central atom bears a direct relation to the refraction (and strength) of the hydrogen bond to the addend.

The potassium salts are available for purchase; we prepared the ammonium salts, the ferrocyanide, by the method of [3], in which it is stated that neutralization of $H_4Fe(CN)_6$ with ammonia gives $(NH_4)_4Fe(CN)_6 \cdot 3.5H_2O$. The acid is readily prepared in pure form from $K_4Fe(CN)_6 \cdot 3H_2O$ [4]; titration with alkali (to phenolphthalein) showed that the product was of high purity. However, neutralization with ammonia gave a salt whose composition was not that stated in [3], but $(NH_4)_4Fe(CN)_6 \cdot 1.5H_2O$.

TABLE 1

Compound	n	λ (mμ)						
		486	520	555	589	620	656	∞
$K_4Fe(CN)_6 \cdot 3H_2O$	n_g	1.594	1.587	1.583	1.580	1.577	1.574	1.555
	n_m	1.587	1.581	1.578	1.575	1.572	1.569	1.550
	n_p	1.582	1.576	1.573	1.570	1.567	1.564	1.545
$K_4Fe(CN)_6$	n_g	1.610	1.602	1.596	1.591	1.587	1.584	1.555
	n_m	1.608	1.600	1.594	1.589	1.585	1.582	1.553
	n_p	1.605	1.596	1.590	1.585	1.581	1.578	1.549

This was analyzed for NH_3 in the usual way (distillation from alkali), while the $[Fe(CN)_6]^{-4}$ was titrated with zinc sulfate. The results for ammonia were 21.9 and 22.0%; calculation for $(NH_4)_4Fe(CN)_6 \cdot 1.5\ H_2O$ gives 22.05%. The other titration gave 68% of $[Fe(CN)_6]^{-4}$, which also corresponds to $(NH_4)_4Fe(CH)_6 \cdot 1.5H_2O$. Ammonium ferrocyanide might be prepared in other ways, e.g., passage of dry ammonia gas into $H_4Fe(CN)_6$ dissolved in alcohol. The yellow product rapidly turns green in air; analysis showed its composition to be precisely that obtained with aqueous solutions. The sesquihydrate is also produced in Briggs' method [5]. In all cases where the product has been stated to be the trihydrate, the workers give no reliable analyses, and there is doubt as to whether they actually produced this compound, since precisely the method given in [4] for the trihydrate has also been recommended in [6] for the anhydrous compound. All our attempts to make the anhydrous salt were unsuccessful. The ammonium analog of potassium ferricyanide which we made by the method of [7] had the composition $(NH_4)_3Fe(CN)_6$, whereas Gmelin (Handbuch der anorganischen Chemie) assigns it the composition $(NH_4)_3Fe(CN)_6 \cdot 1.5H_2O$. It is notable that Hawliczek gives no analyses.

The position may be summarized as follows. Our ammonium salts had less water of crystallization than is stated in works of reference. The empirical formulas of the ammonium compounds could be assigned by analogy if the analytical data were neglected. No artificial hydrated ammonium salt actually has more water of crystallization than the corresponding potassium one; in most cases it has less, or none at all. The same effect has been observed in the natural zeolites [8]. The reason is not merely that the ammonium ion is larger than K^+, but also that the former ion forms hydrogen bonds to other atoms in the salt, which reduces the scope for hydrogen bonding of the water. This indicates that ammonium ferrocyanide and ferricyanide cannot contain more water than the correspond-

TABLE 2

Compound	M	d_4^{20}	$\bar{n}_\infty$	R_∞	R_{H_2O}
$K_4Fe(CN)_6 \cdot 3H_2O$	422.41	1.897	1.550	70.94	3.89
$K_4Fe(CN)_6$	368.36	1.986	1.552	59.27	

TABLE 3

Compound	n	λ (mμ)						
		486	520	555	589	620	656	∞
$H_4Fe(CN)_6$	n_m	1.669	1.658	1.651	1.644	1.640	1.636	1.602
$H_3Fe(CN)_6$	n_g	1.786	1.772	1.763	1.755	1.749	1.744	1.700
	n_m	1.705	1.693	1.685	1.678	1.672	1.668	1.628
$(NH_4)_4Fe(CN)_6 \cdot 1.5\ H_2O$	n_m	1.608	1.601	1.595	1.590	1.586	1.585	1.554
$(NH_4)_3Fe(CN)_6$	n_m	1.601	1.592	1.586	1.581	1.578	1.575	1.549
$K_3Fe(CN)_6$	n_g	1.603	1.594	1.588	1.583	1.580	1.577	1.551
	n_m	1.586	1.578	1.574	1.569	1.566	1.563	1.537
	n_p	1.583	1.576	1.571	1.566	1.563	1.56.	1.534
NH_4N_3	n_g	1.712	1.700	1.692	1.685	1.679	1.675	1.635
	n_m	1.690	1.679	1.671	1.664	1.660	1.656	1.618
	n_p	1.506	1.502	1.499	1.496	1.494	1.49.	1.471
KN_3	n_m	1.681	1.670	1.662	1.656	1.651	1.647	1.611
	n_p	1.416	1.414	1.412	1.410	1.409	1.40.8	1.397
NH_4CNS	n_g	1.723	1.711	1.703	1.696	1.690	1.685	1.645
	n_m	1.711	1.699	1.691	1.684	1.678	1.674	1.634
	n_p	1.548	1.542	1.537	1.533	1.530	1.527	1.506
KCNS	n_g	1.784	1.770	1.761	1.753	1.747	1.742	1.700
	n_m	1.723	1.712	1.704	1.697	1.691	1.686	1.646
	n_p	1.532	1.528	1.524	1.520	1.517	1.514	1.494

ing potassium salts, or even as much, so the formulas $(NH_4)_3Fe(CN)_6$ and $(NH_4)_4Fe(CN)_6 \cdot 1.5H_2O$ are altogether more probable than $(NH_4)_3Fe(CN)_6 \cdot 1.5H_2O$ and $(NH_4)_4Fe(CN)_6 \cdot 3.5H_2O$.

Table 3 gives refractive indices for various ammonium and potassium salts; these are generally the first values to be published, except for the thiocyanates.

The densities then give the molar refractions of Table 4; the refraction arising from the hydrogen bonds in $(NH_4)_4Fe(CN)_6 \cdot 1.5H_2O$ has been found by subtracting the refraction for the water in hydrated potassium ferrocyanide, i.e., 3.89 cm^3.

The exaltation has been shown to be correlated with the electronegativity [2] for hydrogen bonds to oxygen; thus, it was assumed that all the hydrogen atoms in the ammonium group form such bonds. This simple interpretation gave satisfactory results, but it actually stands in need of some revision.

Ammonium thiocyanate has only two $_NH\ldots N$ bonds [10], so the exaltation per NH_4^+ ion should be divided by two, not four, which gives 0.20 cm^3 for $_NH\ldots N$ in the thiocyanate. This large value is due to the excess negative charge on the nitrogen in the thiocyanate ion, because the structure analysis [10] indicates that the CNS ion has the structure $\dot{(}S = C = \bar{N})^-$. The nitrogen has a coordination number of four; two bonds go to the carbon atom, so there are two bonds to hydrogen. In fact, the number of hydrogen bonds to the nitrogen is four minus the number of other bonds. This principle may be extended to other atoms that form hydrogen bonds, because these have coordination numbers relative to hydrogen of four. The refraction of a hydrogen bond must thus be calculated on the basis of the number of other bonds, the molar increase in refraction being divided by the difference between this number and four. The number of possible hydrogen bonds may equal or exceed the number of hydrogen atoms, in which case the exaltation per ammonium ion may be divided by four. This case occurs in the ammonium oxysalts considered in a previous paper.

The cyanide group in the hexacyanides may be taken to have the structure $\dot{C} = \bar{N}$, by analogy with the thiocyanate group. This is confirmed by the very high refraction (0.24 cm^3) of $_OH\ldots N$ in $K_4Fe(CN)_6 \cdot 3H_2O$, for the refraction of hydrogen-bonded water of crystallization usually does not exceed that of ice [2], where the intermolecular bonds are strongest. The excess refraction must be due solely to the excess negative charge on the nitrogen.

The $[Fe(CN)_6]^{-n}$ thus can give 12 $_NH\ldots N$ bonds; three bonds are already taken up in $(NH_4)_4Fe(CN)_6 \cdot 1.5H_2O$ in the formation of $O-H\ldots N$ bridges, so there are only nine possible $N-H\ldots N$ bonds. Hence, the exaltation in ammonium ferrocyanide should be divided by 9, not by 16 (the number of hydrogen atoms in the NH_4^+ ions) to obtain the refraction of one $_NH\ldots N$ bond. The principle that the number of hydrogen bonds is maximal under suitable conditions [11] indicates that we should consider possible $_NH\ldots O$ bonds to the water molecules. We have shown [2] from the dibasic phosphates of potassium and ammonium that the refractions of $_NH\ldots O$ and $_OH\ldots O$ to the same oxygen atom are 0.12 and 0.13 cm^3, respectively, so we may assume here that these bonds from ammonium to water molecules will have refractions as for ice, i.e., 0.13 cm^3. Then $R_{NH\ldots N}$ in $(NH_4)_4Fe(CN)_6 \cdot 1.5H_2O$ is to be found from the total exaltation of 2.56 cm^3 by subtracting 0.39 cm^3 (three $_NH\ldots O$ bonds), the balance being divided by nine.

The ionic exaltation must be halved to find the refraction of $_NH\ldots N$ in ammonium thiocyanate, while it must be quartered for the azide and ferricyanide.

Table 5 gives $_NH\ldots N$ refractions for these compounds.

These are directly related to the effective negative charges on the nitrogen atoms in each case. For instance, increase in the valence of the iron in

TABLE 4

Compound	M	d_4^{25}	$\bar{n}_\infty$	R_∞	ΔR_{NH_4}	ER_∞
$(NH_4)_4Fe(CN)_6 \cdot 1.5H_2O$	311.13	1.346*	1.554	74.08	2.24	0.64
$K_4Fe(CN)_6$	368.36	1.986	1.552	59.27		
NH_4N_3	60.06	1.350	1.573	14.66	2.14	0.54
KN_3	81.12	2.024	1.537	12.52		
$(NH_4)_3Fe(CN)_6$	266.00	1.382*	1.549	61.25	2.01	0.41
$K_3Fe(CN)_6$	329.26	1.871	1.540	55.21		
NH_4CNS	76.13	1.305 [9]	1.593	19.77	2.00	0.40
$KCNS$	97.18	1.868 [9]	1.611	17.77		

TABLE 5

Compound	$R_{NH...N}$
$(NH_4)_4Fe(CN)_6 \cdot 1.5H_2O$	0.24
NH_4CNS	0.20
NH_4N_3	0.14
$(NH_4)_3Fe(CN)_6$	0.10

the hexacyanides reduces the refraction per hydrogen bond from 0.24 cm^3 (Fe^{2+}) to 0.10 cm^3 (Fe^{3+}).

The azide and thiocyanate ions have [10] the structures $\bar{N} = \dot{N} = \bar{N}$ $(\dot{S} = C = \bar{N})^-$ which agree with the present results, because the effective charges in the first case lie closer together, and so are more nearly neutralized than in the second; the refraction of $_N$H...N in NH_4CNS is correspondingly higher than in NH_4N_3.

Refractions of H...N bonds thus resemble those of O...H bonds in being directly related to the effective negative charge on the atom.

LITERATURE CITED

1. S. S. Batsanov, "Refractions of hydrogen bonds in inorganic compounds, Part I," Vestn. Mosk. Univ., 9, 95-108 (1954).
2. S. S. Batsanov and A. S. Sonin, "Refractions of hydrogen bonds in inorganic compounds. Part 2," Kristallografiya, 1, 1, 49-55 (1956).
3. W. Cumming and W. Goog, "The estimation of ferro- and ferricyanide," J. Chem. Soc., 1924-1928 (1926).
4. E. Müller and W. Treadwell, "Über Ferrocyanide," J. Prakt. Chem. [2], 80, 170-182 (1909).
5. S. Briggs, "The isomerism of ferrocyanides," J. Chem. Soc., 99, 1019-1035 (1911).
6. A. Mittasch and E. Kuss, "Über die Ammoniaksynthese mit Katalysatoren," Electrochem., 34, 159-170 (1928).
7. I. Hawliczek, C. B., 2, 1748 (1926).
8. Basic Concepts of Geochemistry [in Russian], Issue 3 (1957).
9. B. Gossner, "Beiträge zur Kenntnis der Isomorphie," Z. Krist., 44, 417-518 (1907).
10. G. S. Zhdanov and Z. V. Zvonkova, "Chemical crystallography of metal thiocyanates," Usp. khim., 22, 1-35 (1953).
11. J. Robertson, Organic Crystals and Molecules (New York, 1953), p. 228.

STRUCTURAL CHANGES IN CRYSTALS STUDIED ON LOW-TEMPERATURE SPECTRA

V. L. Broude and A. F. Prikhot'ko

Physics Institute, Academy of Sciences of the Ukrainian SSR

Translated from Kristallografiya, Vol. 1, No. 3,
pp. 334-341, May-June, 1956
Original article submitted March 9, 1956

Absorption spectra in polarized light are reported for molecular crystals at 77 and 20.4°K; these indicate the symmetry of the crystal and the molecular orientation. Only spectra observed with the direction of polarization along the axes of the ellipsoid should be recorded, because the spectrum is dependent on the orientation of the light vector. The spectra also show that the substrate affects the crystallization of the material.

Introduction

The electronic spectrum of a compound in the form of free molecules (vapor) contains a band corresponding to the purely electronic transition and others corresponding to this in combination with excitation of various modes of molecular vibration. The result is a spectrum consisting of several overlapping series of bands.

The state of aggregation affects the spectrum to an extent dependent on the strength of the intermolecular forces. Molecular crystals (those formed by nearly all organic compounds) have only weak forces; evaporation begins well below the melting point. Such crystals are very convenient in studying the effects of the state of aggregation; the general structure of the spectrum remains that found for the free molecule, while the well-defined changes [1] indicate the effects of the lattice.

The effects are seen especially well if polarized light is used at hydrogen or helium temperatures.

The theory neglects the molecular interaction to a considerable extent, especially in the oriented gas representation; this, if the molecules are represented as electric dipoles, gives the ratio of the absorption coefficients for two mutually perpendicular directions as equal to the square of the tangent of the angle between the projection of the dipole moment for the transition on the relevant plane and the principal refractive index in that plane.

This model thus enables one to locate the dipole moment relative to the ellipsoid; the orientation of the moment in the molecule then gives the orientation of the molecule relative to the crystallographic axes.

Low-temperature spectra [2,3] have revealed some pairs of strongly polarized bands or lines that are not represented in the vapor and that do not fit into the oriented-gas model at all. These have been called crystalline bands, and exciton theory [4] shows that the lattice symmetry and number of molecules in the cell control the number, position, and polarization of these bands.

The polarization and selection rules for these exciton bands thus indicate the possible symmetry of the crystal and even more detailed features of the structure.

Methods

We have used aromatic compounds, mainly hydrocarbons of the benzene and naphthalene series. These must be made into monocrystalline plates around a hundredth of a micron thick by the use of a special quartz cell (Fig. 1). The thickness may be estimated from the color produced between crossed polarizers.

A polarizing microprojector [5] was used to record the spectra of these small crystals, the head (Fig. 2) being placed directly in the cryostat. This head is especially convenient for substances that are liquid at room temperature. Solid materials may be melted on the slide.

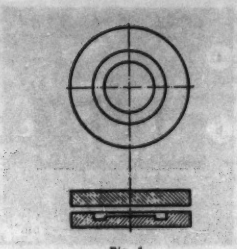

Fig. 1.

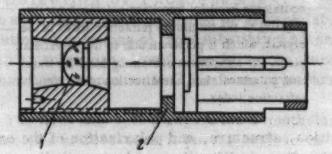

Fig. 2. 1) Lens; 2) cell holder.

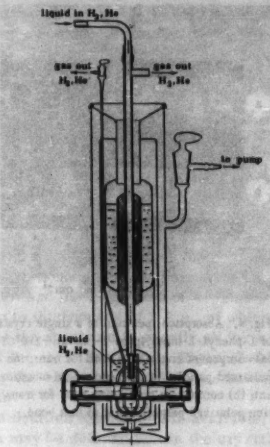

Fig. 3.

Figure 3 shows the cryostat, which can be used with single crystals of size 0.1 mm at hydrogen temperatures. The cryostat of [5] was used at nitrogen temperatures.

This projector may also be used to observe melting and crystallization, to detect photochemical reactions, and to control the growth of small crystals via temperature manipulation.

We used Q-12 and KS-55 spectrographs with a high-pressure xenon arc; the polarizer was usually a crystal of Iceland spar, which gave images of both spectra in the focal plane simultaneously.

Examination of a Crystalline Specimen

Identification of Planes. The universal stage shows that many compounds crystallize in our cell as two or more types of platelet, whose planes contain different axes of the indicatrix. This enabled us to detect differences in the spectra for several planes of polarization.

The universal stage was used to confirm the orientation of the indicatrix deduced from the spectra for compounds such as hexamethylbenzene and hexaethylbenzene. Only the birefringence and the polarized absorption could be used for the xylenes (o- and m-) and benzene; the spectra of the latter show [6] that the recrystallization which it undergoes near the melting point enables one to grow platelets whose planes are close to the *ac*, bc, and *ab* lattice planes.

These platelet planes are very valuable if the molecule of the compound has two overlapping transitions polarized mutually at right angles, one corresponding to the O– O band and the other to combination with some vibrational mode lacking total symmetry [7]. The two dipoles differ in inclination to the plane of polarization and hence differ in absorption. For instance, the monosubstituted benzenes fit this condition very closely, and it is then a simple matter to establish the molecular orientation, which serves to identify the section of the unit cell. Figure 4 shows the spectrum of 1-phenyl-2-methylprop-2-ene, which indicates that the molecule has an orientation such that two transitions polarized mutually at right angles correspond very closely to the two directions of polarization of the incident light.

Figure 5 shows the spectrum of hexaethylbenzene, which indicates an orientation such that one component is almost free from absorption, which can occur only if the molecular plane is perpendicular to the direction of polarization for that component; the plane of the substrate is then perpendicular to the *ac* face of the lattice, which contains the molecular plane.

These results show that the intensities of the components (for a given electronic transition) have a definite ratio in any given section; but the inclination of the transition moment to the polarization direction cannot be found directly from this via the oriented-gas model, for the relationship is

Fig. 4. Absorption spectrum of a single crystal of 1-phenyl-2-methylprop-2-ene at −190°C: (a) component containing band for transition polarized parallel to the bond to the substituent; (b) component containing band for transition polarized perpendicular to that bond.

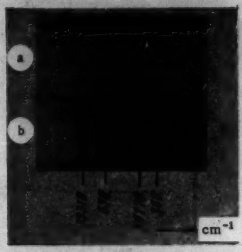

Fig. 5. Absorption spectrum of a single crystal of hexaethylbenzene at −190°C: (a) component containing band for transition polarized nearly parallel to the minimum refractive index of the crystal, which is perpendicular to the molecular plane; (b) component containing band for transition polarized along the direction of maximum refractive index.

much more complicated [8]. The reason is that the molecular interaction can be neglected only as a very rough approximation.

The absorption spectrum reflects the lattice anisotropy in the same way as do the refractive indices, expansion coefficient, etc. Only spectra polarized along the three axes of the indicatrix are significant; any other is a combination of these.

Identification of Modifications. Stepwise changes in birefringence (interference color) and shape have been observed near the melting points of many of these compounds; the effects are often irreversible and occur only on heating. The spectra indicate that these are polymorphic transitions, which occur as follows. Rapid cooling of the melt gives a homogeneous isotropic mass, which remains amorphous at nitrogen temperatures during recording of the spectrum. Subsequent slow heating causes the specimen to crystallize, usually near the melting point. The specimen is at once recooled, the spectrum being recorded with polarized light at the low temperature. A second heating cycle causes crystals of a new modification to grow at about the temperature of the previous transition. Here again this may be frozen for recording. The usual case is to find two crystalline modifications, but mesitylene and hexamethylbenzene have given three.

The transition causes a general shift of the spectrum, a change in the relation of the components, and (most important), radical changes in the position, structure, and polarization of the exciton bands. Two modifications of hexamethylbenzene show [9] that the molecular series are largely unaltered, whereas the absorption near the O–O band is radically changed. This band is forbidden in the vapor but is partly allowed in the crystal and is seen as exciton bands strongly polarized in a way determined by the symmetry of the crystal. The triclinic high-temperature form goes over to a monoclinic form.

These modifications of a single compound show that the strongly polarized bands are of exciton origin and have selection rules governed by the crystal symmetry.

Detection of Impurities. Chemical purification of a complicated organic compound is often unsatisfactory, especially because there may be no rapid method of detecting impurities. Absorption and fluorescence spectra often prove of assistance here.

Many aromatic compounds give very strong absorption; e.g., 0.001% of anthracene can be detected in this way. Fluorescence gives access to even smaller amounts. In addition, the spectra of mixed crystals sometimes indicate the orientation and distribution of the trace component in the lattice.

Tolane and dibenzyl containing a little stilbene give very narrow bands from the stilbene at hydrogen temperatures; some of these are strongly polarized (occur only in one component), while others occur in both (weakly polarized). This gives evidence on the orientation of the stilbene molecules.

The strongly polarized bands must arise from molecular layers of the trace component or from exciton interactions. Concentration effects should serve to distinguish between these possibilities; the preliminary evidence indicates that the intensity differences arise from an orientation of the trace component determined by the structure of the host lattice. The same conclusion may be drawn on anthracene in the hydroanthracenes and phenanthrene, naphthalene in durene, etc.

These trace components could scarcely be examined by x-ray methods; spectroscopy plays here the decisive part.

Detection of Photochemical Reactions. Dimers are produced by ultraviolet irradiation of solutions of monosubstituted anthracenes or anthracene itself. The forces in these dimers have been examined for 9-methylanthracene [10].

The first absorption region for 9-methylanthracene lies at 3000-4000 Å (as for anthracene and the alkylanthracenes generally); it consists of broad strong bands. Irradiation causes a gradual change in the birefringence; the crystal loses its characteristic yellow color and the absorption in this region weakens, finally to disappear and be replaced by absorption in the region characteristic of benzene (2700 Å and below). This may be followed very conveniently with an instrument used in the paper cited above, which presents the absorption spectrum directly on an oscilloscope.

The altered spectrum points to elimination of the conjugation between rings by rupture of bonds at the meso atoms, the free valences linking up to adjacent molecules (dimerization). Figure 6 shows a possible structure for the dimer [10].

Surface and Thickness Effects. Naphthalene (including deuteronaphthalene) crystals were used at 20.4°K. The specimens were made by sublimation or from melts.

A sublimed very thin film gives up to 300 bands (some only 2-3 cm^{-1} wide) in the range 2800-3100 Å; the spectrum starts with a fairly broad band seen only in the component parallel to the b axis of the crystal. At 340 cm^{-1} from this lies (at 31,960 cm^{-1}) a strong narrow band, which represents the head of many series.

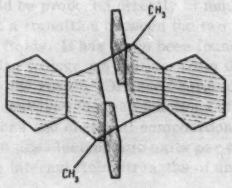

Fig. 6.

The main bands broaden somewhat as the specimen becomes thicker; weaker satellites also appear.

Crystals grown from melts showed pronounced anomalies. The very thinnest ones gave very closely the spectrum of sublimed films, apart from a shift of 83 cm^{-1} to the short-wave side.

Larger thicknesses gave the unexpected effect of very pronounced broadening and a shift in the peaks toward the long-wave side. This shift occurs only up to thicknesses of 1-2 μ, at which point the form of the spectrum is exactly as for a sublimed film of the same thickness. Figure 7 shows schematically the effects for thicknesses between 10^{-6} and 10^{-4} cm.

No detailed explanation is available, though one reason may be deformation in the crystal tightly clamped between the quartz plates [11]. The very sharp bands occurring for very thin crystals would indicate that the translational symmetry is retained. It would seem that the surfaces of the quartz exert some orienting action on crystals grown from a melt, which extends to the whole crystal when this is very thin; the crystal structure is altered, which is reflected in the 83 cm^{-1} shift. The effect is unequally distributed in thicker crystals; the central parts tend to have a normal lattice, whereas the surface layers are still affected. The absorption spectrum is therefore diffuse, because the strict selection rules imposed by the translational symmetry of the crystal are violated. The relative im-

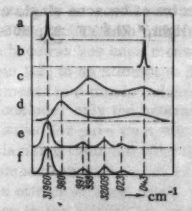

Fig. 7. Thickness effects at −253°C for an absorption band of crystalline naphthalene: (a) very thin specimen, made by sublimation; (b) the same, made from melt; (c)-(e) successively thicker specimens, from melts; (f) sublimed specimen of the same thickness as in (e).

portance of the surface layers is much reduced in very thick crystals, so the spectrum is the one normally found for naphthalene and coincides with that of sublimed platelets.

This is being tested by the use of other substrates.

The effects of substrate and crystallization are revealed by these low-temperature spectra; it may thus prove possible to evaluate the surface forces involved.

Conclusions

The spectra of molecular crystals give rise to the following conclusions on the structure effects.

1. Low temperatures (liquid hydrogen or lower) enable one to relate details of the spectrum to the crystal structure.

The spectrum of a molecular crystal reflects the symmetry of the unit cell, the inclination of the molecule to the crystallographic axes, the distribution of any trace components, the polymorphic transitions in the compound, etc.

2. Spectra having narrow bands (at hydrogen temperatures) under high resolution reveal effects from external factors such as the crystallization conditions.

3. The effects of the crystal structure and external factors can be determined correctly only by the use of light polarized along the axes of the indicatrix.

4. No spectroscopic study can be considered complete unless the actual structure and growth conditions are examined.

LITERATURE CITED

1. A. Prichotyko, "Absorption spectra of crystals at low temperatures," J. Phys., 8, 257-263 (1944).
2. A. F. Prikhot'ko, "The electronic and vibrational levels of the crystal and molecule of naphthalene," ZhÉTF, 19, 383-395 (1949).
3. V. L. Broude, V. S. Medvedev, and A. F. Prikhot'ko, "The electronic and vibrational levels of the crystal and molecule of benzene," ZhÉTF, 21, 665-672 (1951).
4. A. S. Davydov, "Theory of the absorption of light in molecular crystals," Tr. Inst. Fiz. AN UkrSSR, 1, 1-286 (1951).
5. V. L. Broude and V. S. Medvedev, "Apparatus for spectroscopic work at low temperatures," Zavodsk. lab., 17, 486-488 (1951).
6. V. L. Broude and A. F. Prikhot'ko, "Absorption spectra of benzene single crystals in polarized light," ZhÉTF, 22, 605-609 (1952).
7. V. L. Broude, "Absorption spectra of benzene homologs. Part II," Opt. i Spektroskopiya, 1 (1956) (in press).
8. D. P. Craig and P. C. Hobbins, "The polarized spectrum of anthracene. Parts I, II, III," J. Chem. Soc. (London), 539-551, 2302-2308, 2309-2319 (1955).
9. V. L. Broude, "A polarized-light study of the modifications of hexamethylbenzene," ZhÉTF, 22, 600-604 (1952).
10. V. S. Medvedev, B. M. Mikhailov, A. F. Prikhot'ko, and O. P. Kharitonova, "A spectroscopic study of the products from photochemical reactions in solutions and crystals of 9-methylanthracene," Tr. Inst. Fiz. AN UkrSSR, 4, 93-101 (1952).
11. V. L. Broude and A. F. Prikhot'ko, "On McClure and Schnepp's paper," Opt. i Spektroskopiya, 1, 102-103 (1956).

SOVIET PHYSICS - CRYSTALLOGRAPHY VOL. 1, NO. 3 MAY-JUNE, 1956

THE HETEROCHARGE ON CARNAUBA WAX ELECTRETS

A. I. Froiman and V. M. Fridkin

Institute of Crystallography, Academy of Sciences of the USSR

Translated from Kristallografiya, Vol. 1, No. 3,
pp. 342-350, May-June, 1956
Original article submitted October 15, 1955

The charge is examined as a function of polarizing field and polarization temperature by discharge on heating below the melting point.

Introduction

There has recently been much interest in permanent internal polarization in dielectrics and photoconductors. An electret is a body that retains a bulk polarization over a long period (months or even years). The electret state throws fresh light on the mechanisms of polarization and charge absorption in amorphous and crystalline insulators. An electret having artificial anisotropy is also of interest as a texture of dipole elements that corresponds to Shubnikov's symmetry group $\infty \cdot m$.

Eguchi [1,2] made the first experiments with electrets in 1921. A molten mixture of wax and rosin was allowed to set in a strong electric field; it then had a steady internal polarization, with a negative charge on the end facing the positive electrode and a positive one at the other end. This type of charge was afterwards called heterocharge. The heterocharge decreases somewhat in the first few days but thereafter remains nearly constant. The polarity may reverse if the polarizing field is very strong; the heterocharge falls to zero in a few days and is then replaced by a reversed charge (positive at anode end), which is called homocharge.

Several studies were soon made [3-5] on the production of these charges; only heterocharge was produced in fields below 10 kV/cm, but homocharge could be produced directly in much stronger fields, with a transition between the two types in intermediate fields. It has since been found [6] that the polarizing voltage (as distinct from the field) also affects the result. Surface charge densities have been measured [3-5] as functions of polarization conditions and chemical composition; they vary from 5 to 10 cgs electrostatic units per cm^2 and give rise to internal field strengths of up to 30 kV per cm. The density and field are restricted by gas breakdown; they increase with the pressure.

The published work has been reviewed in detail [7]; the known and possible practical uses have also been surveyed [8].

Particular interest attaches to work on the charge and discharge mechanisms. Gross [9,10] made simultaneous measurements of the charge and of the current in the external circuit between the electrodes when the electret was heated below its melting point. This enabled him to distinguish processes that produce heterocharge from those that produce homocharge. The heterocharge arises by absorption of charge within the dielectric, while the homocharge is produced by breakdown at the interfaces with the electrode and by subsequent decay of the internal polarization.

Gemant and others have shown that the stability of the heterocharge can be explained satisfactorily only if ion and dipole mechanisms are considered together; the stability even points to a domain structure [11]. The heterocharge on mixtures of Carnauba wax with beeswax has been measured as a function of time [12] in an attempt to distinguish ionic displacement from dipole orientation.

Here we consider only the heterocharge, which has been measured for pure Carnauba wax as a function of polarizing field and polarization temperature. Comparison with theory is employed to distinguish the effects of ionic displacement and dipole orientation in the destruction of the heterocharge.

Methods

The charge was measured from the effect of repeated heating; the current in the external cir-

cuit (from a contact electrode) was not measured, as it was sufficient to record the displacement current in the external circuit during repeat heating.

The material was not melted during polarization or depolarization, for it has been stated [9,10] that stable electrets with fairly large charges can be produced in this way. In addition, the true surface charge density can be deduced by integrating the discharge current. Also, the thermodielectric effect can produce a charge if the material is melted, and this is difficult to distinguish from the polarization effect at low field strengths.

Carnauba wax also enabled us to obtain results comparable with those previously reported.

Disks 60 mm in diameter and 1 mm thick were cast from carefully filtered wax; the surfaces were polished and then were chemically silvered. One face was then inscribed with a groove to separate the guard ring from the central electrode, whose area was 1.4 cm^2. The silver provided good contact with the electrodes at all points. The electrodes A_1, A_2, and A_3 (Fig. 3) were silvered metal rings; A_1 and A_2 were the electrodes proper, while A_3 was a guard ring. The system was placed in a thermostat providing temperatures up to 100°. A_2 was joined via the protective resistor R_2 to an EHT supply; it could be grounded via key K_2. A_1 was joined via the amber insulators I_1 to the grid of the electrometer tube T_1. Guard ring A_3 was grounded. Key K_1 provided grounding of the grid.

The current during charging and discharging was measured with a vacuum-tube electrometer operated in the constant-deflection mode (Fig. 1). The electrometer section (standard resistor R, amber key K_1, tube T_1, and resistors for this) was enclosed in a grounded case fixed to the thermostat; the section was linked via a cable to the rest of the system, which was enclosed in a separate box.

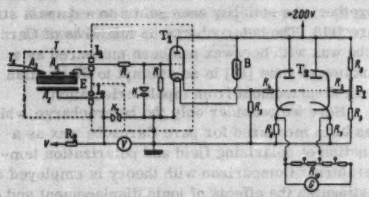

Fig. 1. The apparatus. E) Electret; A_1) upper electrode; A_2) lower electrode; A_3) guard ring; T_1) thermocouple; T) thermostat; I_1) amber insulator; I_2 high-voltage insulator; T_1) RV12P2001 electrometer tube; T_2) 6N8 tube; B) barreter; K_1) amber key; K_2) high-voltage key; V) S-95 voltmeter; G) M-91/A galvanometer; R) standard resistor; P_1) 50-kΩ potentiometer; R_1) 0.1 MΩ; R_2) 1.0 MΩ; R_3) 1.0 MΩ; R_4) 0.1 MΩ; R_5) 0.1 MΩ; R_6) 50 kΩ; R_7) 50 kΩ; R_8) 1 MΩ; R_9) 0.2 MΩ; R_{10}) shunt.

The equipment was powered from the line via an electronic stabilizer, pulse noise being eliminated by a circuit previously described [13].

The electrometer gave stable readings after it had been on for 20 min (zero drift 1-2 mV/h). The instrument was usually operated with a response of 15-400 divisions per volt, with R from 10^9 to $1.12 \cdot 10^{10}$ Ω, which gave readings to ±3% on currents between $2 \cdot 10^{-12}$ and 10^{-9} A.

The operations were conducted as follows. The specimen was left for at least 2 h at the set temperature with K_2 closed; K_2 was then opened to apply the EHT. K_1 was open if the charging current was to be measured. The disc was left for 2 h at the high temperature to polarize and then was cooled to room temperature under voltage over 1.5 h. The mode of cooling was kept strictly constant, although it has been shown [9] that the stored charge is independent of the cooling rate. The EHT was then switched off, K_2 being closed. The second heating was usually started immediately, the discharge current through R being measured (K_1 open). Again the rate of change of temperature was kept strictly constant, the discharge current being followed down to $2 \cdot 10^{-13}$ A. This gave complete discharge, because further cycles produced no more discharge current.

The temperature was measured with a thermometer placed next to the condenser and also with a differential copper–constantan couple attached to the guard ring. The polarizing voltage was measured with the electrostatic voltmeter V.

Results

First we recorded the charge and discharge currents as functions of time for various temperatures at E = 2.1 kV/cm (Figs. 2 and 3); the results were in good agreement with those of [9]. The curves for different temperatures did not intersect.

The charge Q was then measured as a function of polarizing field at 50°, the cooling and heating being strictly as above. Figure 4 shows the discharge-current curves, and also the temperature as a function of time during the discharge. The peak occurs roughly at the same time in each case; the peak current for 15 kV/cm was $1.1 \cdot 10^{-10}$ A and occurred at 200 min. The corresponding quantities for 2.1 kV/cm are $1.3 \cdot 10^{-11}$ A and 110 min. Figure 5 shows Q as a function of E; the one is directly proportional to the other between 2.1 and 12

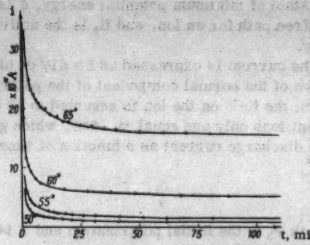

Fig. 2. Absorbed current as a function of time at E = 2.1 kV/cm for various temperatures.

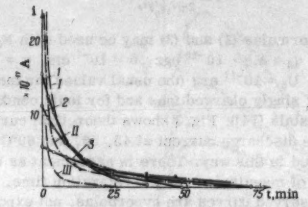

Fig. 3. Discharge (desorption) current as a function of time for E = 2.1 kV/cm. I-III) From experiment; 1-3) from theory; I and 1) at 60°C; II and 2) at 55°; III and 3) at 45°.

kV/cm, but the reproducibility was poor for E > 10 kV/cm, perhaps because homocharge was produced (the reproducibility was good at low fields, which produce only heterocharge). The total charge at 15 kV/cm was 0.25 μC, which is equivalent to $1.8 \cdot 10^{-8}$ C/cm^2. The densities are somewhat less than those quoted in [12], but mixtures of Carnauba wax with beeswax were used in that case.

Figure 6 shows discharge curves following polarization at 5 kV/cm at several temperatures (temperature–time curve during discharge as for Fig. 4). Comparison with Fig. 4 shows that the polarization temperature and polarizing field have completely different effects on the discharge curve; the peak becomes broader and shifts to the right as the polarization temperature is increased, and the rate of decay of the discharge current is substantially reduced. The effect is especially pronounced at low polarizing fields; at 2.1 kV/cm with a polarization temperature of 59°, the peak has a flat top (duration about 15 min), the subsequent decay also being very slow.

Figure 6 gives discharge curves, from which Q may be deduced as a function of polarization temperature T; Fig. 7 shows $\ln (Q \cdot 10^5)$ against $1000 \cdot T^{-1}$. The heterocharge evidently involves an activation energy, because $Q = Q_0 \exp(-U/kT)$; the slope of the line in Fig. 7 gives U as $1.3 \cdot 10^{-12}$ erg, or 18,500 cal/mole, which agrees closely with the

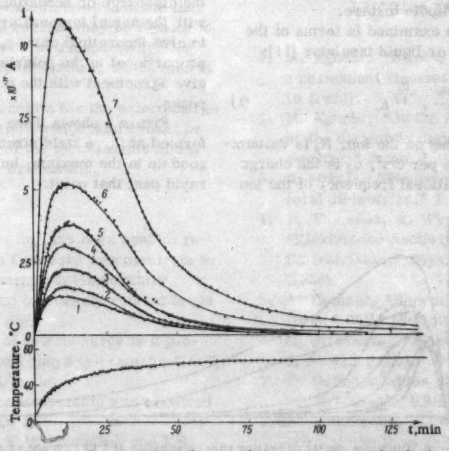

Fig. 4. Discharge current on heating after polarization at 50° in fields (kV/cm) of (1-7): 2.1, 3, 4, 5, 6.2, 9.9, and 15.2.

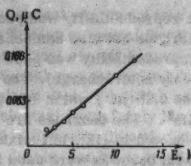

Fig. 5. Charge Q (μC) as a function of polarizing field E (kV/cm); polarization temperature, 50°C.

16,000 cal/mole reported [12] for Carnauba wax mixed with beeswax.

The electret was reheated after a certain delay in certain cases (up to 3 months in a few instances). The discharge current fell only slightly with lapse of time.

Discussion

It is now known [9-12] that macroscopic ion displacements and dipole orientation occur together in the production and removal of the heterocharge.

The proportion of dipole component has been found [12] to diminish gradually, the effect increasing with the polarization temperature, perhaps on account of motion of the ions within the electret.

The effects of heating are to be interpreted as due to migration of weakly bound ions in the electret in response to the internal field, in conjunction with disordering of the dipole texture.

This motion may be examined in terms of the ion current in a crystal or liquid insulator [14]:

$$i = \frac{N q_0^2 \delta^2 \nu}{6kT} e^{-\frac{U_0}{kT}} E. \qquad (1)$$

Here, E is the field acting on the ion, N_0 is the number of weakly bound ions per cm^3, q_0 is the charge on an ion, ν is the vibrational frequency of the ion in its state of minimum potential energy, δ is the mean-free path for an ion, and U_0 is the activation energy.

The current is expressed as $i = dP/dt$ (the derivative of the normal component of the polarization vector); the field on the ion is assumed to be due to adjacent ions only and equal to $-4\pi P$, which gives us the discharge current as a function of time:

$$i = -\frac{P_0}{\tau} e^{-\frac{t}{\tau}}, \qquad (2)$$

in which P_0 is the initial polarization and τ is the relaxation time:

$$\tau = \frac{3k}{2\pi N_0 q_0^2 \delta^2 \nu} T e^{\frac{U_0}{kT}}. \qquad (3)$$

Formulas (2) and (3) may be used with $N_0 = 10^{13}$ cm^{-3}, $q_0 = 4.8 \cdot 10^{-10}$ cgs, $\delta = 10^{-7}$ cm, $\nu = 10^{13}$ sec^{-1}, $U_0 = 10^{-12}$ erg (the usual values for mobilities of singly charged ions and for ionic conduction in crystals [14]); Fig. 3 shows theoretical curves for the discharge current at 45, 55, and 60°C constructed in this way. There is agreement as to order of magnitude over the relaxation time, but the observed curves are hyperbolas, not exponentials. There is no especial point in computing the absolute discharge current and particularly τ from (2) and (3) because U_0 cannot be established precisely.

The same mechanism can be used to discuss the discharge on reheating; Eq. (2) has been used with the actual temperature – time curves of Fig. 4 to give theoretical curves, in which P_0, which is proportional to the polarizing field, was chosen to give agreement with the observed curves at the peaks.

Figure 8 shows these curves for electrets formed at three field strengths; the agreement is good up to the maxima, but the observed fall is less rapid past that point.

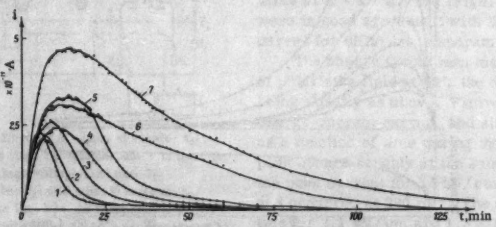

Fig. 6. Discharge current on heating after polarization at 5 kV/cm and various temperatures; curves 1-7 are for 30, 35, 38.5, 43, 47, 52.5, and 59°, respectively.

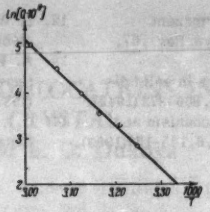

Fig. 7. $\ln(Q \cdot 10^9)$ versus $1/T$, for Q, in C.

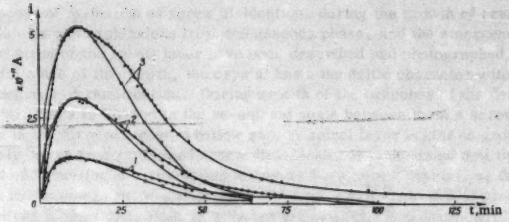

Fig. 8. Observed and theoretical discharge-current curves for polarization at 50° in fields (kV/cm) of: (1) 2.1; (2) 5; (3) 9.9. The theoretical points are indicated by circles.

These rather rough calculations indicate that the rise in the discharge current may be related to the ion motion; the subsequent unexpectedly slow fall may be due to the dipole texture, which also is disrupted by the heating.

A satisfactory explanation for the heterocharge as a function of polarization temperature must be sought in a combination of the mechanisms of ion displacement and dipole orientation.

Conclusions

1. Discharge by heating has been used to relate the heterocharge on Carnauba wax electrets to polarizing field and polarization temperature.

2. The heterocharge is linearly related to the field from 1.2 to 12 kV/cm.

3. The production of heterocharge is a process of activation type and obeys $Q = Q_0 \exp(-U/kT)$, in which U is 18,500 cal/mole.

Assistance in the measurements was received from A.I. Delova.

We are indebted to A.V. Shubnikov and I.S. Zheludev for discussions of the present results.

LITERATURE CITED

1. M. Eguchi, "Effects of electric force on a permanent electret," Japan. J. Phys., 1, 1, 10 (1922).
2. M. Eguchi, "On the intensity of polarization of the dielectric displacement of a permanent electret," Japan. J. Phys., 1, 1, 10 (1922).
3. S. Mikola, "The permanent polarization of solid dielectrics," Z. Phys., 32, 476 (1925).
4. P. Thiessen, A. Winkel, and K. Herrmann, "Elektrische Nachwirkungen im erstarrten Dielektrikum," Phys. Z., 37, 14, 511-520 (1936).
5. A. Gemant, "Recent investigations on electrets," Phil. Mag., 20, 136, 929-952 (1935).
6. C. Jamanaka, "Electret," J. Phys. Soc. Japan., 9, 3, 425 (1954).
7. F. Gutmann, "The electrets," Rev. Mod. Phys., 20, 3, 457-472 (1948).
8. A. Rabinovich, V. Fridkin, and A. Froiman, "Use of electrets in metrology," Izmerit. Tekhn., 4, 31-32 (1955).

9. B. Gross and L. Denard, "On permanent charges in solid dielectrics," Phys. Rev., 67, 8, 253-259 (1945).
10. B. Gross, "On permanent charges in solid dielectrics," J. Chem. Phys., 17, 10, 866-872 (1949).
11. A. Gemant, "Electrets: Their mechanism and potentialities," Direct Current, 1, 6, 145-157 (1953).
12. S. Wikström, "Studies of the heterocharges of electrets," Arkiv. Fys., 7, 20, 213-220 (1954).
13. A. Froiman, "Chemical analysis from x-ray fluorescence," Zavod. lab., 17, 2, 184-195 (1951).
14. G. I. Skanavi, The Physics of Dielectrics [in Russian] (1949).

FORMATION OF SCREW DISLOCATIONS IN THE GROWTH PROCESS OF A CRYSTAL

G. G. Lemmlein and E. D. Dukova

Institute of Crystallography, Academy of Sciences of the USSR

Translated from Kristallografiya, Vol. 1, No. 3,
pp. 351-355, May-June, 1956
Original article submitted March 15, 1956

The process of formation of screw dislocations during the growth of crystals of p-toluidine and naphthalene from the gaseous phase, and the emergence of the first turns of the spiral layer have been described and photographed. In the initial stage of its growth, the crystal has a dendritic character with different degrees of ramification. During growth of the branches of the dendritic crystal, there is formed in the re-entrant angle between them a screw dislocation in the form of a closed hollow gap. A spiral layer begins to grow immediately on the freshly formed screw dislocation. It is assumed that the process of formation of a screw dislocation in the growing crystal, as described in the foregoing, is analogous to the process of formation of screw dislocations in the initial stage of a nucleating crystal. Displacement of the sites of emergence on the crystal surface of screw dislocations of different signs (right-hand and left-hand) on encountering each other, their coalescence, and mutual destruction have been observed.

At the center of a spiral layer, growing on the face of a crystal, as is known, there is situated a structural defect which has been termed a screw dislocation. In 1949, Frank proposed a theory for the growth of a real crystal and indicated the part played by screw dislocations in the process of its growth [1]. He considered that the principal causes of the formation of dislocations in crystals could be the following:

1. Simultaneous formation of nuclei on the same face in correct and incorrect positions, for example twinning positions. At their meeting point, a dislocation is formed.

2. Formation of one-dimensional dislocations in the edge of a growing terrace. Such one-dimensional dislocations possess an energy of the order of the latent heat of vaporization per molecule, and are therefore in a state of thermal equilibrium. Rapid growth at high supersaturation results in their transformation into two-dimensional and three-dimensional dislocations.

3. Presence of impurities, capable of causing stresses in the crystal lattice, resulting in the formation of screw dislocations.

4. Formation on the faces of grains of a system of dislocations setting up stresses in perfect crystals, and capable of forming new members of the growing system.

5. Occurrence at low temperature of accumulations of vacant places in the lattice, which are unoccupied by molecules. The combination of these vacant places represents a plane cavity, the edges of which are dislocation loops.

6. Increase in the number of already existing dislocations under the influence of plastic flow during mechanical stressing.

Without discussing in the present article Frank's foregoing propositions, it will merely be pointed out that none of these mechanisms for the formation of dislocations in a crystal have been studied experimentally. In 1954, Forty, in a review article [2] on dislocations in crystals, also discussed the question of their formation. He pointed out that a dislocation is not essential in the very first stage of growth of a crystal, but becomes important only after the crystal has attained a considerable size. Forty agrees with Frank's view of the function of impurities in the formation of spi-

rals. While observing the spiral growth of CdI_2 crystals from a slightly supersaturated pure solution, he noticed that the spiral growth hillocks on the crystal faces were quite insignificant. On addition of a certain, generally very small, quantity of PbI_2 to the solution, the sculpture of the faces (particularly of the spiral on the faces) became more noticeable. Forty also observed the influence which the mechanical damage of the surface of a crystal face exercises on its growth. If a crystal of CdI_2, without marked sculpture of the faces, is lightly rubbed with a glass rod and is then immersed in a slightly supersaturated solution, spiral-growth hillocks appear at places where the surface of the crystal was damaged. Consequently, mechanical damage to the surface also plays a part in the occurrence of screw dislocations forming spiral-growth centers. Forty expressed the view that dendritic growth of a crystal may lead to the formation of screw dislocations in the crystal. He did not, however, carry out any experiments to confirm this view. It may be thought that the nature of the formation of vicinal hillocks on the surface of the face is similar to, if not identical with, the nature of the formation of spirals on crystal faces. This is shown by an experiment made by Lemmlein in 1934 [3], which was similar to Forty's experiment. The experiment consisted of slightly scratching with a needle an alum crystal on the faces of which no definite vicinals were to be seen, and immersing it for a short time in a slightly supersaturated solution. When the face was examined later, a continuous chain of vicinals was seen to have formed where the surface layer of the crystal had been damaged. The vicinals formed along the joint between two quartz crystals which have grown together or on the edge of healed cracks in crystals, which Lemmlein called "scar" vicinals [4], are related to similar phenomena.

In 1955, Ellis, on etching germanium crystals, obtained etch figures having a spiral character. In this connection, he also discussed the question of the origin of screw dislocations in a crystal [5]. In his view, screw dislocations are produced as the result of primary dendritic growth of the crystal. The scheme he gave, however, was rather primitive, and failed to provide any concept of the mechanism and kinetics of the formation of screw dislocations.

In our first article on the observation of spiral growth on the surface of a face of a p-toluidine crystal, it was noted that dislocations with spiral layers were usually situated close to the re-entrant angles of skeletal or dendritic crystals [6]. We expressed the supposition that the initial growth of a crystal was skeletal, then a joint was formed when the branches of the skeleton coalesced, and this joint preserved the trace of the not quite exact congruence of the lattice at the junction of the layers. This structural defect (i.e., screw dislocation), if supersaturation is suitable, is a constantly effective active center of spiral growth of the face. The same article contained photographs showing spirals inside which the closed joint of the skeleton growth was clearly visible. We were faced with the problem of examining the mechanism of formation of this skeletal growth joint which was the center of a spiral representing a screw dislocation with a site of emergence on the crystal surface. For this purpose, we investigated the growth of very thin crystals of p-toluidine from the gas phase under the same conditions as those obtaining when spiral growth occurs on the faces of already formed crystals.

Observations showed that in the very initial stage of their growth, crystals rarely have a regular shape, but invariably grow in the form of dendrites or skeletons with some degree or other of ramification. It is known that the degree of ramification depends primarily on supercooling. With considerable supercooling, ramification increases, and the crystals begin to resemble more and more ordinary dendrites with thin branches; with slight supercooling, ramification diminishes and the individual branches are coarser. On further growth, the branches of the dendrites coalesce and the crystal assumes a more isometric shape. However, on the coalescence of the branches of the same dendritic crystal, a screw dislocation is formed in the re-entrant angle between them. The process of formation of a screw dislocation and its transformation into a spiral growth center which we observed was photographed on a motion picture film. Exposures were made under a magnification of 200 times with intervals of 1 and 3 sec between the frames.

Figure 1 reproduces enlarged portions of some frames of the motion picture film we took, showing successive stages of formation of a screw dislocation and the spiral surrounding it during the period of growth. For greater clarity, some successive stages of this process are shown diagrammatically in Figs. 2a-2e. In Figs. 1a-1h is shown a portion of a dendritic crystal of p-toluidine. Two branches of a dendrite form a re-entrant angle (Fig. 1a). In the initial stage of growth of this dendritic crystal, the acute re-entrant angle between the dendrite branches, in consequence of its irregularity resulting from the diffusion process, is transformed into a rounded angle (Fig. 2b).

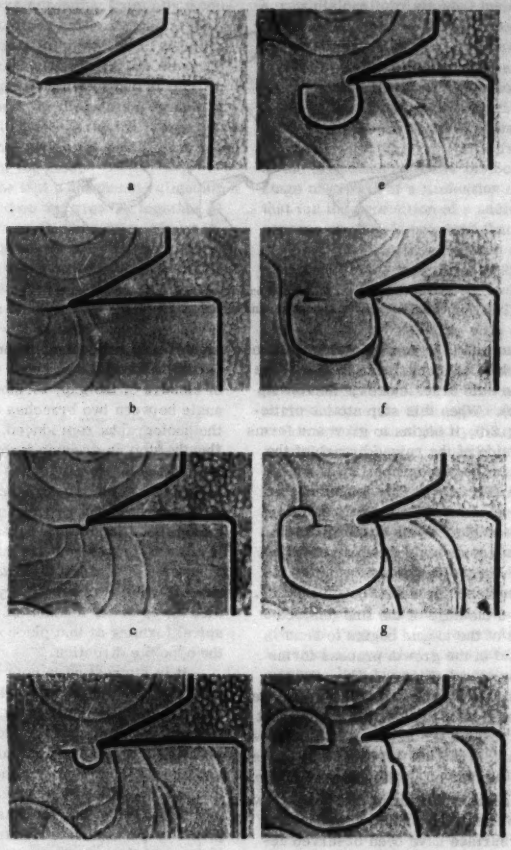

Fig. 1. Process of formation of the first turn of a spiral at the junction of the branches of a dendritic crystal of p-toluidine. Enlarged frames of a motion picture film. Between photographs a and b is an interval of 3.3 min; b and c, 1.5 min; c and d, 1.5 min; d and e, 1.5 min; e and f, 2.8 min; f and g, 0.8 min; g and h, 0.5 min. Magnification 1000.

Further growth proceeds with the formation of a gap between the two branches of the crystal. During this growth, which we shall not consider at the present moment, for some reason or other one branch of the crystal appears somewhat raised above the other (Figs. 2a, b). After a certain time, the gap in the re-entrant angle closes, leaving behind the junction, evidently a cavity in the form of a flattened cylinder, to be seen under the microscope in the form of a line (Figs. 1b and 2c). The mechanism of the growth of a re-entrant angle of a dendritic crystal with the formation of a hollow gap resembles the mechanism of the formation of inclusions in the dendritic healing of cracks in a crys-

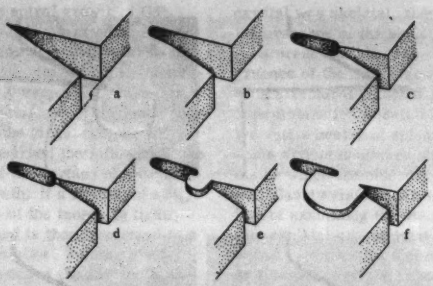

Fig. 2. Diagram of the formation of a screw dislocation on coalescence of the branches of a dendrite, and the initial growth of a spiral layer.

tal studied by Lemmlein [7]. In consequence of the fact that one branch of the dendrite is raised above the other, when the said crack closes, a small step is formed (Fig. 2c). When this step attains critical dimensions (Fig. 2d), it begins to grow and forms a tongue from the side of the raised branch of the crystal, as shown in the photograph (Figs. 1c, d), and in the diagram (Fig. 2e). This tongue begins to grow further, one of its sides extending along the edge of the closed gap, which still remains visible under the microscope in the form of a line, while the other side of the tongue moves along the edge of an as yet unclosed branch (Figs. 1e and 2f).

Having reached the edge of the line (dislocation gap), the edge of the tongue begins to bend around the line, and in the growth process forms the first turn of the spiral (Figs. 1f-1h). Successive bends produce more and more new turns of the spiral. The phenomenon of the bending of the front of a growing layer around obstacles on its path was described by Lemmlein in 1952 [8] in a study of the morphology of the surface of a silicon carbide face.

Similar phenomena of the formation of a screw dislocation and the resulting formation of a spiral layer on a crystal surface have been observed repeatedly by us on both p-toluidine and naphthalene.

The analyzed mechanism of the formation of spirals on crystal faces explains the appearance of spirals of different signs on the same crystal. If several growing spirals are observed in the field of view, it may be seen that a number of spirals are so arranged that their centers are located on one line. This line is the overgrown trace of the former re-entrant angle between dendritic branches of the crystal. The spirals formed may be of one sign, but they may also be of different signs. As follows from the mechanism described in the foregoing, the sign of a spiral depends upon which branch of the dendritic crystal was above the other at the moment of closure of the gap, formed in the re-entrant angle between two branches of the crystal. From the photographs reproduced, it is clearly to be seen that the step, in growing, forms a tongue extending toward the lower part of the crystal. The formation of a spiral of one sign or the other depends on the side from which the edge of the layer (tongue) begins to bend around the screw dislocation formed. If after a certain time, in the case of the successive formation of a screw dislocation, the branch of the crystal which was previously situated higher is situated lower at the moment of closure of the gap, the spiral forming at that place will be "rolled up" in the opposite direction.[1]

It is interesting to note that a screw dislocation is not necessarily formed when a re-entrant angle of a dendritic crystal grows together. A screw dislocation forms if there is closing of the gap, leaving a cavity between the two branches of the crystal, and closure should take place with the already-formed step, the height of which is a multiple of the unit cell parameter, i.e., is equal to the "screw pitch" of the dislocation (Burgers vector). If, on closure of the gap, a step is not formed, a screw dislocation may not appear and, on further growth, this "inclusion" may simply be overgrown without forming a spiral. If on the junction of two branches the height of the step is equal to or is slightly less

[1] During a lengthy observation of the sites of emergence on the crystal surface of two screw dislocations—a left-hand one and a right-hand one—their movement toward each other was noticed. After they had coalesced, growth of the spiral layers stopped at this position, and the last turns of the coalesced right-hand and left-hand spirals became a continuous expanding ring.

This dislocation question, of such importance for theory, should be subjected to a more detailed study.

than the height of layers spreading from other centers, the screw dislocation, newly formed at that place, has little influence on the relief of the crystal surface, since the propagating layers do not enable an independent spiral to be formed at that place. In the case where the dislocation formed has a very small screw pitch compared with other closely situated dislocations, its action has almost no influence on the relief of the face.

Observations show that a continuous dislocation array is rarely formed on the growing together of re-entrant angles in dendritic crystals. There is almost always a discontinuity between the dislocations. Figures 3a, b show a general view of the crystal for which a detailed analysis of the mechanism of the formation of one of its spirals has been made (see Fig. 1). It will be seen that there are several spiral growth centers on one line of the crystal surface. The spiral centers shown, with screw dislocations situated inside, are at some distance apart, the spirals growing from these centers having different signs. Consequently, on their formation in the growth process, at first one branch was raised slightly, and then another.

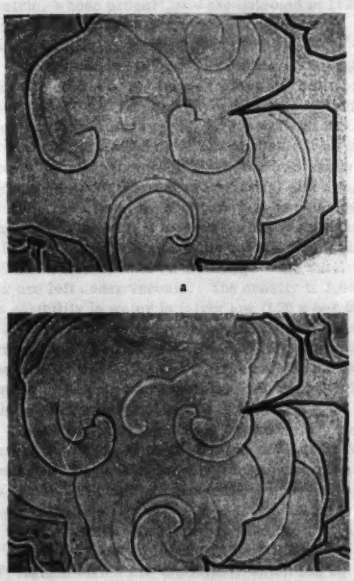

a

b

Fig. 3. General view of a p-toluidine crystal in which the formation of spiral centers was investigated. Two frames from a motion picture film with an interval of 5 min. Magnification 800.

The mechanism, described in the foregoing, of the formation of a screw dislocation in a growing crystal must differ very little from the mechanism of the formation of screw dislocations in the initial stage of growth of a nucleating crystal. We know that for the production of a nucleus, a much higher supersaturation is required than that which is necessary for the subsequent growth of the crystal. Under such conditions, it is difficult to expect that the crystal will have a regular, isometric shape in the initial stage of its growth. It will rather have a skeletal or dendritic form with different degrees of ramification. The degree of ramification, and, consequently, the number of dislocations, will depend on the supersaturation of the medium in which the nucleus appears. The higher the initial supersaturation and the more the system is contaminated by impurities, the greater will be the ramification of the nucleus, and the more probable will be the occurrence of a considerable number of dislocations in the subsequent growth of the crystal. In substances prone to dendrite formation, there is always the greatest number of dislocations. For example, metals form dendrites more readily than other substances, and, as a rule, they have the greatest number of dislocations. According to the figure given by Frank [1], there are 10^8 dislocations per 1 cm^2 of a crystal of annealed metal. In other substances, less prone to dendrite formation, the number of dislocations is much less. In view, however, of the possibility of the occurrence of dendritic forms in the nucleating stage of crystal growth, the presence of screw dislocations may always be expected. Consequently, even in the purest single crystals, grown under the most ideal conditions, the presence of a certain number of screw dislocations will always be fairly probable.

LITERATURE CITED

1. F.C. Frank, "The influence of dislocations on crystal growth," Dis. Faraday Soc., 5, 48-54 (1949).
2. A.I. Forty, "Direct observations of dislocations in crystals," Adv. Phys., 3, 1-60 (1954).
3. G.G. Lemmlein, "Experimental production of vicinals on a growing crystal," DAN SSSR, 2, 554 (1934).

4. G.G. Lemmlein, "Scar vicinals on amethyst crystals," Tr. Lomonosov. Inst. AN SSSR, 6, 13-16 (1953).
5. S.G. Ellis, "Dislocation in germanium," J. Appl. Phys., 26, 1140-1146 (1955).
6. G.G. Lemmlein and E.D. Dukova, "Observations of spiral growth of p-toluidine crystals," DAN SSSR, 102, 77-79 (1955).
7. G.G. Lemmlein, "Process of crack healing in a crystal and transformation of the form of cavities of secondary liquid inclusions," DAN SSSR, 78, 685-688 (1951).
8. G.G. Lemmlein, "Encompassment of obstacles by the front of a growing layer of a crystal face," DAN SSSR, 84, 1167-1169 (1952).

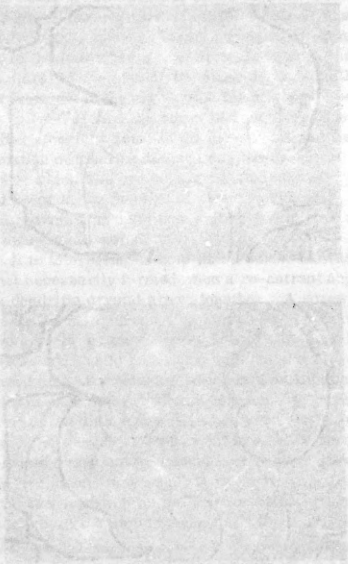

SOVIET PHYSICS – CRYSTALLOGRAPHY VOL. 1, NO. 3 MAY-JUNE, 1956

PREPARATION OF LITHIUM SULFATE CRYSTALS*

P. G. Pozdnyakov

Division 10, Ministry of the Electronics Industry of the USSR

Translated from Kristallografiya, Vol. 1, No. 3,
pp. 356-359, May-June, 1956
Original article submitted January 18, 1956

Results obtained in 1950-1951 are reported; these are of value in the organization of laboratory and commercial crystal production.

Lithium sulfate monohydrate, $Li_2SO_4 \cdot H_2O$, or LS,[1] is of considerable interest as a strong piezoelectric, whose properties were detected in 1925 [1]. LS has since been the subject of several studies [2, 3].

Modulus d_{22} is $45 \cdot 10^{-8}$ cgs units. The longitudinal modulus is the largest known in linear piezoelectrics and can be used to produce strong vibrations in the thickness mode. Hydrostatic pressure produces polarization along the diad axis, and this also is the largest known. These features make the crystals of great interest in acoustical electronics.

LS grows from aqueous solution as colorless transparent crystals whose water of crystallization is firmly bound; it begins to be released only at 105°C. There is no obvious change when the crystals are left under vacuum. The density is 2.06; the solubility in water is fairly low (130 g per liter of solution at room temperature) and has a negative temperature coefficient (average 0.15 g/liter-deg). The last is unusual; it is the first such compound that we have grown as crystals. The density of the solution at room temperature is about 1.23.

The solution is extremely corrosive to most metals, so no metal parts that can contact the solution should be used in the crystal-growing apparatus; glass and plastics, especially Plexiglas, are best.

The crystals (Fig. 1) are monoclinic (dihedral axial class), the angle being 92°08'. Right- and left-handed forms are deposited, which has an important bearing on some practical uses. The habit is usually one of combination of the $\{011\}$ and $\{0\bar{1}1\}$ dihedra with the $\{100\}$ $\{001\}$ pinakoids; $\{101\}$ and $\{10\bar{1}\}$ pinakoids also occur. The cleavage on (001) and (100) is perfect.

We have used grades labeled "analytical" and "pure," but these contained substantial amounts of various impurities, principally sulfates, calcium carbonate, and iron oxides; the solutions were turbid and unsuitable for crystal growing. The materials were therefore purified by recrystallization and washing with hot water until they gave perfectly clear solutions satisfactory for the purpose.

The first trials were done with glass vessels with stagnant solutions at room temperature; they showed that the pure compound usually gave small elongated flat crystals. Highly supersaturated solutions are not formed (limit 3-4%); the metastable region is narrow.

The growth was most rapid along the b (diad) axis, there being no marked difference between the two directions, as for potassium tartrate and ethylenediamine tartrate. Taking the growth rate on b as unit, the rates on *a* and c become 0.2-0.3 and 0.5-0.6.

The pure salt gave solutions of pH 6.0-6.5; addition of LiOH, to bring the pH to 7.5, caused no appreciable change in the growth. The growth rates of the faces became equal when sulfuric acid was used to bring the pH to 5; the crystals grew uniformly, mainly on account of increase in the growth rate along the *a* axis. This led to a long series of unsuccessful attempts to grow the crystals from solutions of pH from 2.5 to 5; the growth rates were only 0.4-0.5 mm/day and parasitic crystals were nearly always formed. The stability of the solution was found to increase with the pH; the uni-

*Read at the First All-Union Conference on Piezoelectricity, November 25, 1952.

[1] LS is a trade designation used in the USSR.

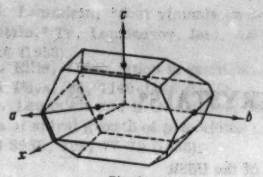

Fig. 1.

formly developed crystals growing at pH from 2.5 to 5 were accompanied by numerous parasitic crystals. Neutral and weakly alkaline pH gave lower growth rates on the *a* faces, which produced flat crystals shortened along the *a* axis, but not so many parasitic crystals were formed, so the supersaturation could be raised to a level giving a growth rate of 1.5 mm/day. The loss in growth rate along the *a* axis may be compensated by using rod seeds with the long axis along *a*; the crystals elongated on *a* needed for this purpose may be grown in acid solutions.

The early experiments involved raising the temperature from normal to 90°C, but the temperature did not affect the growth, either as regards habit or growth rate. However, the crystals are very sensitive to impurities, which give rise to networks of small cracks. This makes it especially necessary to purify the starting material and to prevent contamination of the solutions.

Subsequently, the crystals were grown by rotation or reciprocation in the solution; the speed was found to have an important effect, and vigorous stirring greatly facilitated the production of homogeneous crystals.

At first we used very small seeds, held with cement or rubber tubes in a flat horizontal disk, the b axis of the crystal being perpendicular to the plane. These were grown to 30-50 g in weight and 20-25 mm diameter, and formed the basis of the seeds cut as rods along the *a* axis subsequently used.

Solutions of pH 2.5-5 gave growth rates of only 0.4-0.6 mm/day, whereas pH 6-7.5 gave about twice this; a rate of 2 mm/day would appear to be the limit for ordinary methods. These low rates are characteristic of sparingly soluble compounds generally.

It has been found (e.g., for ammonium and potassium dihydrogen phosphates, potassium tartrate, ethylenediamine tartrate) that solutions containing compounds that retard the growth of certain faces are much more stable and allow much higher supersaturation without spontaneous crystallization. This appears to be a very general rule that can be used to accelerate growth. The loss of growth rate on certain faces may be balanced by the use of long rods or broad plates as seeds of appropriate orientation.

Seed crystals of LS may be grown from solutions brought below pH 5 with sulfuric acid. The temperature coefficient of the solubility is very low, so the temperature-variation method is unsuitable; only about 12 g would be deposited per liter of solution on raising the temperature from normal to 100°C. A better method is evaporation at constant temperature; removal of half the water from a liter of solution should give about 65 g of material deposited.

We have used cylindrical glass vessels of capacity six liters, with the nichrome heater wound directly on the outside. A mercury thermostat provided maintenance of any set temperature between 60 and 90° to 0.5°. The close-fitting cover bore the shaft of the crystal holder, which was rotated or reciprocated at about 30 rpm.

The water was removed by passing a stream of air through the vessel, the water vapor being condensed and collected in order to monitor and control the evaporation rate. The exit tube had a heater to prevent premature condensation. A few turns of rubber tubing carrying cold water were fitted around the vessel at the level of the surface of the solution; these caused water to condense on the sides and run back into the solution, which suppressed the formation of parasitic crystals along the line of contact.

A subsequent, simplified design [5] employed as condenser a lid of conical shape, with an annular trough to collect the water, which could be tapped off at the rate indicated by the evaporation graph.

An apparatus of this type has been used [6] in the method in which the solute is introduced via a hopper into the water collector as the crystal grows. The salt then dissolves in the collector, from which the unsaturated solution trickles slowly back into the vessel. This method allows either continuous or periodic addition of the salt.

This method has several advantages, in that the temperature, composition, supersaturation, and volume of solution may all be kept constant. In addition, the only restriction on the size of the crystal is that imposed by the size of the vessel; the solubility is irrelevant, as is the temperature coefficient of the solubility. The method makes efficient use of the solution (allows one to grow large crystals from small volumes of solution) in the case of sparingly soluble substances such as LS. A single six-liter vessel used in this way can grow

three or four pure homogeneous crystals each of weight 80-100 g in two weeks. The method has obvious advantages for the commercial production of LS crystals.

Crystals grown in this way have been used in research and in the manufacture of devices ordered by various organizations.

We are indebted to A.V. Shubnikov for his comments on the draft of this paper.

LITERATURE CITED

1. E. Gibe and A. Schaibe, "A simple method of detecting piezoelectric response in crystals," Z. Phys., 33 (1925).
2. W. Mason, Piezoelectric Crystals and Their Application in Electroacoustics [Russian translation] (IL, 1952), pp. 200-205.
3. R. Bechman, "Elastic and piezoelectric properties of lithium sulphate monohydrate," Proc. Phys. Soc., 65, 375 (1952).
4. Recent Research in Chemical Crystallography, Collection II [in Russian] (Moscow, 1950), pp. 81-82.
5. A.V. Shubnikov, How Crystals Grow [in Russian] (1935).
6. P.G. Pozdnyakov, Authors certificate No. 96,229, September 25, 1951.

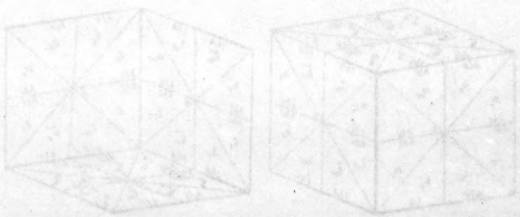

BRIEF COMMUNICATIONS

THE 48-HEDRON GROUP

N. V. Belov and T. N. Tarkhova

Institute of Crystallography, Academy of Sciences of the USSR

Translated from Kristallografiya, Vol. 1, No. 3,
pp. 360-361, May-June, 1956
Original article submitted March 29, 1956

The most complete representation of any group is its Cayley square. For the highest crystallographic group with 48 operators this square is too cumbersome, and the filling of some of its 48^2 cells causes difficulty in the multiplication of operations involving axes (rotation and mirror) by reflection from mirror planes set obliquely to the axes.

All the difficulties can easily be overcome if, after fixing the initial face (1) on two identical crystallographic 48-hedra, on all the remaining faces we write the symbols of the unique symmetry elements by which face (1) transforms into the others. Symmetry elements with order greater than two will be written on two faces since, for such elements, both right-hand and left-hand rotations are possible. We denote the latter by a negative index (–1).

In order to find the product of two operations, on one of the 48-hedra let us fix the initial face (1) and a (face)-multiplier operation. We set the second 48-hedron in a parallel position, so that the multiplicand operation (the face with the symbol of this operation) corresponds to the (1) face of the first 48-hedron. Then on the face of the second 48-hedron which corresponds to the face multiplier on the first we find the product operation (expressed by the symmetry element).

The second 48-hedron will only come into the strictly parallel position when the face with the multiplicand and face (1) are connected with each other by an operation of the first kind – pure rotation. Twenty-four such faces [including face (1)] are known to exist. On the remaining 24 faces there will be the symbols of symmetry elements of the second order, and such faces cannot be combined with face (1). In these cases, instead of face (1) on the first 48-hedron we choose a face with the symbol of a center of symmetry $C = \bar{1} = \overset{\circ}{2}$. In finding the product of two operations as before, we further multiply it (in order to secure the desired result) by an inversion, which can be done especially simply by way of a theorem found in the first few pages of an elementary treatise on crystallography.

For greatest convenience in handling, we take (stock together) a 48-hedron with a symbol hkl in which h is much greater than k and l. In other words, this will be traced as a cube in which each face is divided into eight triangles. Figures 1a and 1b give pictures of such a 48-hedron for the three front and three back faces separately, the latter, as

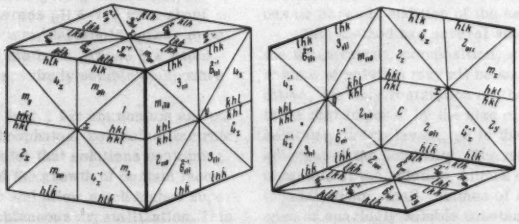

Fig. 1.

they appear when the front three are removed (not a view from the rear).

Symmetry planes are shown by the letter m, axes by the numbers 1,2,3,4,6. In order to denote mirror axes it would be desirable to use lines over the figures, but these are already taken (in "international" notation) for inversion axes, and we therefore indicate mirror axes by circles over the figure. As we know, $\bar{3} = 6^{-1}$ and $3 = \bar{6}^{-1}$. For simplicity, axes parallel to the coordinate directions and mirror planes perpendicular to these have suffixes x, y, z. For diagonal (with respect to the coordinate triad) symmetry elements, their developed notations are given.

CRYSTALS OF COMPLEX COMPOUNDS OF METALS OF THE PLATINUM GROUP (PART 13)*

K. N. Baranskii, L. A. Gribov, and V. P. Prikhod'ko

N. S. Kurnakov Institute of General and Inorganic Chemistry

Translated from Kristallografiya, Vol. 1, No. 3,
pp. 361-365, May-June, 1956
Original article submitted January 11, 1956

Complex compounds of platinum and cobalt have been synthesized by the methods of various authors. Crystal optical measurements have been made by the immersion method. The crystals have been measured on a two-circle Goldschmidt goniometer. The angles of the optical axes have been measured on a Fedorov stage.

112. Dibromodipyridinecobalt (II)

The compound $CoPy_2Br_2$ was synthesized by Hantsch's method [1]. The deep blue flat needles of $CoPy_2Br_2$ were grown from an ethanol solution by slow crystallization in a desiccator (Fig. 1). The results of the goniometric measurements are given in Table 1.

The crystals of $CoPy_2Br_2$ belong to the prismatic class of the monoclinic system. The blue color of the crystals interfered with the precise determination of the refractive index under the microscope, so that the refractive indices are given only to two places: $n_g = 1.67$; $n_m = 1.65$; $n_p = 1.57$; $2V = 52°$; $n_m = y$; $n_p^z = 26\text{-}29°$.

Fig. 1.

113. Dichlorodipyridinecobalt (II)

The compound $CoPy_2Cl_2$ was prepared by Reizenshtein's method [2].

Two modifications of this compound are reported in the literature and we obtained crystals of both modifications. The crystals of α-$CoPy_2Cl_2$ were obtained from alcohol solution by slow crystallization in a desiccator over sulfuric acid as blue-violet acicular flat crystals (Fig. 2). The results of measurements are given in Table 2.

The crystals belong to the rhombodipyramidal class of the rhombic system.

The refractive indices are: $n_g = 1.767$; $n_m = 1.750$; $n_p = 1.580$; $2V = 33°$.

The crystals of β-$CoPy_2Cl_2$ were obtained by dissolving α-$CoPy_2Cl_2$ in chloroform and pouring the hot solution into a mixture of ethyl acetate and benzene with subsequent slow crystallization in a desiccator over sulfuric acid by A. V. Babaeva's method. The intense blue crystals of β-$CoPy_2Cl_2$ are acicular (Fig. 3).

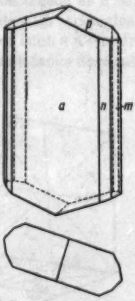

Fig. 2.

*The previous twelve parts were published by various authors in Trudy Instituta Kristallografiya.

TABLE 1

Symbol of face	Designa. of face	Measured value		Calc. value		Quality of signals	Number observed
		φ	ρ	φ	ρ		
100	*a*	90°00′	90°00′	—	—	Average	3
010	*b*	0°00′	90°00′	—	—	Good	4
110	*m*	65°25′	90°00′	—	—	Good	6
011	*p*	22°41′	27°20′	—	—	Good	6
121	*q*	−42°15′	51°35′	−41°27′	52°11′	Average	2
001	*c*	—	—	90°00′	11°16′	—	—

$a : b : c = 0.4665 : 1 : 0.4769$, $\beta = 101°16'$.

TABLE 2

Symbol of face	Designation of face	Measured value		Calculated value		Quality of signals	Number observed
		φ	ρ	φ	ρ		
100	*a*	90°00′	90°00′	—	—	Good	10
110	*m*	26°30′	90°00′	—	—	Good	10
210	*n*	44°30′	90°00′	44°55′	—	Average	6
021	*p*	0°00′	23°33′	—	—	Good	10

$a : b : c = 2.0057 : 1 : 0.2176$.

TABLE 3

Symbol of face	Designation of face	Measured value		Calculated value		Quality of signals	Number observed
		φ	ρ	φ	ρ		
110	*m*	65°10′	90°00′	—	—	Good	12
010	*b*	0°00′	90°00′	—	—	Average	8
011	*p*	23°45′	27°40′	—	—	Very good	12
$\bar{1}21$	*q*	−41°50′	51°15′	−40°11′	52°12′	Average	10
001	*c*	—	—	90°00′	11°58′	—	—

$a : b : c = 0.4702 : 1 : 0.4798$, $\beta = 101°58'$.

Goniometric measurements showed that these crystals belong to the prismatic class of the monoclinic system. The results of the measurements are given in Table 3.

A comparison of the results of the measurements shows that β-$CoPy_2Cl_2$ and $CoPy_2Br_2$ are isomorphous. The refractive indices are: β-$CoPy_2Cl_2$; $n_g = 1.652$; $n_m = 1.62$; $n_p = 1.551$; $2V = -65°$; $n_m = y$; $n_p \hat{} z = 26°$.

Because the crystals have a deep blue color, absorbing at the Becke line, the value of n_m was only determined to the second figure.

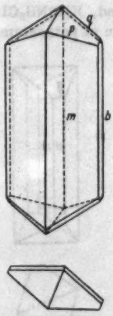

Fig. 3.

114. Potassium Tribromo-π-ethyleneplatinate (II)

The compound with the composition $K[PtC_2H_4Br_3]H_2O$ was synthesized by Gel'man's

TABLE 4

Symbol of face	Designation of face	Measured values		Calculated values		Quality of signals	Number observed
		φ	ρ	φ	ρ		
100	*a*	90°00′	90°00′	—	—	Poor	2
120	*m*	37°53′	90°00′	—	—	Good	12
106	*r*	90°00′	17°32′	90°00′	18°11′	Good	12
102	*q*	90°00′	37°45′	90°00′	38°01′	Average	12
146	*p*	28°53′	33°30′	—	—	Poor	2
001	*c*	90°00′	6°00′	—	—	Average	2

$a : b : c = 0.6462 : 1 : 0.8697$; $\beta = 96°00'$.

method [3]. Brownish-orange crystals in the form of short prisms were grown by slow crystallization from aqueous solution at room temperature. The results of measurements are given in Table 4.

The crystals of potassium tribromo-π-ethyleneplatinate (II) belong to the prismatic class of the monoclinic system (Fig. 4). The refractive indices are: $n_g > 1.780$, $n_m = 1.780$, $n_p = 1.588$. This compound is isomorphous with the compound $K[PtC_2H_4Cl_3]H_2O$.

115. Potassium Trichloro-π-ethyleneplatinate (II)

This compound, $K[PtC_2H_4Cl_3]H_2O$, was synthesized by Gel'man's method [3]. Goniometric measurements on the short yellow prisms coincided completely with the literature data [4]. The crystals belong to the prismatic class of the monoclinic system. The refractive indices are: $n_g = 1.717$, $n_m = 1.700$; $n_p = 1.552$; $2V = -32°$; $n_g = y$; $n_p \wedge z = 20°$.

116. Potassium Chlorodinitroammineplatinate (II)

This compound, $K[PtNH_3Cl(NO_2)_2]$, was synthesized by the action of potassium nitrite on potassium trichloroammineplatinate (II). The transparent, colorless or slightly yellow, elongated hexahedral prisms and rhombuses were obtained by slow crystallization from aqueous solutions at room temperature. Six crystals were measured on the goniometer. The results are given in Table 5.

TABLE 5

Symbol of face	Designation of face	Measured value		Quality of signals	Number observed
		φ	ρ		
$11\bar{2}0$	*l*	60°20′	90°00′	Good	6
$11\bar{2}1$	*p*	60°00′	60°09′	Good	6

$a : c = 1 : 0.8713$.

The precision of measurement of the coordinates was $\varphi_{11\bar{2}0} = \pm 0°30'$, $\rho_{11\bar{2}1} = \pm 0°25'$.

From the results of the goniometric measurements with a precision of up to 0°30′, the crystals belong to the hexagonal system. The crystals appear as combinations of hexagonal prisms and rhombohedra (Fig. 5). From the crystal-optical measurements the crystals are pseudo-uniaxial and

Fig. 4.

Fig. 5.

Fig. 6.

positive. The refractive indices are: $n_g = 1.752$; $n_m = 1.638$; $n_p = 1.630$; $2V = +26°$.

117. Potassium Trichlorotrinitroplatinate (IV) (Ribbed Form)

The compound, $K_2[Pt(NO_2)_3Cl_3]$, was synthesized by Vezes' method [5]. The very thin yellow planar needles were grown from aqueous solution in a Dewar flask (Fig. 6). Sixteen crystals were measured on the goniometer, but the precision of measurement was only less than ±3°. The crystals frequently had adhesions on [100]. The following simple forms were observed: {100}, {010}, and {111}.

Within the limits of the measurement the crystals belonged to the prismatic class of the monoclinic system.

From the crystal-optical measurements the crystals are biaxial and negative. The refractive indices: $n_g = 1.785$; $n_m = 1.761$; $n_p = 1.724$. The angle of extinction is 25°; $2V = -75°$.

LITERATURE CITED

1. A. Hantzsch, "Solvation und Komplexbildung als Ursache des Farbenwechsels der Kobaltohaloide," J. Anorg. Allg. Chem., 159, 273-303 (1927).
2. F. Reitzenstein, "Über die Einwirkung reduzierender Mittel auf Metallcyanide und einige Metallsalze mit organischen Basen," Ann. Chem., 276-280 (1894).
3. A.D. Gel'man (Nikitina), Complex Compounds of Platinum with Unsaturated Compounds [in Russian] (1945), p. 45.
4. S.M. Jörgensen, "Zur Konstitution der Platinbasen," Z. Anorg. Chem., 24, 153-182 (1900).
5. M. Vézès, "Sur les sels azotés du platine," Compt. Rend. Acad. Sci., 115, 44 (1892).

CRYSTALS OF COMPLEX COMPOUNDS OF METALS OF THE PLATINUM GROUP* (PART 14)

É. E. Burovaya

N. S. Kurnakov Institute of General and Inorganic Chemistry

Translated from Kristallografiya, Vol. 1, No. 3,
pp. 365-368, May-June, 1956
Original article submitted January 18, 1956

118. Potassium Trichlorotrinitroplatinate (IV) (Faceted Form)

A. B. Babaeva synthesized crystals of the compound $K_2Pt(NO_2)_3Cl_3$ at the Institute of Inorganic and General Chemistry of the Academy of Sciences of the USSR (IONKh AN SSSR). The crystals were short prisms (Fig. 1) or tablets bounded by faces of the zone 001 and three pinacoids. Seven crystals were measured on a goniometer, and from the measurements (Table 1) the crystals belong to the prismatic class of the monoclinic system. The refractive indices are: $n_g = 1.879$, $n_m = 1.791$; $n_p = 1.740$.[1]

119. Ammonium Hexachlororhenate (IV)

V. G. Tronev (IONKh AN SSSR) synthesized crystals of the composition $(NH_4)_2ReCl_6$. The muddy green crystals had the form of skeletal octahedra about 1 cm in size (Fig. 2). They were isotropic in polarized light with n = 1.790. To confirm that the compound was isomorphous with potassium hexachloroplatinate (IV), a Debye photograph was taken. As frequently happens with complex compounds, the splitting of the $K\alpha_1 - K\alpha_2$ doublet was not observed. The lattice parameter was estimated by extrapolation from the x-ray photograph as $a = 10.07 \pm 0.02$ Å. Comparison of the line intensities on x-ray photographs of $(NH_4)_2ReCl_6$ and $(NH_4)_2IrCl_6$ confirmed that they belonged to the same group of complex compounds of the type $M_2^{I}M^{IV}Cl_6$.

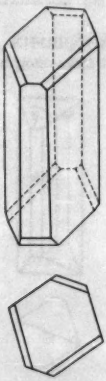

Fig. 1.

120,121. Sodium and Potassium Trisulfitotriammineiridate (III)

Z. M. Novozhenyuk (IONKh AN SSSR) synthesized crystals of the compounds $Na_3[Ir(SO_3)_3(NH_3)_3] \cdot 7H_2O$ and $K_3[Ir(SO_3)_3(NH_3)_3] \cdot 7H_2O$. The crystals were pointed colorless rhombohedra, 1-2 mm in size. The basic rhombohedra were $\{10\bar{1}1\}$ with the rhombohedra $\{01\bar{1}2\}$ developed in very narrow bands. The crystals rapidly tarnished in air because of efflorescence. Vicinals were observed on

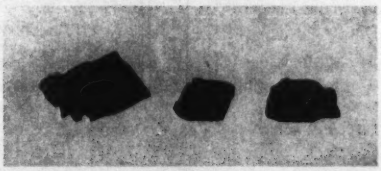

Fig. 2.

*A description of crystals of a complex compound of rhenium are described in addition to those of platinum group metals.

[1]Measured by S. S. Batsanov.

TABLE 1

Symbol of face	Designation of face	Measured value		Calculated value		Number observed
		φ	ρ	φ	ρ	
100	*a*	90°00′	90°00′	—	—	4
110	*m*	35°15′	90°00′	—	—	4
101	*p*	90°00′	38°40′	—	—	4
$\bar{1}01$	*q*	−90°00′	49°	—	50°25′	1
123	*l*	11°42′	41°31′	—	—	1
001	*c*	—	—	90°00′	11°30′	—
$\bar{1}23$	*k*	−29°36′	44°16′	30°36′	46°38′	1

$a : b : c = 1.39 : 1 : 1.37$; $\beta = 101°30'$. Precision of measurement $\Delta\varphi_{110} = \pm 0°30'$.

TABLE 2. $Na_3[Ir(SO_3)_3(NH_3)_3] \cdot 7H_2O$

Symbol of face	Designation of face	Measured value		Calculated value	
		φ	ρ	φ	ρ
10$\bar{1}$1	*f*	90°00′	74°48′	—	—
01$\bar{1}$2	*p*	30°00′	61°40′	30°00′	61°31′

$a : c = 1 : 3.192$.

TABLE 3. $K_3[Ir(SO_3)_3(NH_3)_3] \cdot 7H_2O$

Symbol of face	Designation of face	Measured value		Calculated value	
		φ	ρ	φ	ρ
10$\bar{1}$1	*f*	90°00′	75°10′	—	—
01$\bar{1}$2	*p*	30°00′	62°00′	30°00′	62°05′

$a : c = 1 : 3.270$.

the faces, and only close to the vertices of the crystals were the faces more even, making it possible to measure the crystals on the goniometer with sufficient precision. Five crystals of each compound were measured. The results are given in Tables 2 and 3.

The crystals are uniaxial and negative with the refractive indices: $n_m = 1.573$, $n_p = 1.541$.

Crystals of both compounds have cleavage planes relative to the rhombohedra $\{10\bar{1}1\}$. They belong to the ditrigonal scalenohedral class of the hexagonal system. The crystals are isomorphous with $Na_3Rh(SO_3)_3(NH_3)_3 \cdot 6H_2O$ [2]. It should be noted that the presence of six water molecules in place of seven is more in accord with the symmetry of the crystals.

The crystals are uniaxial and negative with the refractive indices: $n_m = 1.568$, $n_p = 1.546$.

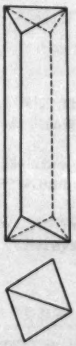

Fig. 3.

TABLE 4

Symbol of face	Designation of face	φ	ρ	Number observed
110	m	37°58′	90°00′	7
101	p	90°00′	33°01′	7

$a : b : c = 1.281 : 1 : 0.832.$

122. Potassium Bromodichloroammineplatinate (II)

E. F. Karandasheva synthesized the compound $K[PtNH_3Cl_2Br] \cdot H_2O$ and sent it to us for crystallographic study. The crystals are yellow prisms, 1-2 mm in size. The development of the crystals is extremely simple (Fig. 3) – only two simple forms were observed {110} and {101}. The measured coordinates of the faces are shown in Table 4. The precision of the measurements was ± 0°05′.

The crystals belong to the rhombodipyramidal class of the rhombic system. The refractive indices are: $n_g = 1.780$, $n_m = 1.678$; $n_p = 1.545$; $2V = -66°$. The crystals are isomorphous with the compounds $K[PtNH_3Cl_3] \cdot H_2O$ and $K[PtNH_3Br_3] \cdot H_2O$ [3].

LITERATURE CITED

1. G. B. Bokii and P. I. Usikov, "X-ray study of the structure of $(NH_4)_2IrCl_6$," DAN SSSR, 26, No. 8 (1940).
2. G. B. Bokii, "Crystals of sodium trisulfitotriamminerhodate (III) hexahydrate," Tr. Lab. Krist AN SSSR, 1 (1939).
3. M. N. Lyashenko, "Crystals of complex compounds of platinum group metals. Part 12," Tr. Inst. Kristallogr., 9 (1954).

REFRACTIVE INDICES OF ROCHELLE SALT NEAR PHASE-TRANSITION POINTS

K. N. Baranskii, L. A. Gribov, and V. P. Prikhod'ko

M. V. Lomonosov State University, Moscow

Translated from Kristallografiya, Vol. 1, No. 3, pp. 368-369, May-June, 1956
Original article submitted February 3, 1956

The upper Curie point of Rochelle salt is at +24°C; the dielectric constant there has a sharp peak, which is observed at frequencies up to 10^8 cps.

Mueller [1] observed a small anomaly in the birefringence at this point, which indicates that the refractive indices should also show anomalies.

Quartz has a second-order phase transition at +573°C; it has anomalies in the static dielectric constant and in the refractive indices in the visible region [2].

Valasek [3] measured the refractive indices of Rochelle salt at –70, –11.5, 0, +21.3, and +40°; but he paid no particular attention to the behavior near the transition point. We have made careful measurements near that point from the angles of minimum deviation given by a 60° prism with the lines of mercury. The temperature coefficients (rather than the indices themselves) were of interest, so the faces were covered with thin glass plates and castor oil in order to present a better surface to the rays.

The spectra were photographed at various temperatures; a change of 10^{-5} in the refractive index was detectable.

The prism was heated in a cylindrical oven having windows to pass the beams; any temperature between +18 and +35° could be maintained to ±0.1° and was measured to ±0.01° with a copper-constantan couple inserted in a hole drilled in the prism. In addition, capacitance measurements at 10^4 cps were made on the prism. The peak in the lower curve of Fig. 1 represents the transition point.

Two prisms differing in orientation were used; prism I had its refracting edge parallel to the c axis, while prism II had it parallel to the *a* axis. The directions of propagation were along the b axis and along the c axis, respectively, measurements in each case being made of n' and n" (n' > n") for

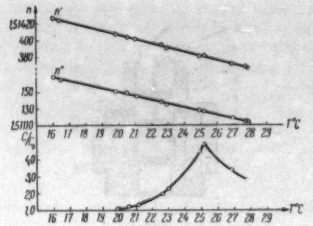

Fig. 1. Prism I.

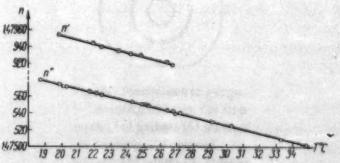

Fig. 2. Prism II.

λ = 5460 Å (Figs. 1 and 2). The results were processed by least squares; straight lines were obtained.

There is thus no deviation from a constant temperature coefficient within the errors of measurement.

We are indebted to I. A. Yakovlev for proposing the topic, and to M. A. Chernysheva for providing the specimens.

LITERATURE CITED

1. H. Mueller, "Properties of Rochelle salt. IV," Phys. Rev., 58, 805-811 (1940).

2. F. Rinne and R. Kolb, "Optisches zur Modifikationsänderung in Quarz," Neues Jahrb. Min., 2, 138-158 (1910).

3. J. Valasek, "Properties of Rochelle salt related to the piezoelectric effect," Phys. Rev., 20, 639-664 (1922).

SOVIET PHYSICS – CRYSTALLOGRAPHY VOL. 1, NO. 3 . MAY-JUNE, 1956

MEASUREMENT OF PRESSURE IN EXPLOSIONS OF GASEOUS MIXTURES BY MEANS OF A PIEZOELECTRIC GAUGE

I. S. Zheludev and V. M. Makarov

Institute of Crystallography, Academy of Sciences of the USSR
Central Scientific Research Institute for Fire Prevention
Translated from Kristallografiya, Vol. 1, No. 3,
pp. 370-372, May-June, 1956
Original article submitted February 24, 1956

Introduction

The considerable inertia of mechanical pressure gauges does not permit their use for the measurement of pressures in high-speed explosions of gaseous mixtures, lasting milliseconds. Of the large number of existing methods [1] of measuring pressures of such durations, the piezoelectric method was selected for work carried out by us at the Central Scientific Research Institute for Fire Prevention for recording the pressures set up in the explosion of some gaseous mixtures.

The piezoelectric method is widely used for recording and measuring pressures in internal combustion engines [2]. There is, however, some difference between the explosion of gaseous mixtures and the explosion of other fuel mixtures (for example, in internal combustion engines). In view of this, the method of measuring pressures, recording, calibrating, etc., developed by us is to some extent specific. In addition, the use of ceramic barium titanate, previously used by us in other work [3,4], as piezoelement, made it possible to simplify considerably the device for recording the pressures in the explosion process of a gaseous mixture.

Apparatus for Recording Pressures during the Explosion Process

The apparatus as a whole comprises the piezoelectric gauge (Fig. 1), dc amplifier and loop oscillograph MPO-2. The piezoelement in the gauge was a disk of barium titanate ceramic, 22 mm in diameter and 2 mm thick. Silver electrodes were brazed onto the lateral surfaces of the disk. After application of the electrodes, the barium titanate was polarized for 1 h in a static electric field having a strength of 20 kV/cm.

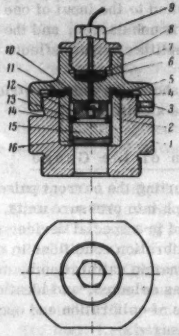

Fig. 1. Piezoelectric gauge. (1) Housing; (2) cup; (3) stop screw; (4) gasket; (5) washer; (6) packing; (7) conical washer; (8) cover; (9) stopper; (10) insulation spacer; (11) screw; (12) contact plate; (13) crystal; (14) ring; (15) base; (16) support.

As a result of the action of the pressure of the explosion wave on the piezoelement of the gauge, the barium titanate is polarized. The resulting potential difference between the grounded and insulated electrodes is proportional to the magnitude of the pressure. The considerable capacitance of the titanium piezoelement, in the specific case equal to 1800 pF, makes it possible to secure a fairly high time constant of the instrument when using the simple dc amplifier which we have previously described [5]. The time constant of our instrument was about 0.5 sec, which exceeds the duration of

Fig. 2. General view of piezoelectric gauge and dc amplifier. (1) Gauge; (2) amplifier.

the explosion process by approximately one order. The amplifier is built up on a balanced circuit using two 6Zh4 tubes. When the signal from the piezocrystal is applied to the input of one of the tubes, the amplifier is unbalanced, and the unbalance current at the amplifier output deflects the oscillograph loop.

Figure 2 shows the piezoelectric gauge together with the amplifier.

Calibration of the Gauge

For converting the current pulses recorded on the oscillograph into pressure units, the gauge was first calibrated in a special device. For approximating the calibration conditions to the operational conditions, dynamic calibration by means of compressed air was selected, and identical temperature conditions of calibration and operation of the gauge were ensured.

During calibration, the gauge was connected through a quick-acting valve to a cylinder filled with compressed air to the required pressure. The pressure in the cylinder was measured by means of a standard manometer. When the handle was pressed, the valve opened momentarily, and the gauge was subjected to the action of the air pressure imitating the explosion pressure of a gaseous mixture. As the result of the calibration, taking into account the errors introduced by the manometer and the "dead space" (variation in volume of the chamber with the valve open), a calibration graph (Fig. 3) was constructed. The pressure was plotted in kg/cm^2 on the axis of abscissas and the amplitude of the current pulses in mm, as recorded on the oscillograph film, on the axis of ordinates. Calibration was repeated for greater reliability. As will be seen from the graph, the calibration points from different calibrations coincide, and thus up to 28 kg/cm^2, linear relationship between amplifier output current and measured pressure is ensured.

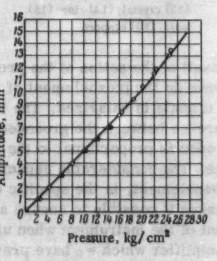

Fig. 3. Calibration graph of piezoelectric gauge.

Limits and Accuracy of the Measurements

The explosion pressures which had to be measured were expected to be of the order of 10-25 atm. The recording device was therefore designed to permit reliable pressure measurements in the range from 2 to 25 kg/cm^2. For reducing the error of measurement to a minimum, the following precautions were taken: (1) calibration and measurement were carried out at the same temperature of the ambient medium to eliminate the effect of temperature fluctuations on the properties of the piezoelement and gauge as a whole; (2) for eliminating errors introduced by the dc amplifier through variations in mains voltage, the rectified voltage was stabilized. In consequence, for fluctuations of the mains voltage of ±7.5%, the stabilized voltage varied by 0.08%; (3) the effect of variations in the emission of the tubes was eliminated by preliminary conditioning of the tubes under operational conditions.

Calculation showed that under these conditions the total error was approximately 2.5%.

Testing the Gauge

The gauge was tested in experimental explosion apparatus for measuring the explosion pressures of hydrogen–air and propane–air mixtures of different concentrations. Figure 4 shows an oscillogram obtained from the explosion of a hydrogen–air mixture with a concentration of 34%, according to the partial pressure. The direction of the recording of the process is indicated by the arrow. The recording speed was 25 cm/sec. The time marks are recorded in the top part of the oscillogram (time mark frequency 50 cps). Recording of the explosion process was effected with a loop having a sensitivity of 3.3 mm/mA. The process was recorded on motion-picture film, and the oscillogram was enlarged on printing.

The oscillogram obtained makes it possible to determine the maximum pressure and study the character of the explosion. By means of the calibration curve (Fig. 3), it was found that the maximum explosion pressure in the present case was 26 kg per cm^2.

The work which has been carried out demonstrates the complete suitability of the apparatus described for recording the explosion processes of gaseous mixtures, and measuring the pressures set up in such processes. Obviously, the apparatus may also be used for recording other processes having similar characteristics.

The authors are grateful to L. M. Dzhulardyan and I. B. Ognievich for their assistance in carrying out the work.

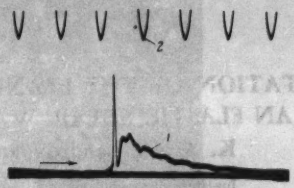

Fig. 4. Oscillogram of the explosion process of a hydrogen–air mixture. (1) Oscillogram of the explosion; (2) time marks.

LITERATURE CITED

1. A. M. Turichin, Electrical Measurements of Nonelectrical Quantities [in Russian] (1954).
2. L. Volchok, Piezoelectric Indicators for Internal Combustion Engines [in Russian] (1945).
3. I. S. Zheludev, A. S. Shein, B. I. Shteinberg, and N. A. Galybin, "Piezoelectric gauge for pressure measurement," Zavod. lab., 7, 852-855 (1953).
4. B. I. Shteinberg, N. A. Galybin, A. S. Shein, and I. S. Zheludev, "Measurement of pressure in industrial peat briquetting presses," Torf. prom., 4, 25-30 (1953).
5. I. S. Zheludev and I. B. Ognievich, "Piezoelectric instrument for measuring pressures and stresses in periodically operating mechanisms (PID-2)," Tr. Inst. Kristallogr., 12 (1956).

ROTATION OF THE PLANE OF POLARIZATION OF AN ELASTIC SHEAR WAVE

K. S. Aleksandrov and V. Ya. Khaimov-Mal'kov

Institute of Crystallography, Academy of Sciences of the USSR

Translated from Kristallografiya, Vol. 1, No. 3,
pp. 373-374, May-June, 1956
Original article submitted March 22, 1956

Theory [1] shows that the tetrad axis in a cubic crystal can carry a longitudinal wave whose speed is governed by c_{11} and a shear wave whose speed is governed by c_{44} no matter what the polarization of the exciting wave. The two shear waves propagating along [110] and having [$\bar{1}$10] and [001] as displacement directions show birefringence and have difference velocities: $v_{[001]} = (c_{44}/\rho)^{1/2}$; $v_{[110]} = [(c_{11} - c_{12})/2\rho]^{1/2}$. An incident wave with an arbitrary direction of displacement is split up into two waves differing in velocity [2].

We have observed rotation of the plane of polarization on rocksalt cleaved on [100] and cut along [110]. The specimens were heated to 600-700°C in an oven and were twisted through the required angle around the cutting direction in a gas burner, as shown in Fig. 1.

Optical tests revealed no stress after annealing.

A short ultrasonic pulse from a Y-cut quartz plate (polarizer) operating at 1.67 Mc was applied to a specimen with polished ends; a similar plate (analyzer) received the signals.

Figures 2-4 show oscillograms for [110] cut NaCl, undeformed and after twisting through 90° (sizes 100 and 90 mm, respectively). The deformed specimen had been turned to cylindrical form to eliminate effects from the sides. Figure 2a shows that the transmitted pulse is maximal when the analyzer is parallel to the polarizer when the wave is excited along [$\bar{1}$10] in the undeformed specimen, whereas the twisted specimen then gives no signal (Fig. 2b). Figure 3 is for the analyzer at 45° to the polarizer, the direction of polarization being unchanged. The undeformed crystal (Fig. 3a) transmits a smaller signal, while the deformed one (Fig. 3b) transmits a small pulse. No signal is seen from the undeformed crystal (Fig. 4a) when the polarizer and analyzer are crossed, whereas the deformed one (Fig. 4b) then gives its maximal signal.

A twisted NaCl crystal thus rotates the plane of polarization of a shear wave through the angle of twist and in the sense of the twist, so rotation of either sense can be produced. The effect occurs only for a direction of propagation having a difference in the speeds of the two shear waves and fixed displacement directions. The effect was not observed in rocksalt cleaved on [100].

The effect may be explained by reference to optics, where it has been studied in detail. We may

Fig. 1. Twisted NaCl crystal (length of specimen 75 mm).

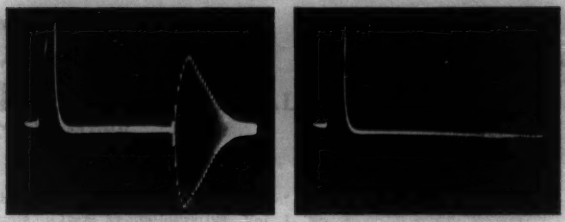

a b

Fig. 2.

a b

Fig. 3.

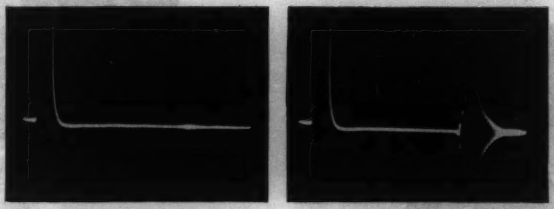

a b

Fig. 4.

Figs. 2-4. Oscillograms of pulses of elastic shear waves in a nondeformed, a, and twisted specimen, b, of [110]-cut NaCl.

consider a [110]-cut twisted crystal as the limiting case of a stack of identical birefringent plates each twisted relative to the next through the same angle; the effect is analogous to the optical activity of a nematic liquid crystal sheared by twisting the coverslip [3]. Then a twisted [100]-cut crystal may be represented as the limit of a stack of plates either isotropic or cut perpendicular to an optic axis in a crystal not showing optical activity. Clearly, no rotation occurs in that case.

We are indebted to Academician A. V. Shubnikov for his interest, and to E. M. Akulenok for assistance.

LITERATURE CITED

1. M. J. P. Musgrave, "On the propagation of elastic waves in aeolotropic media," Proc. Roy. Acad. Sci., A226, 339-355 (1954).
2. K. S. Aleksandrov, "A particular case of the propagation of elastic waves in crystals," Kristallografiya, 1, 1 (1956).
3. A. V. Shubnikov, Optical Crystallography [in Russian] (1950), pp. 231-242.

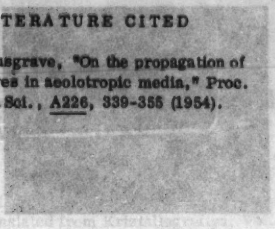

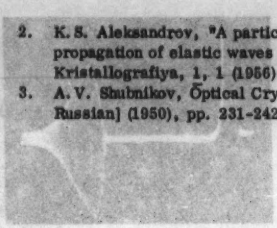

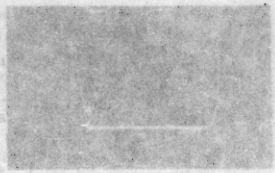

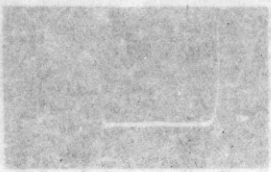

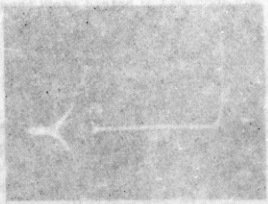

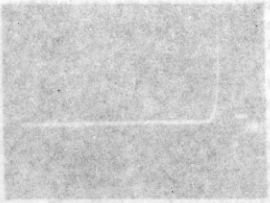

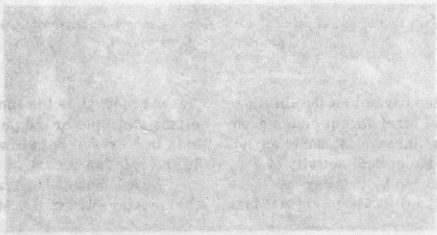

SOME ASPECTS OF THE CRYSTALLIZATION OF DIPHENYLAMINE

A. V. Shubnikov

Institute of Crystallography, Academy of Sciences of the USSR

Translated from Kristallografiya, Vol. 1, No. 3,
pp. 374-375, May-June, 1956
Original article submitted March 17, 1956

While preparing some lecture demonstrations on crystal growth, we noticed that diphenylamine containing a trace of rosin gives rise to radially rayed crystals (spherulites, but clearly not spherical) during the initial stage of crystallization (Figs. 1 and 2).

The products are not spherical because they arise by branching from single crystals to give the fan-shaped figures of Figs. 3-10, which have often been described for other substances [1-6].

These figures are very simple to prepare. A solution of the compound in benzene containing a little damar gum or other rosin soluble in benzene (e.g., Canada balsam) is used; a small drop is placed on a slide previously polished with a cloth moistened with benzene, which allows the drop to spread out as a very thin layer. The compound begins to crystallize in 10-60 sec, the amount of rosin being the decisive feature. The product may be heated and cooled (melting point of diphenylamine, 54°) several times in the production of such figures.

Fig. 1. Radially rayed crystal of diphenylamine of pseudo-square shape seen between crossed polarizers (+); x 80, about.

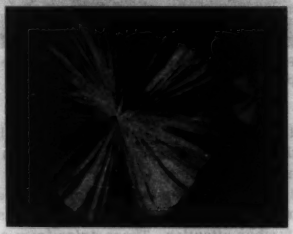

Fig. 2. Radially rayed crystal of diphenylamine of pseudo-square shape with re-entrant parts; +, x 60.

Fig. 3. Initial stage in the splitting of a nucleus; +, x 100.

Fig. 4. Second stage of splitting; +, x 60.

Fig. 5. Splitting completed; +, × 60.

Fig. 6. One of the forms given by diphenylamine; +, × 60.

Fig. 7. Another form of diphenylamine; +, × 60.

Fig. 8. Internal spirals in diphenylamine; +, × 60.

Fig. 9. Spirals of Fig. 8 in ordinary light; × 60.

Fig. 10. Radially rayed crystal of diphenylamine of pseudo-square shape in contact with others; +, × 20.

The asphericity is $(r_1 - r_2)/r_1$, in which r_1 is the maximal radius vector and r_2 the minimal one. This asphericity decreases during growth, and a large crystal would be almost spherical. This explains Popoff's [3] assumption that a spheroidal crystal (a very thin radially rayed structure) of exact spherical form always arises from a single crystal (or a twin); again, only such crystals should be called spheroidal crystals, to distinguish them from the polycrystalline spherulites, which arise from many nuclei close together [7, 8].

Diphenylamine has the characteristic feature of giving striking spirals (Figs. 8 and 9) that deserve further attention. These arise from splitting of the crystal, not from dislocations.

LITERATURE CITED
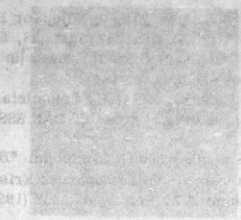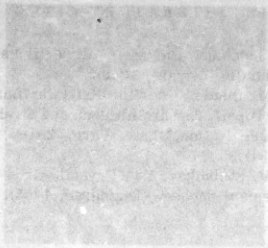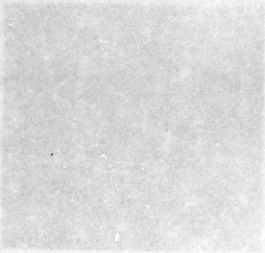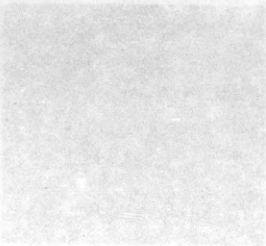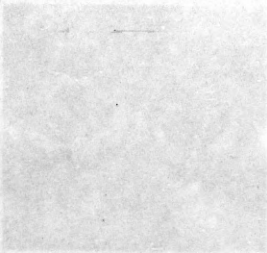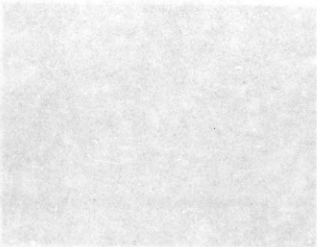
1. O. Lehmann, Die neue Welt der flüssigen Kristalle [Leipzig, 1911).
2. F. Bernauer, Gedrillte Kristalle (Berlin,1929).
3. B. Popoff, "Sphärolithenbau und Strahlungskristallisation," Latv. Farm Zurn., Riga (1934).
4. A.V. Shubnikov, How Crystals Grow [in Russian] (Moscow-Leningrad, 1935).
5. A.V. Shubnikov, "The equation for Popoff's figure," Tr. Lomonosov. Inst., 8, 5-9 (1936).
6. A.V. Shubnikov, Crystal Growth [in Russian] (Moscow-Leningrad, 1947).
7. A.V. Shubnikov and G.G. Lemmlein, "Orthotropism in crystal growth," DAN SSSR, 61 (1927).
8. A.V. Shubnikov and G. Lämmlein, "Beobachtungen über die Orthotropie des Kristallwachstums," Z. Krist., 65, 297 (1927).